[American Journal of Science, Vol. 310, September, 2010, P. 575–628, DOI 10.2475/07.2010.02]

STRUCTURAL CONSTRAINTS ON THE EVOLUTION OF THE CENTRAL ASIAN OROGENIC BELT IN SW MONGOLIA

JÉRÉMIE LEHMANN*,**,†, KAREL SCHULMANN*, ONDREJ LEXA**,***, MICHEL CORSINI§, ALFRED KRÖNER§§,‡, PAVLA ŠTÍPSKÁ*, DONDOV TOMURHUU‡‡, and DORJSUREN OTGONBATOR‡‡

ABSTRACT. We provide a detailed description of the structures along a 300 km long and 50 km wide transect across the Central Asian Orogenic Belt (CAOB) in southwestern Mongolia, covering the Precambrian Dzabkhan continental domain with overthrust Neoproterozoic ophiolites in the north (Lake Zone), a Silurian-Devonian passive margin association (Gobi-Altai Zone) and oceanic domain (Trans-Altai Zone) in the center, and a continental area (South Gobi Zone) in the south. Structural analysis suggests late Cambrian collapse of the thickened Lake Zone continental crust, leading to stretching of the lithosphere and followed by Silurian-Devonian formation of oceanic crust in the Trans-Altai domain. Subsequent emplacement of Devonian-Carboniferous and late Carboniferous magmatic arcs occurred on the Gobi-Altai and South Gobi Zone crusts, respectively, during E-W shortening. Finally, the entire system was affected by N-S convergence from the Permian to Jurassic, leading to heterogeneous shortening of the orogenic domain. The model best fitting these observations is one of generalized westward drift of the Tuva-Mongol-Dzabkhan-Baydrag ribbon continents during the Silurian-Devonian, associated with westward-subduction of the Mongol-Okhotsk Ocean and sequential growth of syn-convergent magmatic arcs. Back-arc basins opened during this period in the area of the western Paleoasian Ocean. The present-day shape of the CAOB in southern Mongolia was probably formed during Permian to Mesozoic anticlockwise rotation and folding of the Tuva-Mongol-Dzabkhan-Baydrag continental ribbons, combined with a strike-slip (transpressional) reactivation of ancient transform boundaries in the Paleoasian oceanic domain. All continental and oceanic crustal domains were reactivated and intensely deformed during this convergence in a style controlled by crustal rheology and a heterogeneous Permian magmatic-thermal input. The sequence of tectonic events is tested against published paleomagnetic data, paleogeographic reconstructions and tectonic models, leading to a revised model for the accretion of juvenile crust to a continental margin in the CAOB of southern Mongolia.

Key words: structural geology, $^{40}Ar/^{39}Ar$ geochronology, Building of the Central Asian Orogenic Belt, Mongolia, oroclinal bending

INTRODUCTION

The Central Asian Orogenic Belt (CAOB) is one of the major regions of crustal growth in the Phanerozoic (Şengör and others, 1993; Jahn, 2004). The formation of this belt, also known as Altaids (Şengör and others, 1993; Şengör and Natal'in, 1996), is due to accretion of magmatic arcs, back-arc and fore-arc terranes, accretionary

* Institut de Physique du Globe—UMR 7516, 4 rue René Descartes, Université de Strasbourg, F-67084 Strasbourg, France
** Czech Geological Survey, Klárov 3, 118 21 Praha 1, Czech Republic
*** Institute of Petrology and Structural Geology, Univerzita Karlova, Albertov 6, Praha 2, Czech Republic
§ U.M.R. 6526, GéoAzur, Université de Nice-Sophia Antipolis, 28, avenue Valrose, 06108 Nice Cedex 2, France
§§ Institut für Geowissenschaften, Universität Mainz, Becherweg 21, D-55099 Mainz, Germany
‡ Beijing SHRIMP Center, Chinese Academy of Geological Sciences, No. 26, Baiwanzhuang Road, Beijing 100037, China
‡‡ Institute of Geology and Mineral Resources, Mongolian Academy of Sciences, P.O. Box 118, Ulaanbaatar 210351, Mongolia
† Corresponding author: jerelehmann@gmail.com

complexes and continental blocks. The period of accretion is considered to have lasted either from the late Neoproterozoic to the late Permian (Şengör and others, 1993; Şengör and Natal'in, 1996) or from the latest Mesoproterozoic to the late Permian (Kröner and others, 2007; Windley and others, 2007). This orogenic complex extends from the Siberian Craton in the north to the Tarim and Sino-Korean Cratons in the south and from far eastern Siberia to the Ural Mountains (fig. 1A).

Şengör and others (1993) suggested that the orogen was formed by a process of successive bending and strike-slip duplication along a large-scale arc system composed of Proterozoic basement and magmatic arcs (the ~7000 km long Kipchak-Tuva-Mongol arc), next to the pre-Uralide and Baikalide orogens. The model of oroclinal bending was extended to the Mongolian part of the CAOB and refined by Yakubchuk and others (2005) and Yakubchuk (2008) who proposed that accretion occurred via oroclinal bending of arc-back-arc systems between the clockwise-rotating Siberian and eastward-moving North China cratons. However, Badarch and others (2002) and Windley and others (2007) proposed north-directed addition of terranes of various composition, followed in the late Paleozoic by stacking of terranes along huge shear zones. Earlier, a model involving the closure of an oceanic basin between two continental blocks by imbrication of magmatic arcs, back-arcs and passive continental margins above a large Paleozoic subduction system was proposed by Zonenshain (1973), Zorin and others (1993), Zorin (1999), and Lamb and Badarch (2001).

All proposed mechanisms of crustal growth must have been associated with deformation of the crustal fragments that were progressively added to the Siberian continental nucleus. The oroclinal bending and strike-slip duplication model (Şengör and Natal'in, 1996; Yakubchuk and others, 2005) requires a succession of distinct tectonic events that should be distinguishable (for example Johnston, 2001) as a result of accretion of terranes above subduction zones (Badarch and others, 2002; Windley and others, 2007). For example, terranes accreted by duplication of obliquely convergent margins are commonly severely sheared, heterogeneously deformed and affected by intrusions of linear and syntectonic plutons of magmatic arcs that are commonly emplaced in both transtensional and transpressive regimes (for example, Hutton and Dewey, 1986; Hutton and Reavy, 1992). However, terrane accretion does not necessarily develop parallel to sets of simultaneously operating subduction zones as was proposed by Badarch and others (2002), but the subduction systems may operate at high angles to terrane boundaries. For example, the Indonesia-Phillipines back-arc system is bounded by two almost perpendicular subduction zones that impose contrasting geometrical and kinematic constraints on the upper plate through time. Here, the magmatic arcs are related to one or both subduction zones at different times, and the directions of extensional and compressive stresses have varied through time (Hall, 2009). Typical features of accretionary orogens are changing cycles of extension and compression that are linked to successive additions of magmatic and sedimentary material (Collins, 2002a) as the result of flipping between roll-forth and roll-back subduction. As a consequence, episodes of low-pressure metamorphism and extensive magmatism associated with the development of subhorizontal extensional fabrics should alternate with phases of burial, medium- to high-pressure metamorphism, and compressive reworking related to the development of steep cleavage fronts and burial fabrics (Collins, 2002b).

To establish which of the above models applies to a given paleo-subduction system, a detailed structural study combined with high-resolution geochronology is required. Structural analysis is a powerful tool providing information about the geometry, kinematics of deformation fabrics, and the superposition of structural patterns. It is possible to recognize whether deformations were superposed at high angles due to far-field plate reorganisation or simply because of mechanical heteroge-

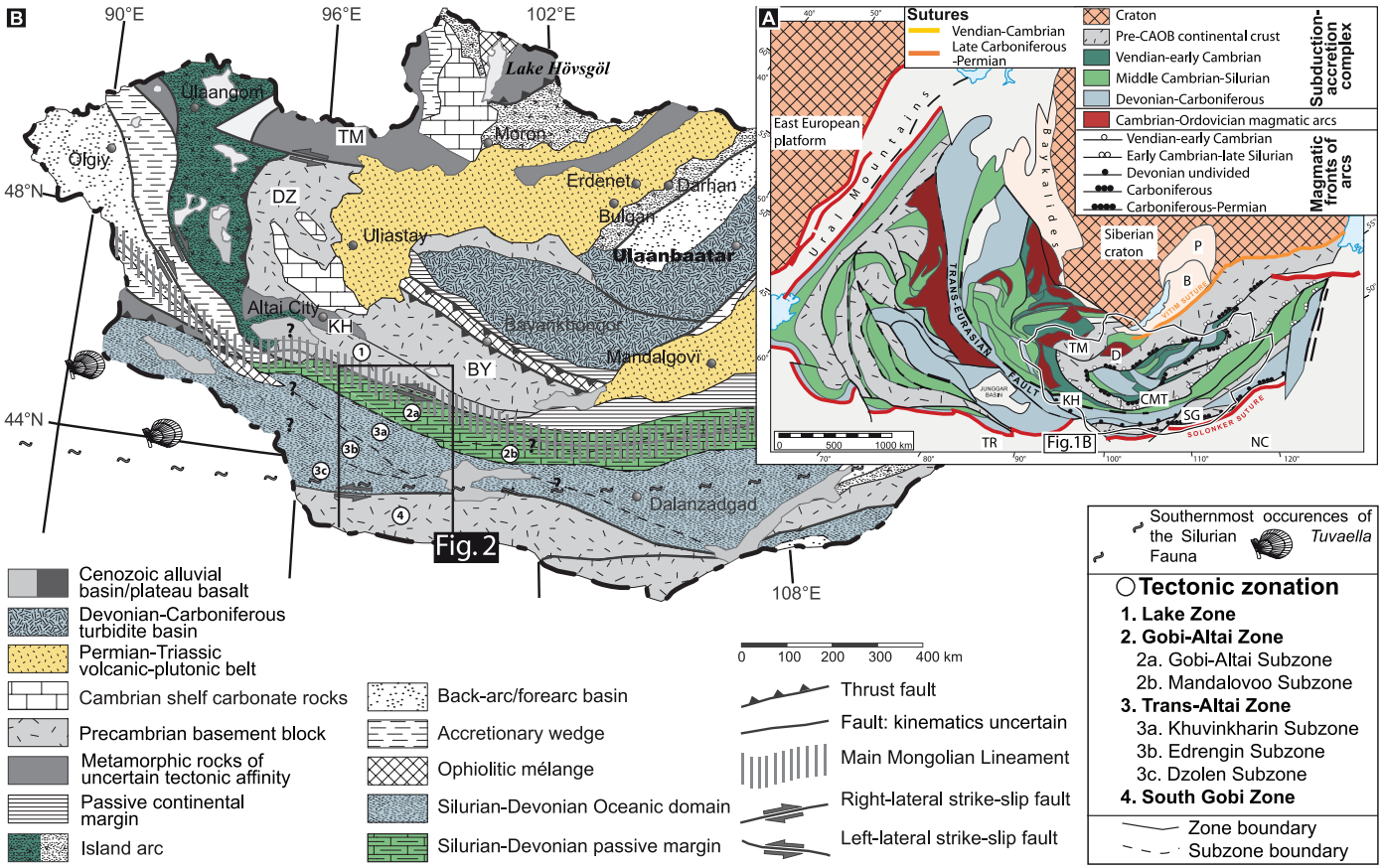

Fig. 1. (A) Simplified tectonic map of the Central Asian Orogenic Belt, modified from Şengör and others (1993) and Xiao and others (2008). B: Barguzin microcontinent; CMT: Central Mongolian Terrane; D: Dzhida island arc; KH: Khantaishir ophiolite; NC: North China Craton; P: Patom belt; SG: South Gobi microcontinent; TM: Tuva-Mongol Massif; TR: Tarim Craton. Note that only the magmatic fronts of arcs located in Mongolia are indicated. (B) Simplified geological map of Mongolia showing lithotectonic associations and location of figure 2. DZ: Dzabkhan microcontinent; BY: Baydrag block; TM: Tuva-Mongolian microcontinent; modified from Badarch and others (2002).Locations of southermost occurences of the Silurian *Tuvaella* Fauna are from Rong and Zhang (1982) and Rong and others (1995).

neities such as basement indentors. In order to fully understand the time-scales of superposed strain patterns, high resolution dating is required, and Schulmann and others (2005, 2008) have given an account of the procedures involved.

In this study, a detailed description is given of the structure along a 300 km long and 50 km wide transect across the CAOB in southwestern Mongolia (fig. 1B). By combining structural analysis with an understanding of lithostratigraphy, based on the age of angular unconformities, sedimentary unconformities, types of volcanic events and large-scale structural patterns, it has been possible to establish a plausible kinematic model of crustal accretion through time in one of the most critical sectors of the CAOB. Structural geology was combined with single zircon ages and the results of $^{40}Ar/^{39}Ar$ mineral dating that provide constraints on the duration of processes of switching from compression to extension and vice versa as has been reported in recent studies of other accretionary orogens (Lister and others, 2001; Collins, 2002a). The leading tectonic models mentioned above have been tested against existing paleomagnetic and paleontological data and our new structural and geochronological datasets, and a revised model for the accretion of juvenile crust to a continental margin in the CAOB is proposed.

Appendix I summarizes the analytical procedures for $^{40}Ar/^{39}Ar$ laser ablation dating, Appendix II provides additional information on published models for the evolution of the CAOB. This summary of existing models, paleomagnetic and paleonotlogy data are crucial for critical assessment of the new structural data and ages presented in this paper.

GEOLOGICAL SETTING

The geology of southern Mongolia can be divided into two major geological domains: the northern domain is dominated by Precambrian basement, and the southern domain consists mainly of Paleozoic sedimentary and volcanic rocks (for example, Zonenshain, 1973, fig. 1B). These domains are separated by a crustal-scale fault zone, the Main Mongolian Lineament, which forms an approximate regional structural boundary (Tomurtogoo, 1997a, 1997b). The northern domain, previously termed Caledonian (Amantov and others, 1970; Marinov and others, 1973), contains metamorphic rocks of Precambrian to early Paleozoic age, Neoproterozoic ophiolites, and early Paleozoic island arc volcanic rocks and associated volcaniclastic sediments (Badarch and others, 2002; Kröner and others, 2007). These rocks are overlain by sediments of Devonian to Carboniferous age and were affected by Permian volcanoplutonic activity with associated marine and non-marine sediments (Kröner and others, 2010). The southern domain, previously termed Hercynian (Amantov and others, 1970; Marinov and others, 1973), is dominated by early to late Paleozoic arc-related volcanic and volcaniclastic rocks with fragments of ophiolites and serpentinite mélanges (Windley and others, 2007 and references therein). Late Carboniferous to Permian volcaniclastic sediments are also widespread (Kovalenko and others, 1995). In the northern area of this domain, Devonian fossiliferous reef marbles are exposed, associated with terrigenous and volcaniclastic passive margin sequences (for example, Zaitsev and others, 1970). Both domains were intruded by post-orogenic granites and are overlain by terrigenous volcanic and sedimentary rocks of Jurassic to Cretaceous age.

The area investigated was affected by Paleozoic and post-Paleozoic strike-slip faults which offset and interfer with the primary accretionary contacts (Baljinnyam and others, 1993; Cunningham and others, 1996; Zheng and others, 1996; Lamb and others, 1999; Calais and others, 2003; Bayasgalan and others, 2005; Walker and others, 2007). Therefore, Badarch and others (2002) proposed a model of accreted terranes in which the different tectono-stratigraphic units were treated as fault-bounded assemblages of rocks or crustal fragments characterized by distinctive geological

histories that are different from adjacent terranes. In SW Mongolia, these supposed terranes form bodies elongated in an E-W direction, parallel to the topographic trend of mountain ranges.

Kröner and others (2010) presented new SHRIMP and Pb-Pb evaporation zircon ages and a thorough analysis of the lithostratigraphy in SW Mongolia, which permits to redefine the tectonic affinities of these suspect terranes in the frame of a new tectonic model for southern Mongolia (fig. 1B). This subdivision takes into account the conservative geological models proposed earlier by Russian geologists (Zaitsev and others, 1970; Zonenshain, 1973) and revised by Lamb and Badarch (1997, 2001). According to the classical subdivision of the CAOB, the tectonic zonation of western Mongolia begins with the "Lake Zone" in the north and extends into the Paleozoic of the Gobi-Tienshan area incorporating the Gobi-Altai and Trans-Altai Zones and the South-Gobi Zone in the south (figs. 1B and 2). The principal topographic units in the transect chosen for the present study are the NW-SE trending Gobi-Altai Range and branches with piedmonts and the southernmost E-W trending Gobi-Tianshan Range with Meso- to Cenozoic intermontane depressions. Our 300 km long and about 50 km wide traverse cuts across the main E-W to WNW-ESE trend of these mountain ranges.

TECTONIC ZONES AND PUBLISHED GEOCHRONOLOGY

Lake Zone

In the north of the section investigated, a Mesoproterozoic to late Cambrian block (defined by Kröner and others, 2010) is described as part of the Lake Zone (figs. 1B and 2). This unit is exposed in a belt north of the Main Mongolian Lineament, elongated E-W and flanked to the north by a Cretaceous basin. It is best characterized by a N-S section along the Khantaishir Range close to the city of Altai where a type section through the Lake Zone is developed (fig. 4A of Kröner and others, 2010). The studied section is exposed along the Zamtyn Range close to the village of Chandman where the existence of Precambrian basement was confirmed at the bottom of the sequence by a SHRIMP zircon age of 950 ± 16 Ma for a granite-gneiss. The basement is tectonically overlain by an eclogitic unit composed of carbonate, a micaschist mélange containing eclogite boudins, and the Khantaishir ophiolite composed of peridotite, gabbro, basaltic pillow lava and deep marine sediments such as chert and shale. The basement unit was affected by a magmatic/eruptive cycle dated as Cambro-Ordovician (fig. 3A) and marked by felsic pyroclastic rocks (501.2 ± 4.7 Ma), leucocratic dikes (500.8 ± 3.8 Ma), cross-cutting banded amphibolites of the basement, and a large concentric composite batholith with an age of ~511 Ma (Hanžl and Aichler, 2007; Kröner and others, 2010). These ages correspond to late Cambrian granitoid intrusions from the adjacent Baga Bogd Massif (Demoux and others, 2009b) and indicate major magmatic reactivation of Proterozoic basement rocks of the Lake Zone. The entire crystalline complex of the Zamtyn Range is overlain by a flyschoid clastic basin of middle Devonian age (detrital $^{206}Pb/^{238}U$ zircon ages between 406 and 394 Ma). Kröner and others (2010) also report a $^{206}Pb/^{238}U$ age of 358.7 ± 5.0 Ma age for felsic volcaniclastic rocks, suggesting early Carboniferous deposition of clastic sediments (fig. 3A). Paleontologically dated Permian volcaniclastic rocks (Rauzer and others, 1987; Hanžl and Aichler, 2007) flank the southern piedmonts of the Zamtyn Range and unconformably overlie older formations. Rare leucocratic granites of presumed Permian age (Rauzer and others, 1987) intrude the Zamtyn complex.

Gobi-Altai Zone

An ESE-WNW trending belt of high-grade rocks and low-grade Paleozoic sequences, 70 km wide and up to 300 km long, occurs south of the Main Mongolian Lineament. These rocks are exposed in the study area between the Chandman, Erdene

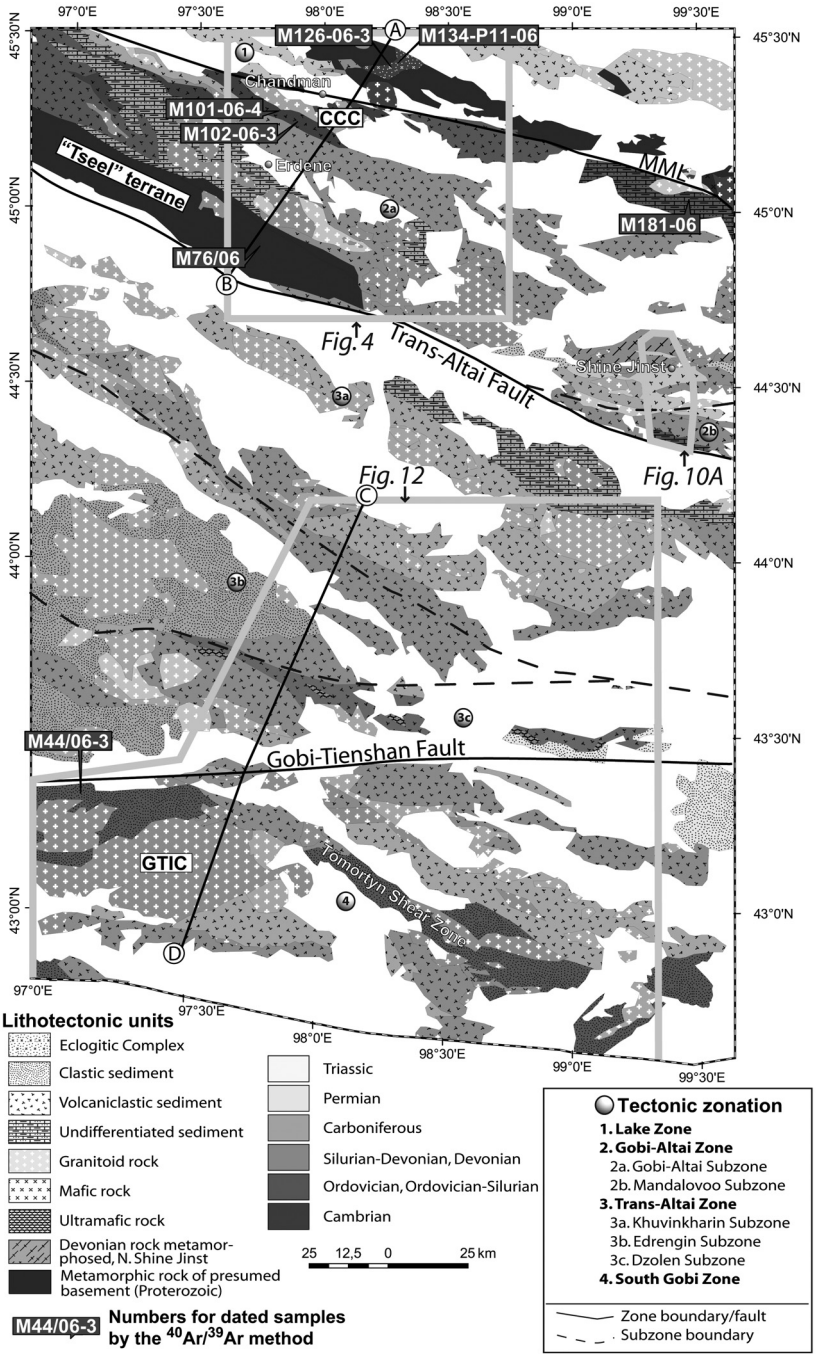

Fig. 2. Lithotectonic map of the geotraverse in SW Mongolia showing the pre-Jurassic units (Rauzer and others, 1987; Tomurtogoo, 1998) with locations of figures 4, 10A and 12 and the location of the geological cross-section of figure 17L. CCC: Chandman crystalline complex; GTIC: Gobi-Tienshan Intrusive Complex; MML: Main Mongolian Lineament. Circled numbers refer to lithotectonic zones (modified from Markova, 1975; Ruzhentsev, 2001).

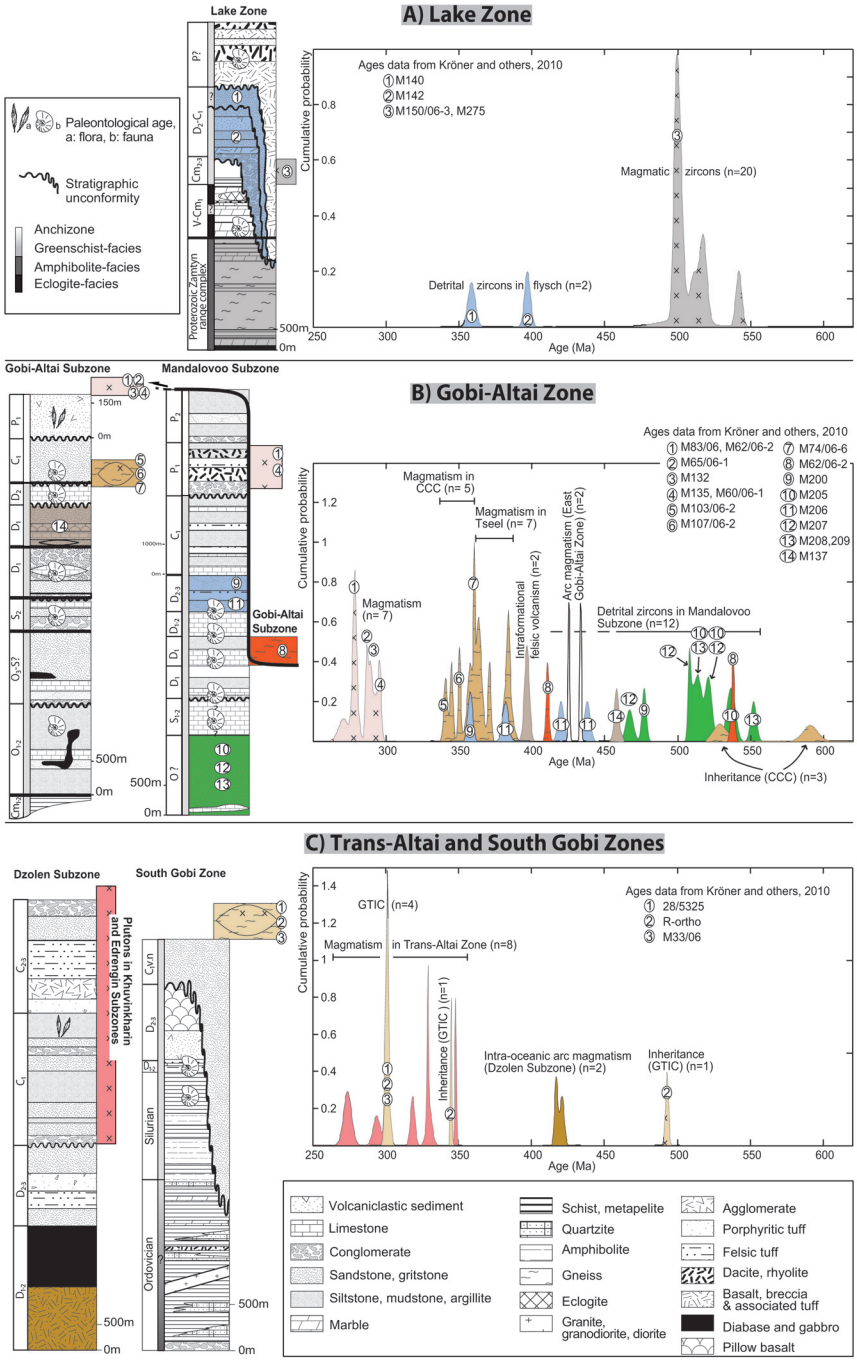

Fig. 3. Generalized lithostratigraphic columns for the study area (modified from Kröner and others, 2010 and references therein) in combination with cumulative probability curves of age histograms to show published zircon ages for (A) Lake Zone, (B) Gobi-Altai Zone and (C) Trans-Altai and South Gobi Zones. Color shading for both lithostratigraphic columns and histograms is identical to indicate which formations were dated. CCC: Chandman crystalline complex, GTIC: Gobi-Tienshan Intrusive Complex. The circled numbers refer to the dated samples of Kröner and others (2010).

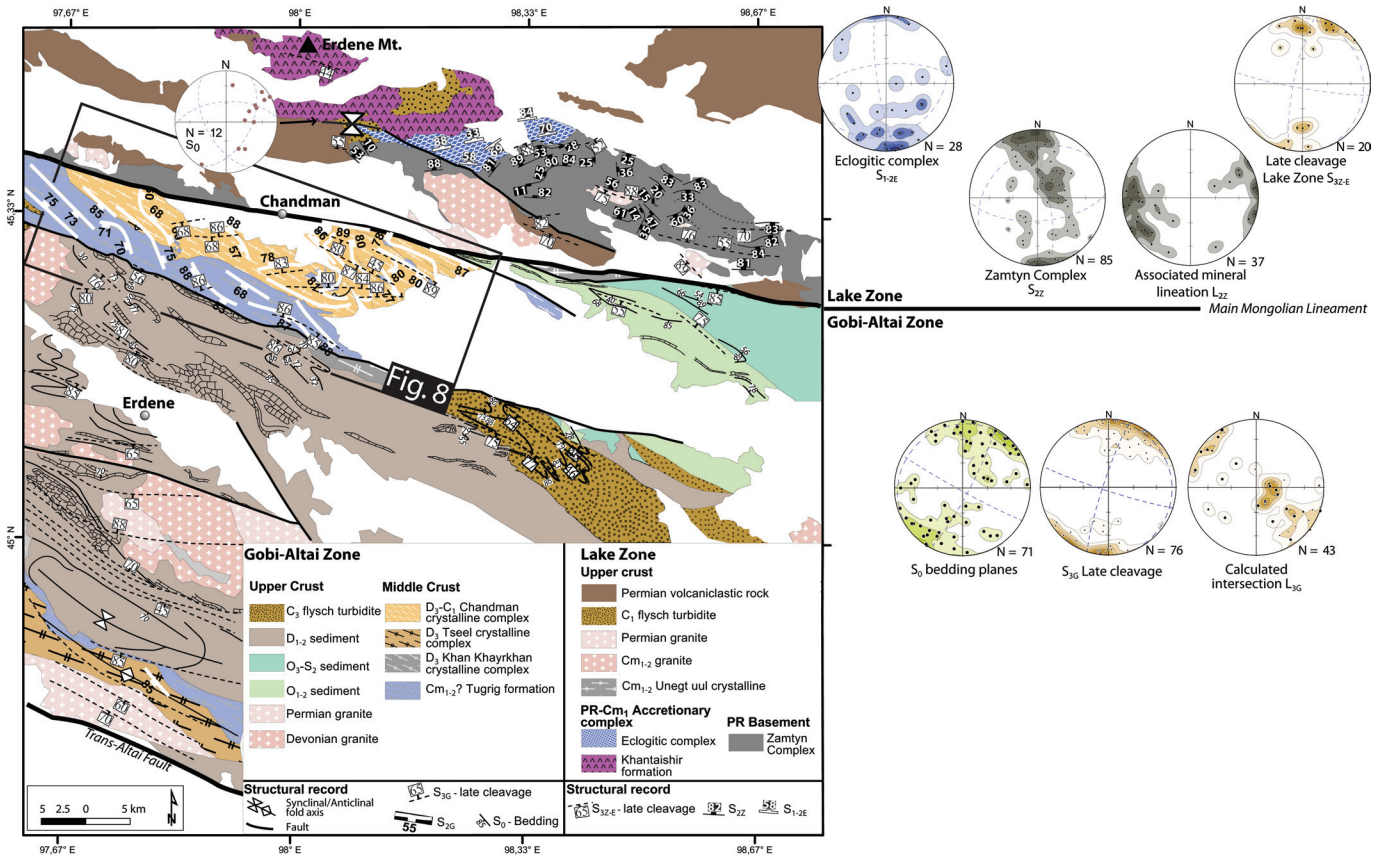

Fig. 4. Structural map for the junction of the Lake and Gobi-Altai Zones summarizing the different fabrics and indicating location of figure 8. The structural trends show extrapolations of major orientations of the structural fabrics in the field (average values were calculated using the Spheristat software). Stereograms represent average poles of folations and orientation of lineations in equal area lower hemisphere projection (averaging consists in reducing the number of measurements per locality to the minimum amount of subpopulations). The different lithotectonic units are categorized according to the published geological maps (Rauzer and others, 1987; Tomurtogoo, 1998). However, new units were defined according to new age data of Kröner and others (2010) and with spatial extent mainly inferred from examination of Landsat imagery.

and Shine Jinst Districts (fig. 2) and are bordered to the south by the active Trans-Altai Fault (Badarch and others, 2002).

The oldest lithostratigraphic unit of this zone is the Tugrig formation, probably of early to middle Cambrian age (Kröner and others, 2010) (fig. 3B). These rocks are exposed south of Chandman village (fig. 2) and consist of garnet-sillimanite-biotite paragneisses, amphibolites and quartz-rich metapelites in the north and andalusite-white mica-biotite schists in the south. The Tugrig formation in the south is unconformably overlain by a thick sedimentary-volcanic early to middle Ordovician sequence (the Bayantsagaan formation), followed by a thick sequence of fossil-free tuffaceous sediments, siltstones and rare limestones of probable late Ordovician or Silurian age, in turn overlain by thick early Devonian coral-rich limestones (Markova, 1975). The Devonian is in tectonic contact with siliciclastic early Carboniferous sediments interpreted as constituting an intramontane basin (Markova, 1975). The structurally deepest rocks exposed in the vicinity of Chandman village are represented by granites with dioritic enclaves, diorites, and xenoliths of migmatitic amphibolitic gneisses and migmatites (fig. 3B). Zircons from granites were dated at 345 ± 2 Ma (Hrdličková and others, 2008) and 340.9 ± 2.5 Ma (Kröner and others, 2010) (fig. 3B). The granites and granodiorites were locally converted into orthogneisses, and a protolith was dated at 350.4 ± 1.7 Ma (Kröner and others, 2010).

The southernmost part of the Gobi-Altai Zone, the Tseel metamorphic "terrane" (fig. 2) of Badarch and others (2002), contains a pink granophyric granite-gneiss, local mylonitic granites and rhyolitic volcanic rocks from which zircons were SHRIMP-dated at 279.6 ± 3.9 Ma and 295.7 ± 2.2 Ma (fig. 3B) by Kröner and others (2010). The core of the "Tseel terrane" is composed of metamorphic rocks consisting of amphibole-rich gneisses and felsic gneisses dated at 363.6 ± 3.9 Ma (fig. 3B) by Kröner and others (2010), as well as paragneisses with garnet and pyroxenite boudins, embedded in andalusite-bearing metapelites. Dating of a tonalitic gneiss from this area corresponds to the age of a granitoid (~360 Ma) located farther west in the area of Tsogt (fig. 3B; Kozakov and others, 2002; Kröner and others, 2007) and to metamorphic zircon ages of ~385 Ma for amphibolite-facies rocks from the Tseel area (fig. 3B; Bibikova and others, 1992; Kozakov and others, 2002). To the north of these high-grade rocks occur low-grade metasediments containing abundant felsic volcanic rocks of early-middle Devonian age (Demoux and others, 2009a). Farther north and west there is a sedimentary basin of middle Devonian age containing siltstones, shales and numerous paleontologically dated reef limestones (fig. 3B) that, according to Rauzer and others (1987), are intruded by Devonian and Permian granites.

The Mandalovoo Subzone (redefined as a terrane by Badarch and others, 2002) (fig. 2) to the east contains a sedimentary sequence that has been described in detail by Lamb and Badarch (1997) and is listed in figure 3B. The section begins with Ordovician slates containing detrital zircons dated by Kröner and others (2010) at 513 to 538 Ma and interpreted to represent the maximum age of sediment deposition. These are overlain by paleontologically dated thick Silurian fossiliferous shallow-marine carbonate sequences (Minzhin and others, 1993 and references therein). This unit is overlain unconformably by early to middle Devonian fossiliferous reef limestones (Alekseyeva, 1993 references therein). The middle to late Devonian volcaniclastic sandstones, siltstones and argillites contain volcanic flows and tuffs of basaltic to rhyolitic composition. The zircons of this formation were also dated by Kröner and others (2010) and provided a maximum depositional age of 382 ± 4 Ma and an emplacement age for intraformational felsic volcanic rocks of 357.8 ± 3.2 Ma. In the Shine Jinst area, the entire Paleozoic sequence is interpreted as shallow-marine to marine with periodic input from proximal volcanic centers (Lamb and Badarch, 1997). The rocks of the eastern termination of the "Tseel terrane" north of Shine Jinst

(fig. 2) are characterized by high-grade metamorphism marked by migmatites and granites that yielded SHRIMP zircon ages of 292.4 ± 3.6 and 277.7 ± 2.0 Ma, respectively. Importantly, the granites contain numerous zircon xenocrysts one of which was dated at 410.8 ± 2.0 Ma and suggesting the occurrence of Devonian magmatism in this area.

Trans-Altai Zone

The northern part of the Trans-Altai Gobi Desert located south of the Trans-Altai Fault and north of the Gobi-Tienshan Fault Zone was divided by Kröner and others (2010) into three Subzones according to earlier authors (Ruzhentsev and Pospelov, 1992; Ruzhentsev, 2001). This large area (fig. 2) consists of the following lithostratigraphic sequences.

The northern section is exposed in the region of the Khuvinkharin Subzone (fig. 2) where the Devonian consists of conglomerates with boulders of granite, quartz-porphyry, micaceous quartzite, gritstone and marble, which pass upwards into strata composed of intercalations of clay-rich siliceous shale, serpentinite, jasper and intercalated basalt flows. The sequence ends with a 2000 m thick graywacke flysch of middle to late Devonian age, followed by mafic volcanic rocks of intermediate composition and belonging to a weakly differentiated low-Ti tholeiitic sequence that probably formed in a rift setting (Ruzhentsev and Pospelov, 1992).

The southern section occurs along the Edrengin Subzone (fig. 2) and is dominated by volcano-sedimentary sequences. These rocks consist of tuff, tuffite and tuffaceous sandstone that contain lenses of limestone containing Emsian brachiopods in the lower part (Ruzhentsev and others, 1985) as well as massive dacite, andesite and basaltic pillow lava, rarely with tuff, in the upper part and interpreted as having formed in an island-arc setting (Ruzhentsev and Pospelov, 1992; Lamb and Badarch, 2001).

According to Ruzhentsev and others (1991) the oldest rocks of this domain are found in the Dzolen Subzone (fig. 2). Numerous strongly serpentinized peridotite fragments are exposed here, locally accompanied by gabbro, pillow lava and associated basaltic tuff. Beds of radiolarian jaspilite of Silurian–early Devonian age, sponges as well as quartz-hematite rocks are common (Zonenshain and others, 1975; Ruzhentsev and others, 1985). These fragments of oceanic lithosphere were interpreted to mark the eastern termination of the Dzolen "terrane" (Badarch and others, 2002). Helo and others (2006) showed that the Devonian volcanic rocks from the Dzolen range are of intermediate, calc-alkaline composition, consistent with formation in a juvenile intra-oceanic arc SHRIMP zircon-dated at 421.0 ± 3.0 Ma and 417 ± 2.2 Ma (fig. 3C). The Devonian sequence is overlain unconformably by early Carboniferous basalt, andesitic basalt, and andesite as well as corresponding tuff, tuffaceous sandstone and siltstone, and tuffaceous conglomerate.

South Gobi Zone

The South Gobi Zone (Ruzhentsev and others, 1985) or Atasbogd "terrane" (Badarch and others, 2002) occupies the southernmost part of the CAOB in Mongolia and is separated from the northern part of the Trans-Altai Gobi by the E-W striking Gobi-Tienshan Fault Zone (fig. 2).

The oldest rocks belong to the Tömörtyn Formation (Sinitsyn, 1956; Markova, 1975), presumed to be of Ordovician to Silurian age. This sequence consists of siliceous clastic rocks, sandstone, gritstone and conglomerate with coarse-grained sediments overlain by metamorphic rocks consisting of amphibolite, amphibolitic schist, and gray-green chlorite and sericite-chlorite schists. Zircons from a mylonitized volcanic rock of this sequence were dated by Kröner and others (2010) at 399.1 ± 1.1 Ma, using the Pb-Pb evaporation method (fig. 3C). The overlying early Devonian consists mainly of volcanic, volcano-sedimentary and sedimentary rocks with lenses and

beds of limestone and quartzite, followed by coarse-grained graywacke and middle Devonian slaty mudstone, metamorphosed sandstone and calc-silicate rocks. All these early Paleozoic rocks are unconformably overlain by early and middle Carboniferous basal conglomerate, tuffaceous sandstone and mudstone and volcanic rocks of basaltic, andesitic, dacitic and rhyolitic composition. The late Carboniferous sequences consist of tholeiitic basalt flows and hyaloclastites, followed by clastic sediments containing sandstone and biogenic limestone.

The lowest structural unit is the E-W trending Gobi-Tienshan magmatic complex, located in the west and covering an area of about 3000 km^2. The structure of the Gobi-Tienshan intrusive complex (GTIC) is made up of high-grade metamorphic rocks at the base, mafic intrusives in the lower part of the magma chamber, a granodioritic core and a hypabyssal granophyric granite that intrudes weakly metamorphosed Devonian and Carboniferous sediments at the top. This sequence indicates that the depth of exposure in this huge magmatic complex increases progressively towards the NW (Kröner and others, 2010). A late Carboniferous age of emplacement was determined for a granodiorite (TIMS zircon age of 302 ± 3 Ma, Yarmolyuk and others, 2008, SHRIMP zircon age of 299.9 ± 1.6 Ma, Kröner and others, 2010) (fig. 3C). The age of partial melting of migmatitic orthogneisses was inferred from the presence of hornblende- and plagioclase-rich leucosomes in gneisses dated using the zircon evaporation method at 301.4 ± 1.2 Ma (fig. 3C). An orthogneiss xenolith stoped in the main granodiorite also reveals a late Carboniferous SHRIMP zircon age of 301.1 ± 1.6 Ma but also contain xenocrystic zircons dated at 345, 493 and 886 Ma, suggesting the presence of Precambrian crust at depth, thermally rejuvenated in early Palezoic times (fig. 3C).

TECTONIC EVOLUTION

Structural investigations were carried out along four cross-sections with the aim to provide a full inventory of deformation fabrics in terms of their orientation, intensity and kinematics, mechanics of structures and relative timing of their evolution. A structural pattern is provided in a series of structural maps and cross-sections. The structural evolution is presented for each of the four lithotectonic zones, and subsequently the fabric sequences are correlated according to their relative geometry and timescale compatibilities.

Structural Evolution of the Lake Zone

The southern part of the Lake Zone provides continuous exposures studied along a 50 × 10 km wide area bounded in the south by the Main Mongolian Lineament (fig. 4). The rock assemblages show contrasting structural patterns in the Zamtyn Complex (ZC), the Eclogitic Complex (EC), the Khantaishir formation, the newly identified early Carboniferous flyschoid sediments (Kröner and others, 2010), and the Permian granite and volcaniclastic sequences.

The high-grade rocks of the Zamtyn Complex (ZC) show a polyphase structural evolution. The earliest amphibolite-facies fabric S_{1Z} of variable attitude is locally preserved as a metamorphic gneissosity in orthogneisses. This earliest structure was almost pervasively reworked by a ubiquitous S_{2Z} metamorphic foliation that is defined by a compositional layering characterized by an alternation of mafic and felsic layers in banded amphibolites, a metamorphic gneissosity in granitoid gneisses and metagabbros, and a continuous schistosity in metapelites and marbles. In the diorites and gabbros, the D_{2Z} event is recorded in a magmatic to high-grade solid state fabric. Melt-bearing shear zones as well as quartzo-feldspathic melt-filled boudin necks indicate that melting occurred during D_{2Z}. S_{2Z} dips gently to the SSW in the north and shows a steep attitude in the southern part of the section. The associated mineral and stretching lineations form a broad maximum around a WSW-ENE direction (fig. 4).

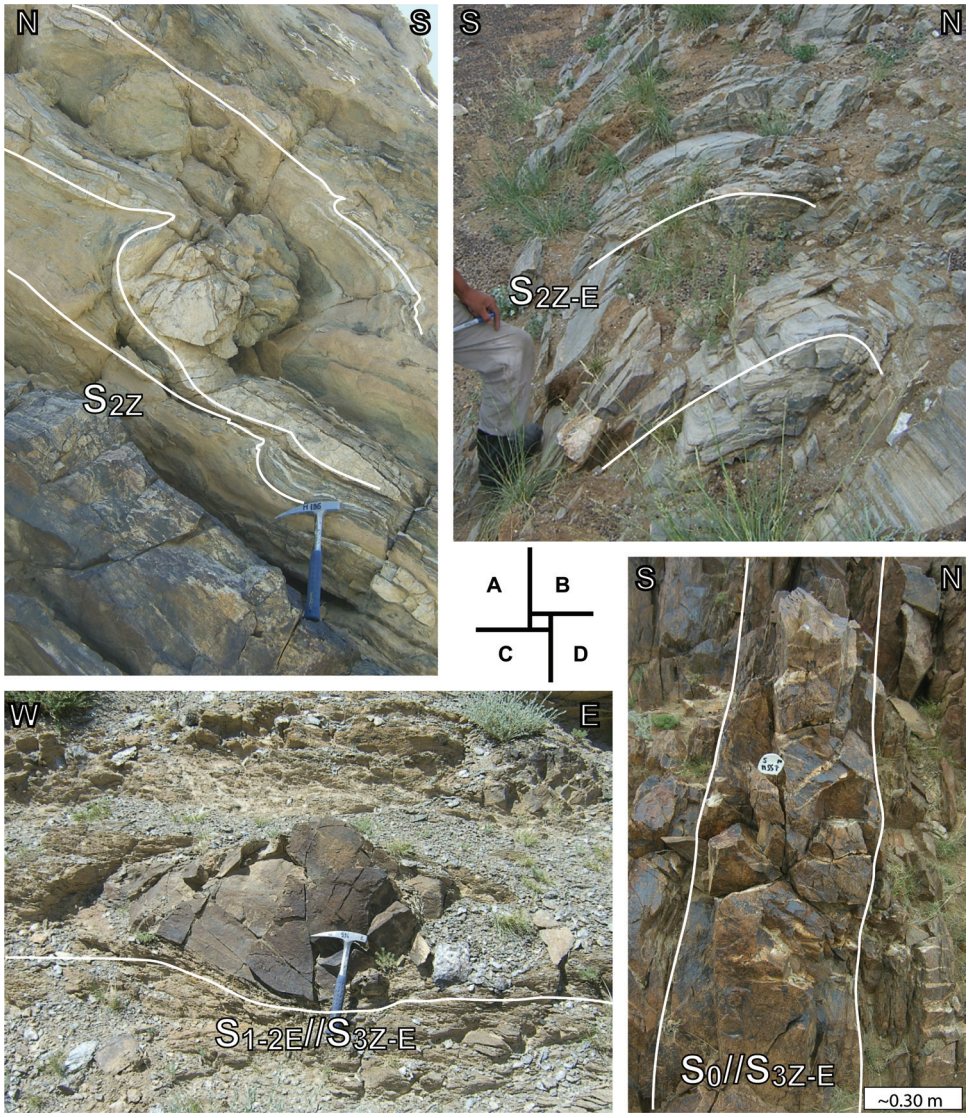

Fig. 5. Field photographs showing structural features along the geological cross-section in the Lake Zone. (A) F_{2Z} non-cylindrical fold in marbles of the Zamtyn basement complex associated with top-to-the SW shearing, vertical view. (B) $F_{3Z\text{-}E}$ buckle fold in paragneisses of the Zamtyn basement complex with steep E-W striking axial plane associated to $D_{3Z\text{-}E}$ N-S shortening event. (C) $S_{1\text{-}2E}$ compositional banding of interlayered marbles and metapelites deflected around an eclogitic boudin in the core of the Eclogitic Complex, vertical view. Note that orientation of the fabric indicates rotation of structures during N-S shortening event $D_{3Z\text{-}E}$. (D) Steep E-W striking beds of late Permian volcaniclastic rocks verticalized during $D_{3Z\text{-}E}$ N-S shortening, vertical view.

Numerous kinematic criteria such as bookshelf feldspar phenocrysts as well as sigma and delta feldspar porphyroclasts in highly deformed orthogneisses and south-verging asymmetrical folds in marbles (fig. 5A) indicate top-to-the SW shearing parallel to the direction of the regional-scale L_{2Z} lineation. This dominant S_{2Z} fabric was rotated by open to tight, meter-scale upright F_{3Z} folds (fig. 5B) associated with a locally developed chlorite-bearing steep E-W striking S_{3Z} cleavage.

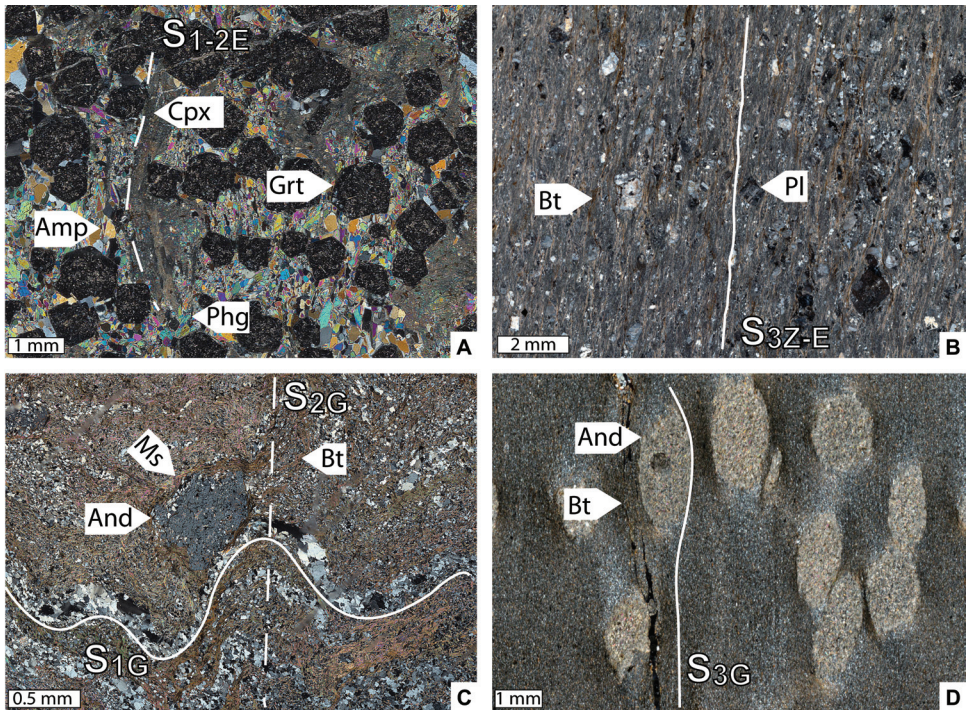

Fig. 6. Photomicrographs of microstructures and distinct deformation-mineral growth relationships. (A) Typical eclogitic assemblage in the eclogites. Štípská and others (2010) dated two phengites from this sample yielding a $^{40}Ar/^{39}Ar$ plateau age of 543.1 ± 3.9 Ma and a mean age of 547.9 ± 2.6 Ma. (B) Early Permian (Hanžl and Aichler, 2007) or late Permian (Rauzer and others, 1987) volcaniclastic rock deformed by a pervasive, steeply dipping, E-W striking micaceous cleavage. (C) Pre- to syntectonic (with respect to D_{2G}) andalusite porphyroblast in quartzitic metapelite of the Tugrig formation on the southern margin of the CCC. A white mica from this rock yielded a $^{40}Ar/^{39}Ar$ plateau age of 365 ± 18 Ma (sample M102-06-3, fig. 15C). (D) Andalusite porphyroblast (pretectonic with respect to D_{2G}) in early Devonian shale with S_{3G} foliation deflected around the porphyroblast. Mineral abbreviations are after Kretz (1983).

The Eclogitic Complex reveals an early S_{1E} fabric that is preserved in isoclinally folded marbles, as inclusion trails in large garnet porphyroblasts discordant to an external fabric in metapelites, or as a clinopyroxene banding in the eclogites (fig. 6A). The subsequent high-grade S_{2E} fabric is characterized by a mylonitic layering S_{2E} in marbles associated with isoclinal folding of relict S_{1E} surfaces, continuous foliation in coarse-grained metapelites, and ductile shear zones in the eclogites which are locally preserved as boudins (fig. 5C). At many sites, this second fabric strikes N-S and gently dips either west or east. This composite fabric is folded into large-scale tight to isoclinal disharmonic folds associated with a vertical E-W striking greenschist-facies S_{3E} axial planar cleavage. Mutual structural relationships between the EC and the southern high-grade ZC reveal that the latter unit occurs in the hanging wall of the EC in the south and in the footwall in the north (fig. 7). The S_{2Z} in the migmatites and orthogneisses is more or less geometrically concordant with the composite folded S_{1-2E} fabric, suggesting that they were deformed together during the D_{3Z-E} shortening event.

The Khantaishir formation, Carboniferous flyschoid sediments and Permian sequences reveal a simple structural evolution. The most intense deformation was observed at the contact with the ophiolite fragments on the southern slope of the Erdene Mountain, which were thrust upon pyroclastic rocks and metabasalts. As a result, this thrusting developed a zone of intense greenschist-facies deformation

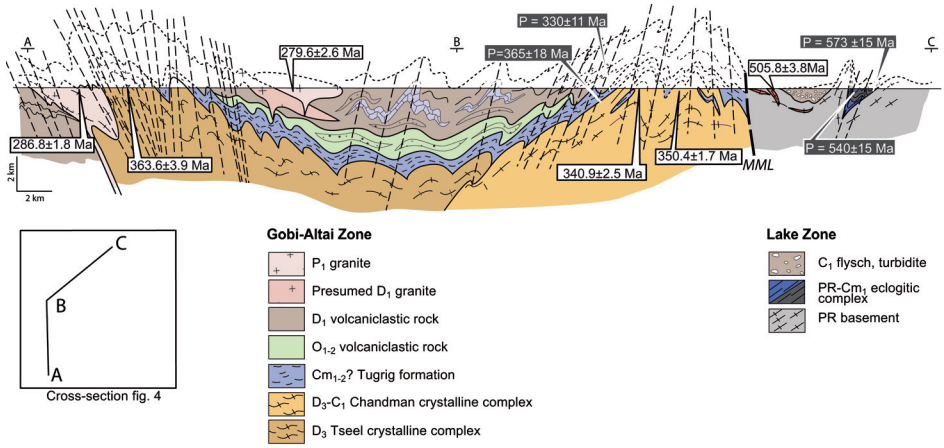

Fig. 7. Interpretative cross-section at the junction of the Lake and Gobi-Altai Zones showing the main structural features as described in the text. White boxes represent zircon ages of Kröner and others (2010), gray boxes represent $^{40}Ar/^{39}Ar$ ages of this study.

marked by strong elongation of lapilli and the development of a mylonitic south-dipping banding. A small (4 × 2 km) Carboniferous molasse sequence (Kröner and others, 2010) is resting on rocks of the Zamtyn Complex and the Khantaishir formation. The bedding is folded and defines a NNE-SSW oriented girddle on the stereogram (fig. 4), interpreted as the result of late NNE-SSW shortening. The axial plane of the fold is geometrically compatible with the cleavage of the Khantaishir formation, the S_{3E} and the S_{3Z} fabrics. Presumed Permian leucocratic granites were also affected by this deformation as exemplified by hinterland-dipping duplexes with northward motion as well as Permian vertically dipping volcaniclastic beds (Štípská and others, 2010) (fig. 5D) affected by intense greenschist-facies and E-W striking and steeply dipping cleavage (fig. 6B).

Structural Evolution of the Gobi-Altai Zone

The area located between the Main Mongolian Lineament and the Trans-Altai Fault (40 × 100 km) exposes a N-S alternation of two granitic and migmatitic domes with a large E-W oriented belt of low-grade Paleozoic sediments and volcanic rocks between Chandman and Erdene villages. The southern high-grade dome corresponds to the "Tseel terrane" of Badarch and others (2002) and continues for 100 km in an ESE direction towards Shine Jinst village. This area enabled us to investigate the structural relationships between a deep arc and shallow crustal sequences (fig. 4).

Deformation of the Chandman Crystalline Complex and its cover.—The Tugrig Formation reveals a penetrative sub-horizontal S_{1G} schistosity that developed during vertical shortening (fig. 8A). This foliation is marked by a syntectonic assemblage of sillimanite, garnet and biotite developed close to the contact with the magmatic rocks. Microstructural analysis of andalusite-bearing schists south of the CCC confirmed that the earliest S_{1G} metamorphic fabric is overgrown by syntectonic andalusite porphyroblasts, indicating the existence of a pre- to syn-D_{2G} high-temperature event (fig. 6C). The second fabric S_{2G} is represented by a steep N-S striking greenschist-facies crenulation cleavage D_{2G} (figs. 8A and 9A) that grades into a migmatitic foliation towards the core of the CCC.

The CCC granitoids are surrounded by a 100 m wide zone of granitoid sills intruding the Tugrig Formation rim that decrease in thickness and density away from

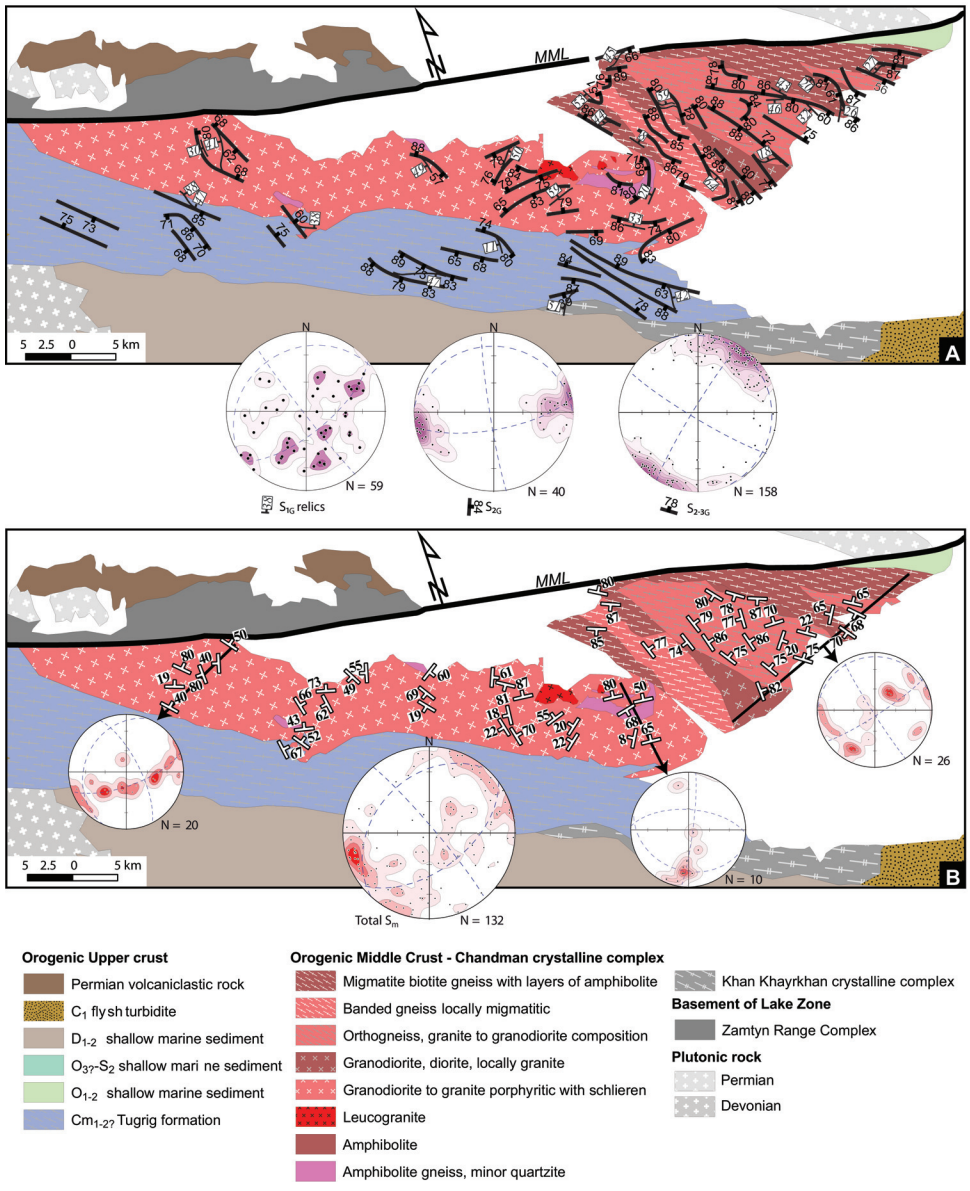

Fig. 8. Detailed structural map of the Chandman crystalline complex in the northern Gobi-Altai Zone. Lithotectonic units are based on Rauzer and others (1987), Hanžl and Aichler (2007), Hrdličková and others (2008) and our own observations. Average orientations on the map and on pole stereograms of (A) S_{1G} and S_{2G} and S_{2-3G} metamorphic foliations; (B) the magmatic foliation S_m.

the pluton. Rare fish-hook F_{2G} folds (fig. 9C) suggest that sills emplaced parallel to the S_{1G} schistosity were solidified and boudinaged during D_{1G} and subsequently folded during D_{2G}. Nevertheless, the bulk of the magmatic sills intruded parallel to the S_{2G} anisotropy (fig. 9B) and exposes either a magmatic fabric defined by hornblende and/or biotite alignment or a solid state foliation characterized by ductile deformation of quartz and feldspars. The core of the granodiorite-granite suite shows a rare,

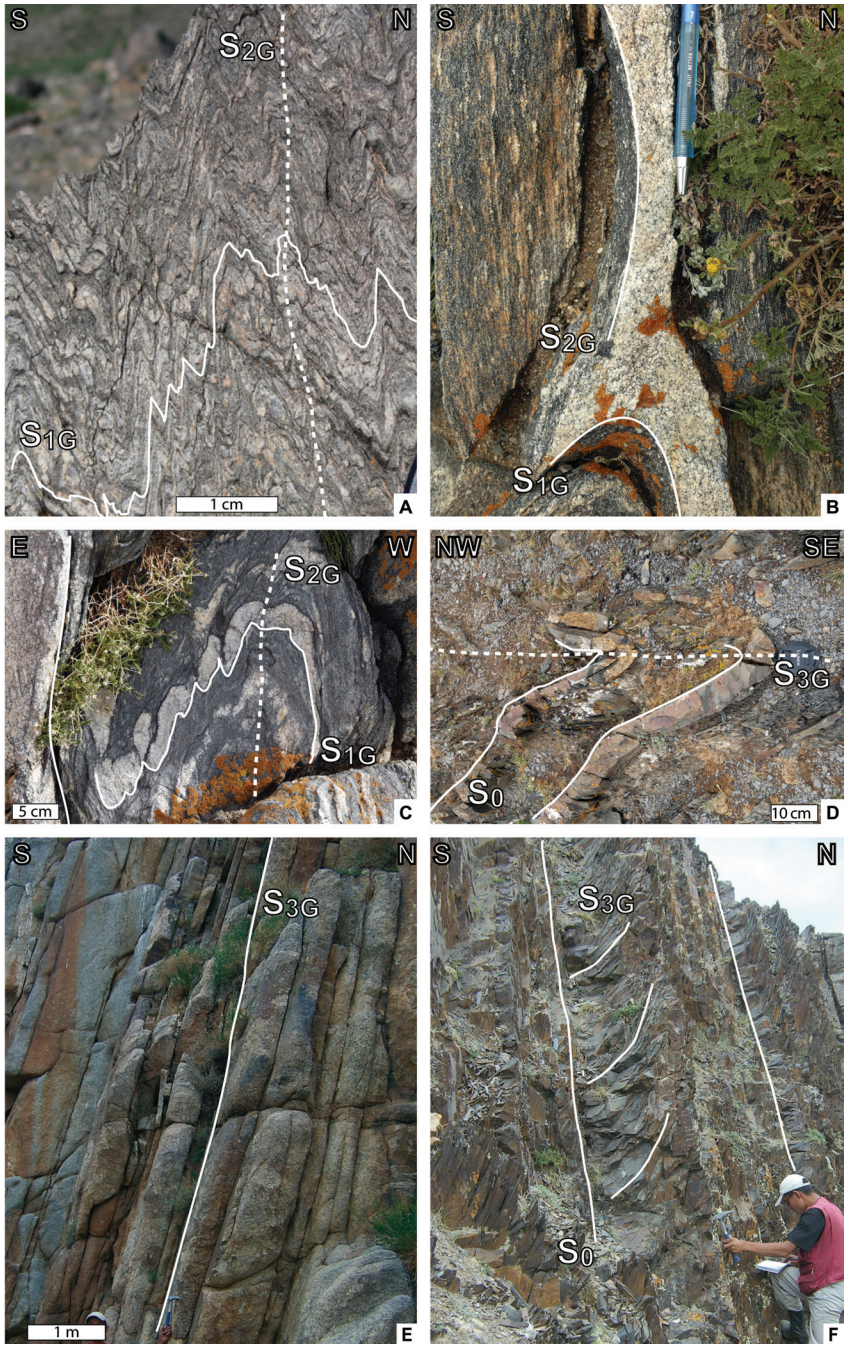

Fig. 9. Field photographs showing the main structural features along the geological cross-section in the Gobi-Altai Zone. (A) S_{1G} compositional banding in quartzitic metapelites of the Tugrig Formation, affected by a steeply dipping, E-W striking crenulation cleavage S_{2G}, vertical view. A white mica from this rock yielded a $^{40}Ar/^{39}Ar$ plateau age of 365 ± 18 Ma (sample M102-06-3, fig. 15C). (B) Felsic magma preferentially collected in the hinge of a F_{2G} fold and in the axial planar cleavage S_{2G}, inclined view. Thicker vein in the hinge region than in the limbs of the F_{2G}-fold suggests syn-D_{2G} magma migration. (C) Folded pinch-and-swell felsic sill, suggesting that the vertical shortening event D_{1G} was still active during the emplacement of this magmatic feature, vertical view. (D) Map view of an early Devonian sandstone/siltstone multilayer folded during the D_{3G} NNE-SSW shortening

flat-lying magmatic foliation marked by the orientation of restitic schlieren and stoped blocks of the Tugrig schists (fig. 8B). Nevertheless, the main fabric in granites and granodiorites is a steep magmatic to solid-state foliation compatible with the S_{2G} fabric of the host rocks and the magmatic sill-bearing rim. These observations suggest that the CCC granitoids were mainly emplaced during intense E-W horizontal shortening and experienced considerable D_{2G} cooling and syntectonic solidification.

Bedding planes in the overlying Ordovician to Carboniferous low-grade rocks located between these two high-grade complexes were also deformed during D_{2G}. This deformation event is deduced from the attitude of steep F_{3G} fold hinges (fig. 9D) and calculated intersection lineations L_{3G} between S_0 and S_{3G}, revealing variable angles of plunge from very steep to subhorizontal (fig. 4). The steep hinges of F_{3G} folds must originate from folding of steeply inclined bedding planes that were rotated into a vertical position by the D_{2G} event.

The entire area was affected by a steep WNW-ESE to E-W striking cleavage associated with intense D_{3G} N-S to NNE-SSW horizontal shortening. The contrasting record of this deformation event in different geological units was controlled by the competence of the deformed material. In rocks of the CCC, D_{3G} is developed as meter-scale asymmetrical F_3 folds with steep fold axes. Long limbs of F_{3G} folds trend NW-SE to E-W, sub-parallel to the associated spaced cleavage S_{3G} (fig. 9E). This suggests that S_{2G} was rotated by large F_{3G} folds reaching hundred meters to even kilometers in wave length (figs. 4 and 8A). Similarly, rocks of the Tugrig formation show heterogeneous D_{3G} deformation, mostly expressed by the rotation of S_{2G} planes towards the S_{3G} striking direction, meter-scale open to close F_{3G} folding of the S_{2G} fabric and development of a discontinuous S_{3G} cleavage. F_{3G} folding thus operated on all scales from cm to km and was responsible for the current shape of the Chandman gneiss antiform and steep WNW-ESE attitude of the Tugrig formation along the southern border of the Chandman crystalline complex.

Deformation of the Southern Tract of the Gobi-Altai Zone.—A similar structural evolution is also preserved in gneisses of the high-grade crustal exposure south of Erdene village (fig. 4). Here, a rarely preserved flat S_{1G} compositional banding is marked by hornblende-rich layers of tonalitic gneiss preserved in meter-scale hinges of F_{2G} folds. An associated pervasive axial plane S_{2G} foliation is steep and strikes NW-SE and developed at still high metamorphic grade. Paleozoic low-grade rocks located between the CCC and the southerly gneissic dome display a heterogeneously developed D_{3G} deformation marked by a high-strain zone adjacent to its southern margin (fig. 7). The D_{3G} deformation is generally characterized by the development of upright folds of variable scale (10 to 100 meters). The zones of intense deformation gave rise to a continuous to discontinuous slaty cleavage (fig. 9F) and associated pressure solution features. These rocks were intruded by a granite pluton of presumed Devonian age whose southern margin was reworked in E-W striking D_{3G} cataclastic zones. The metamorphic aureole of the pluton is marked by pre-tectonic andalusite porphyroblasts as manifested by attenuation of S_{3G} cleavage along their high-strain sides (fig. 6D). In contrast, the isotropic Permian leucogranite (dated at ~279 Ma) exhibits a passive-type of emplacement (fig. 5D in Kröner and others, 2010). Towards the south, S_{3G} cleavage intensity increases in a km-wide highly deformed zone constituting the northern limb of a large-scale synform (fig. 7). It decreases gradually towards the synform core that is marked by gentle dips of felsic volcanic beds dated as early

event. Note that the fold axis is vertical, suggesting that bedding was already steepened prior to the D_{3G} event. (E) Steep S_{3G} ESE-WSW striking spaced cleavage in a vertical cliff of granite-granodiorite of the Chandman crystalline complex. (F) Refracted S_{3G} cleavage in sandstone/siltstone multilayer either of early Carboniferous (Hanžl and Aichler, 2007) or early Devonian age (Rauzer and others, 1987).

Devonian (Demoux and others, 2009a). In the strongly reworked southern limb of the megafold, strongly sheared and retrogressed tonalitic gneiss as well as andalusite-bearing micaschist occur in cores of sub-vertical ENE-WSW striking cusps that are surrounded by extremely shortened and sheared siltstones and sandstones. Here, S_{3G} forms a N-S positive cleavage fan within the core of the crustal-scale dome hosting tonalitic gneiss. D_{3G} greenschist-facies mylonitization has entirely reworked the southern granophyric granite of Permian age (dated at ~287 Ma, Kröner and others, 2010).

Structures of the eastern termination of the "Tseel Terrane" and the Mandalovoo Subzone.—The high-grade gneiss north of Shine Jinst village reveals a well preserved early NW-SE striking migmatitic layering S_{2S}. This fabric is associated with isoclinal folds suggesting the existence of an early S_{1S} foliation (figs. 10A, 10B, 11A, 11B). The late and heterogeneous fabric S_{3S} is represented by north-dipping greenschist-facies shear zones that indicate south-directed ductile shearing (fig. 11C). Farther south, Permian volcaniclastic sedimentary beds and rhyolitic lava flows are buckled into large-scale upright folds associated with the development of a strong E-W striking S_{3S} axial plane cleavage. The folded trace of the bedding planes can be inferred from Landsat image analyses as observed by Badarch (ms, 1990) and Lamb and others (2008) (figs. 10A and 10B). This 15 km wide Permian basin is flanked, in the south, by a presumed Permian magmatic complex consisting of diorite, granite and granophyre with well preserved magmatic fabrics. The southern margin of this igneous unit is thrust over Devonian carbonates of the Mandalovoo Subzone along a several tens of meters wide zone of fault breccia. These limestones are folded by large, hundred meter-scale upright, buckle folds with E-W trending hinges. To the south, Ordovician sediments reveal a similar style of folding and the development of a strong E-W striking S_{3S} fracture cleavage (fig. 11D).

Structural Evolution of the Trans-Altai Zone

This large area includes tectonic imbrications of Devonian to early Carboniferous rocks and early Paleozoic ophiolites in the southern part of the study area, locally covered by Triassic continental sediments which exhibit polyphase folding.

Deformation partitioning between individual subzones.—Deformation of the Trans-Altai Zone mainly includes imbrications of early Carboniferous sediments and volcanic rocks, middle Devonian sandstones and slates and early Devonian lithologically variable volcano-sedimentary sequences, which exhibit variable intensities of folding and cleavage development. This area is divided into regions of low deformation intensity and high-strain domains close to major thrusts that delimitate the boundaries of the individual subzones.

The high strain zones are restricted to the boundaries between the Khuvinkharin and Edrengin Subzones and the Edrengin and Dzolen Subzones. These zones of intense deformation are developed in Devonian and, to some extent, also Carboniferous rocks that show their strongest folding and cleavage development close to three major thrust belts (figs. 12 and 13A) in which several hundred meters to one kilometer wide zones of intense cleavage are developed. The slaty cleavage is associated with ductile strain of pebbles, and often exhibits cleavage refraction between competent graywacke and incompetent slate beds. The orientation of steep cleavage planes along the entire transect is uniformly NW-SE to WNW-ESE (fig. 12, stereogram 1). The thrust zones are associated with the development of spectacular tension gashes filled with quartz that are systematically located in the footwall of major thrusts that is, mostly in the Carboniferous rocks. The poles to steep quartz-filled fractures are homogeneously oriented in the NNW-SSE direction, whereas the main cleavage is dipping SW at intermediate angles. These observations are consistent with a NE-SW oriented compression axis and high fluid pressure in the footwall rocks, associated with dewatering of over-pressurized fluid-rich sediments below thrust ramps. Locally, vertical NW-SE

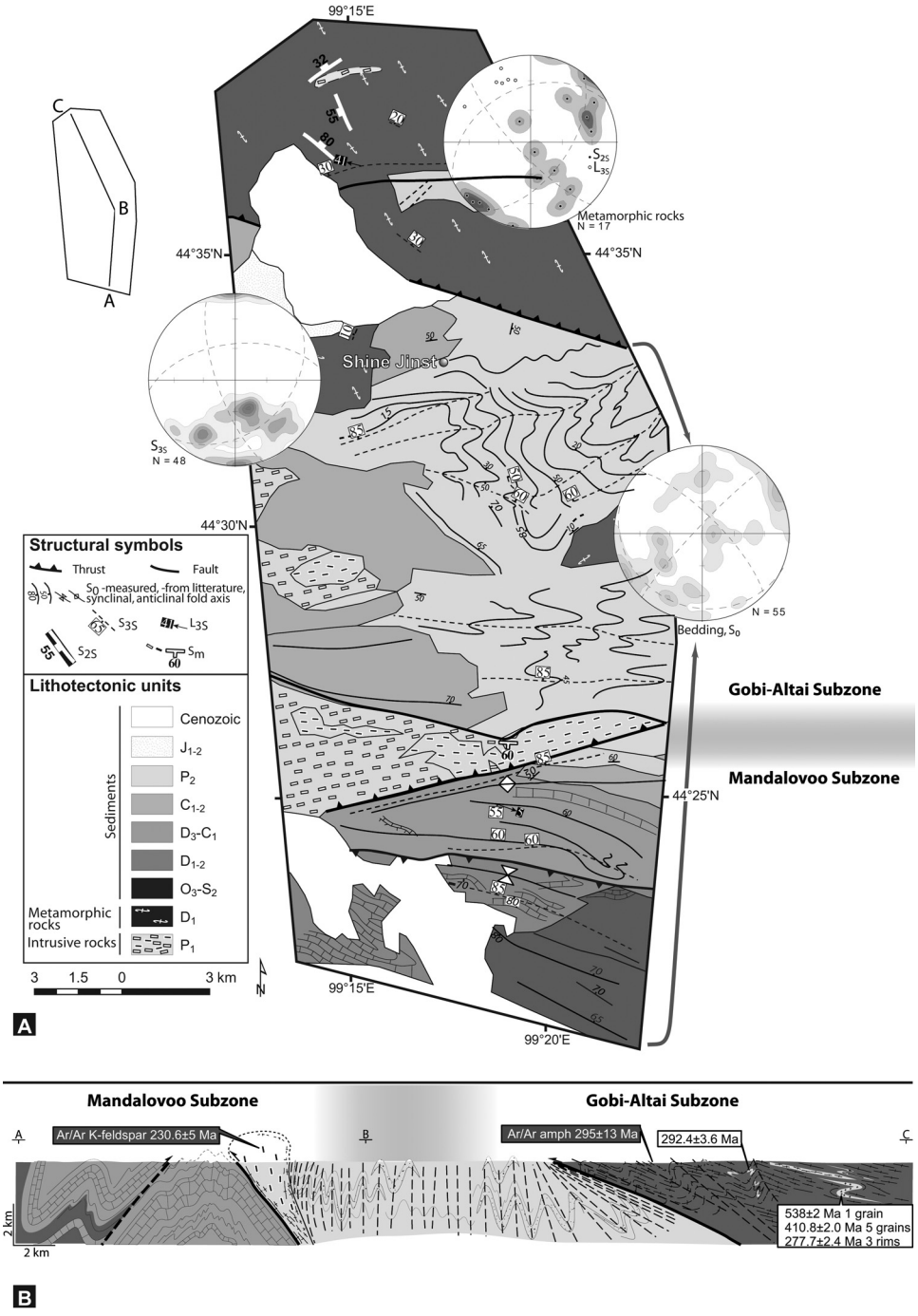

Fig. 10. (A) Structural map at the junction of the Gobi-Altai and Mandalovoo Subzones summarizing the superposition of the deformation fabrics. The structural trends indicate the extrapolation of the major orientations of the structural fabrics in the field. Stereograms represent average poles of folations and orientation of lineations in equal area lower hemisphere projection. The strike of bedding planes is based on interpretation of landsat imagery and Badarch (ms, 1990). (B) Interpretative cross-section at the junction of the Gobi-Altai and Mandalovoo Subzones showing the main structural features described in the text. White boxes represent the zircon ages of Kröner and others (2010) and the gray boxes the $^{40}Ar/^{39}Ar$ ages of Lamb and others (2008).

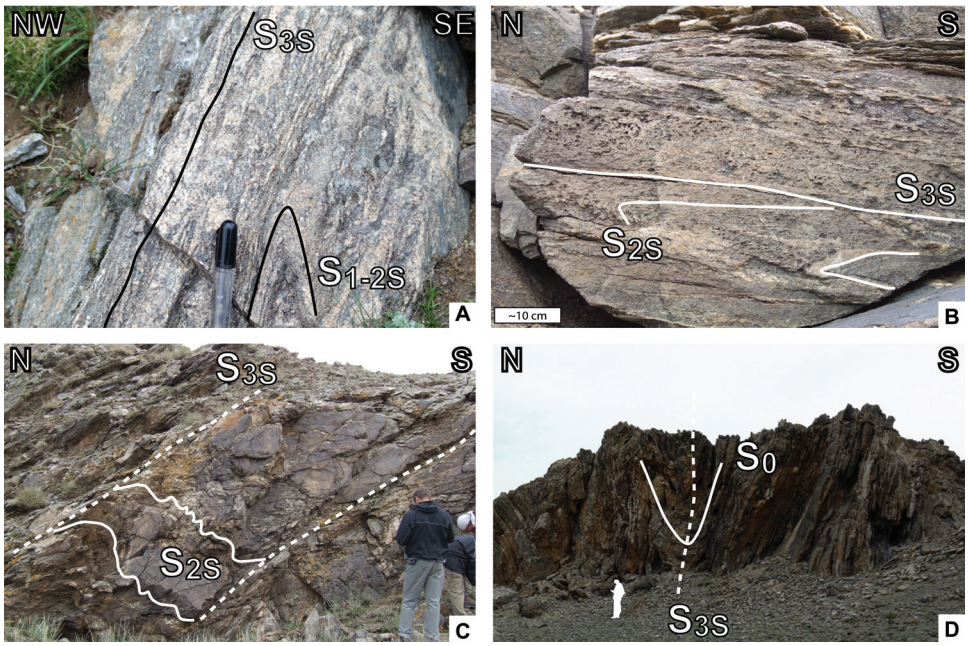

Fig. 11. Field photographs showing structural features at the junction of the Gobi-Altai (A, B, C) and Mandalovoo Subzones (D). (A) Syn-F_{2S} folding in migmatitic gneiss of early Devonian protolith age (zircon age at 410.8 ± 2.0 Ma with rims at 277.7 ± 2.4 Ma, Kröner and others, 2010). (B) Rotated migmatitic S_{2S} fabric during D_{3S}, vertical face. (C) S_{2S} fabric preserved in short limbs of meter-scale assymetric F_{3S} folds. (D) Folded early Devonian carbonates during D_{3S} shortening event.

striking zones are associated with intense refolding of cleavage by strongly non-cylindrical sheath folds. The folded veins are cross-cut by newly formed E-W striking quartz gashes indicating dextral kinematics along these mainly simple shear zones.

The low strain zones occupy most of central parts of the Khuvinkharin and Edrengin Subzones and also part of the Dzolen Subzone. The structural pattern is simple and is represented by folded bedding (fig. 12, stereograms 2, 3 and 4) accompanied by a NW-SE striking heterogeneously developed and steep slaty S_{3T} cleavage. On the geological map, alternations of the Devonian and Carboniferous sequences indicate large-scale folds with open to closed antiforms and synforms and minor thrusts to the NW. A large low strain area of Carboniferous and Devonian sediments reveals relicts of early folding F_{2T}. These meter- to hundred meter-scale open to buckle folds with steep axial planes were recognized through mapping of the orientation of S_0 beds. Stereograms from these low-strain domains show a distribution of poles to sedimentary beds which form a great circle oriented in a NNE-SSW direction (fig. 12, stereograms 2, 3 and 4). However, the poles to S_0 are highly irregular and are parallel to the vertical NNE-SSW striking cleavage planes in the north (fig. 12, stereogram 2), whereas in the center of the basin, S_0 predominantly dips to the NW or ESE at steep to intermediate angles (fig. 12, stereogram 3), and in the south these planes dip to the ESE at intermediate angles (fig. 12, stereogram 4). This irregular distribution of gently folded sedimentary strata is of considerable significance and indicates that the entire area was already gently folded prior to the development of D_{3T} thrusting and folding. The reconstruction of bedding prior to D_{3T} shows that S_0 was dipping mostly to the SE or NW, which indicates a phase of early open folding during a D_{2T} NW-SE oriented compression.

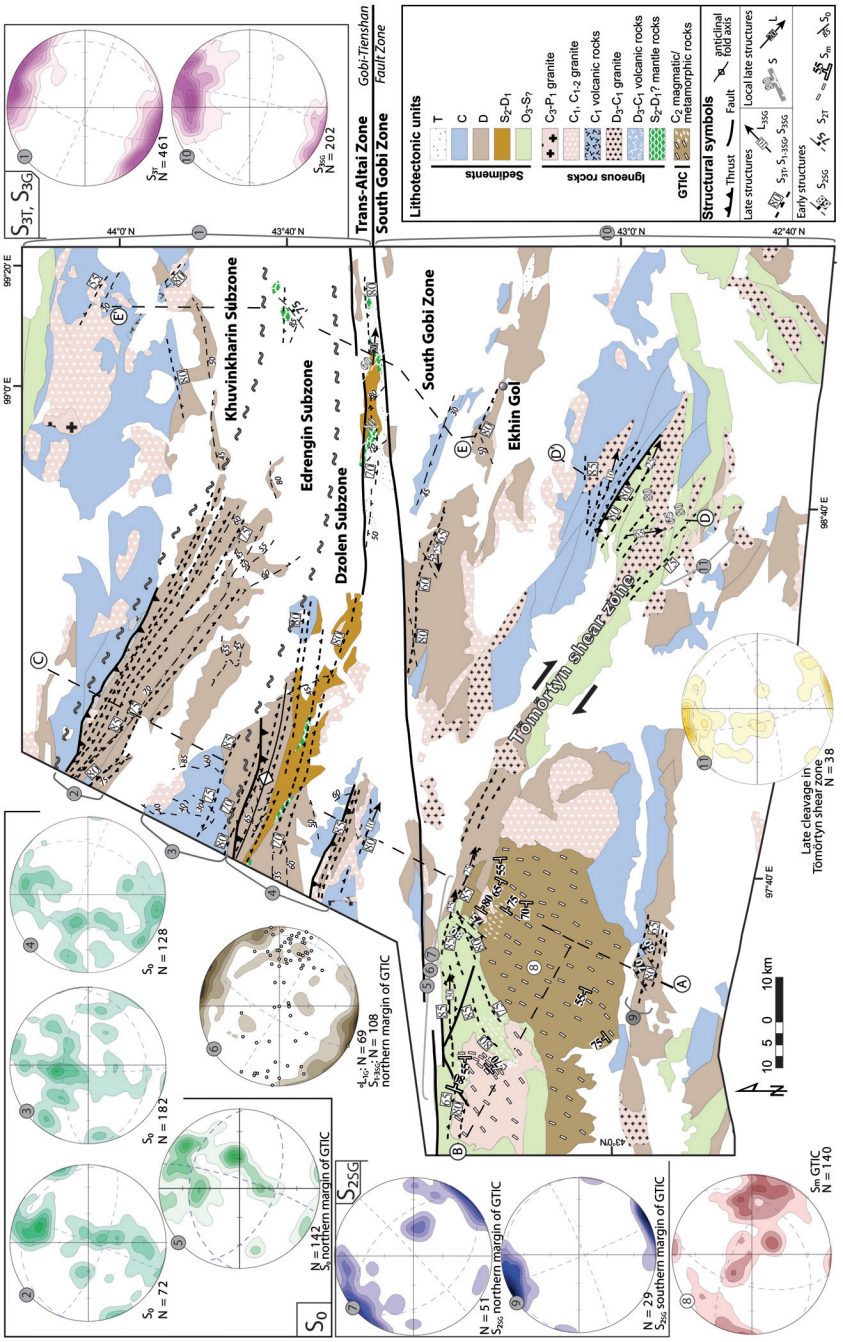

Fig. 12. Structural map of the Trans-Altai and South Gobi Zones. Structural trends indicate extrapolations of major orientations of structural fabrics in the field. Stereograms represent average poles of foliations and orientation of lineations in equal area lower hemisphere projection. Location of geological profiles and block diagram of figure 9 are indicated.

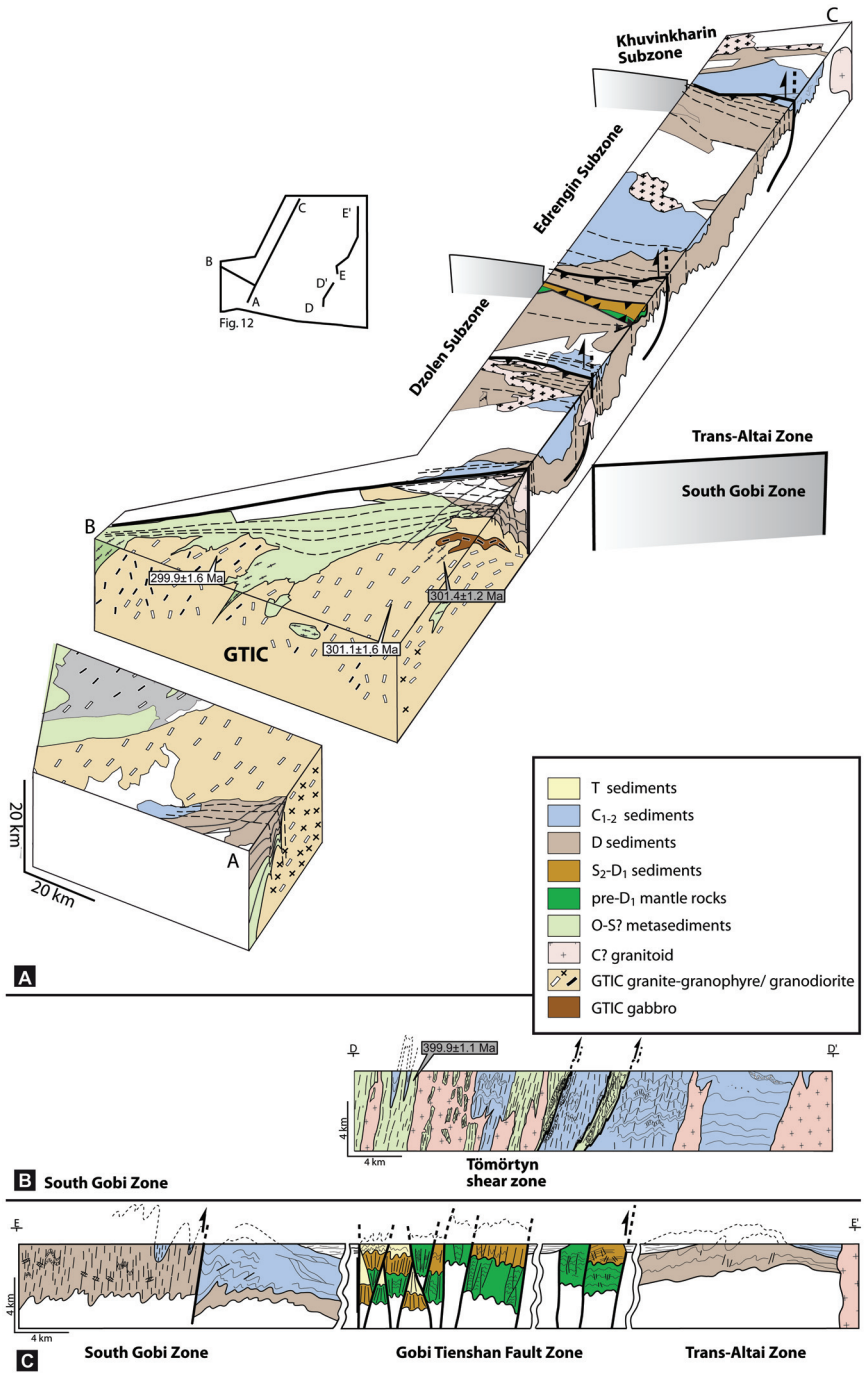

Fig. 13. (A) Block diagram summarizing the main structural features of the South Gobi Zone and the Dzolen, Edrengin and Khuvinkharin Subzones. (B) Interpretative cross-section of main structural features along the Tömörtyn shear zone in the South Gobi Zone. (C) Interpretative cross-section of the main structural features in the Trans-Altai Zone. White and gray boxes represent respectively the SHRIMP zircon and Pb-Pb zircon evaporation ages of Kröner and others (2010).

Deformation of ophiolite fragments of the Dzolen Subzone.—Inside the Devonian-Carboniferous sequence of the Dzolen Subzone occur a few ophiolitic fragments together with deep marine sediments of early Devonian age (see review of Kröner and others, 2010) thrust over late Devonian sequences which do not exhibit signs of the later D_{3T} reworking and metamorphism (Zonenshain and others, 1975; Ruzhentsev and Pospelov, 1992). The 3D model of the area shows that these ophiolitic fragments are surrounded by Devonian rocks in the south and north, indicating that they appear in the core of a large-scale synformal structure (fig. 13A). South of the ophiolite fragments the Devonian and Carboniferous rocks are severely imbricated and folded into large-scale upright folds with NW-SE trending hinges, indicating that the ophiolitic rocks were exhumed prior to the main phase of D_{3T} folding and, during this phase, already acted as rigid obstacles. On the other hand, numerous serpentinite and peridotite fragments occur along zones of intense D_{3T} cleavage development, indicating that these zones were exhumed as weak cusps during the main D_{3T} shortening event. These cuspate structures show a polyphase tectonic evolution marked by numerous superposed cleavage patterns in extremely weak serpentinites.

One of the rare ophiolite fragments of the Dzolen range shows a complete structural sequence (figs. 12 and 13A). Serpentinite and ultrabasic rocks are overlain by deep marine early Devonian sediments with flat bedding affected by a greenschist-facies metamorphic foliation S_{1T} which is also seen in associated gabbroic rocks. The dominant sub-horizontal S_{1T} fabric of the ophiolite is folded by open, kilometer-scale F_{3T} folds that are represented in map view by an alternation of parallel belts of ultramafic rocks and sediments. The serpentinites reveal a superposed cleavage pattern with relic S_{2T} and a dominantly steep, generally E-W striking S_{3T} crenulation cleavage. The tectonically underlying Carboniferous and Devonian sequences show a similar style of F_{3T} folding as the hanging wall ophiolitic rocks (fig. 13A). Even if the thrust plane of ophiolites is not detectable in the field we deduce that the serpentinite mélange and associated rocks with D_{1T} fabric were thrust over the Devonian rocks along a shallow dipping thrust. Thus, the pre-D_{3T} structural disposition of the early Devonian ophiolite fragments sitting above a Devonian-Carboniferous sedimentary sequence represents a unique argument for D_{2T} thrust tectonics in this area.

Structure of Triassic sediments and ophiolite fragments along the Gobi-Tienshan Fault Zone.—The Gobi-Tienshan Fault Zone (Tapponnier and Molnar, 1979) affected Triassic continental clastic sediments and partially affected early Devonian fragments of ophiolites; and produced a hundred meters thick zone of cataclasites, fault breccia and cohesionless gauges (figs. 12 and 13C). The Triassic rocks close to the fault zone exhibit polyphase folding: the earliest folding with steep fold axes was associated with N-S compression characterized by large (10-100 m wavelength) open to tight folds with steeply dipping and E-W striking axial planes. Locally, a fracture cleavage is developed in the hinge zones of most tight folds. These folds were non-coaxially refolded by open folds with steep NW-SE striking axial planes. North of the Triassic sediments, but still inside the Gobi-Tienshan Fault Zone, occur dismembered ophiolites of presumed early Devonian age and composed essentially of serpentinite, altered basalt, sheared ophicalcite and deep marine sediments. The earliest structural element of this ophiolitic sequence is a sub-horizontal greenschist-facies metamorphic fabric S_{1T} affecting sheared ophicalcites that are characterized by dynamic recrystallization of calcite and quartz. In contrast, the serpentinites and deep marine sediments exhibit multiple folding and the development of several cleavage systems from which the most important is an E-W S_{3T} striking crenulation cleavage.

Structural Geology of the South Gobi Zone

The western part of this zone is represented by the huge late Carboniferous Gobi-Tienshan intrusive Complex (GTIC) which is surrounded by metavolcano-

sedimentary host rocks of the Ordovician-Silurian Tömörtyn group in the north and presumed Devonian to Carboniferous volcaniclastic rocks to the south (figs. 12 and 13).

Structural evolution of the Tömörtyn shear zone.—The general structural pattern is shown in two areas, east and north of the Gobi-Tienshan pluton (figs. 12, 13B and 13C). In the east, the structural fabric in the early Paleozoic rocks is characterized by a greenschist-facies schistosity S_{1SG} affecting Ordovician metasediments and Devonian metarhyolites (~400 Ma, Kröner and others, 2010) that were converted into greenschist-facies ultramylonites. The mylonitic fabric dips steeply to the south (fig. 12, stereogram 10) and bears a horizontal mineral stretching lineation. The metarhyolites are locally folded and imbricated together with early Carboniferous conglomerate, metagraywacke and quartzite (fig. 13B). The Carboniferous beds are folded into tight to isoclinal vertical folds up to 100 m in wavelength and associated with the development of an axial cleavage and intense flattening of pebbles and volcanic clasts. In the central part of the section, the mylonitic metarhyolites were intruded by pink, supposedly Carboniferous granites (Yarmolyuk and Tikhonov, 1982) of the eastern extremity of the Gobi-Tienshan Intrusive Complex (GTIC). The granite is isotropic, contains numerous metarhyolite xenoliths (fig. 13B) and intruded parallel to the vertical foliation of the host rocks. These field observations are of first order importance and suggest that the major granite emplacement mechanism was a passive invasion of magma along the main anisotropy surfaces represented by the S_{1SG} metamorphic foliation. As the GTIC show strong magmatic fabrics in the west, the deformation related to pluton emplacement is labeled D_{2SG}.

Farther north, the boundary between the early Paleozoic Tömörtyn group and the early Carboniferous volcano-sedimentary sequence is marked by a several kilometers wide zone of intense ductile deformation which is manifested by a WNW-ESE striking steep mylonitic foliation and a horizontal stretching lineation associated with dextral shearing. This shearing occurred during lower greenschist-facies conditions as shown by dynamic recrystallization of quartz and recrystallization of biotite on mylonitic surfaces. The Carboniferous sediments display a strong E-W striking slaty cleavage and tight folding. The difference in metamorphic grade between the Tömörtyn zone mylonites in the hanging wall and very low-grade rocks of the Carboniferous sequence in the footwall indicates thrusting of early Paleozoic sequences over the Carboniferous rocks. Both the Tömörtyn D_{1SG} mylonites and the strongly deformed Carboniferous rocks were affected by a post-metamorphic late cleavage which dips steeply to the SSE (fig. 12, stereogram 11) and by folds plunging at low angles relative to the main mylonitic fabric. The orientation of this late cleavage and the non-cylindrical character of superposed folds reveal the dextral transpressive character of deformation. Towards the north, the intensity of deformation decreases so that the volcanic layering and sedimentary bedding in the Carboniferous rocks were only weakly folded in conjunction with the development of a faint fracture cleavage. A similar situation exists in the Ekhin Gol area where greenschist-facies Devonian sediments were thrust over Carboniferous rocks (fig. 13C).

The Tömörtyn zone continues to the NW and is exposed in several valleys north of the Gobi-Tienshan pluton (figs. 12 and 13A). Presumed Ordovician and paleontologically dated Silurian, Devonian and Carboniferous sediments were subjected to low- to very low-grade metamorphism and D_{1SG} deformation that is marked by tight to isoclinal folding of S_0 bedding surfaces. The existence of early F_{1SG} folds is also evident from orientation mapping of Devonian beds, the poles of which form a NNE-SSW girdle in the stereonet (fig. 12, stereogram 5). As in the east, the D_{1SG} fabrics were reworked by a strong D_{3SG} steep cleavage zone striking WNW-ESE and associated with steep F_{3SG} folds that rotated the S_{1SG} foliation into a steep position. Here, the vertical

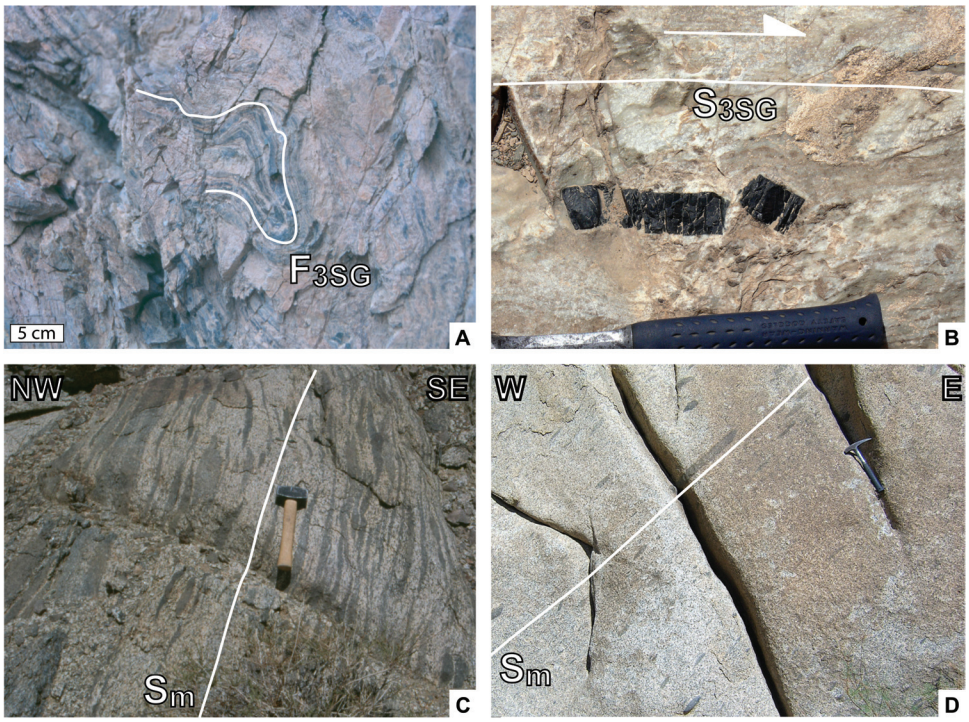

Fig. 14. (A) F_{3SG} sheath fold in mylonitized carbonate rock of the Tömörtyn shear zone in the NE part of the GTIC, vertical view. (B) Marble strongly mylonitized during D_{3SG} N-S shortening of the northern rim of the GTIC, map view. Domino boudins of mafic volcanic rocks indicate a dextral sense of shear, horizontal view. (C) Submagmatic shear zone related to NW-SE shortening D_{2SG} in granodiorite in the NE part of the GTIC, horizontal view. (D) Magmatic foliation (S_m) defined by strongly flattened microdioritic enclaves and related to the D_{2SG} ESE-WNW shortening event in granodiorite in the NW part of the GTIC, vertical view.

S_{1SG} foliation contains stretching lineations of variable plunge from sub-vertical to sub-horizontal (fig. 12, stereogram 6). F_{3SG} sheath folds occur in highly sheared marbles (fig. 14A) with sub-horizontally oriented noses and numerous dextral shear sense criteria (fig. 14B) parallel to a strong L_{1SG} stretching lineation.

Structural Geology of the Gobi-Tienshan Intrusive Complex.—The northern margin of the Gobi-Tienshan Intrusive Complex (GTIC) exhibits a metamorphic aureole marked by chloritoid-bearing spotted slates and hornfels which also coincides with a separate structural aureole. This margin of the pluton is composed of fine-grained granite-gneiss that exhibits features of near-solidus deformation of granite as lock-up shear bands (Ingram and Hutton, 1994) as well as irregular melt pockets developed along the S_{2SG} schistosity and marked by the preferred orientation of biotite and restitic schlieren. At some localities, stromatitic migmatites show isoclinal rootless folds of leucosome layers and discordant granite dikes cutting the migmatitic layering. The granite dikes also intrude chloritoid-bearing slates and are folded into open, steep folds with axial planes parallel to the schistosity. The S_{2SG} foliation in the migmatites and the schistosity in the spotted chloritoid-bearing slates (fig. 12, stereogram 7) strike steeply NE-SW and bear a subvertical mineral lineation. Farther north, this metamorphic fabric is rotated into an E-W direction, parallel to the S_{3SG} cleavage front. The intensity of this late cleavage decreases to the north, away from the metamorphic aureole, indicating that the GTIC behaved as a rigid body during the D_{3SG} event.

Table 1

Analytical $^{40}Ar/^{39}Ar$ data

Sample	Lab n°	Laser Power (mV)	^{40}Ar (moles)	^{40}Ar (V)	±1σ	^{39}Ar (V)	±1σ	^{38}Ar (V)	±1σ
M126-06-03	B87-1			0.003534	0.000039	0.000396	0.000012	0.000236	0.000008
White mica	K87-1	384 mV	0.252653	0.000128	0.000039	0.014515	0.000053	0.000438	0.000020
	K87-2	402 mV	0.656419	0.000439	0.000039	0.040843	0.000061	0.000845	0.000016
	K87-3	422 mV	0.425292	0.000359	0.000039	0.026448	0.000071	0.000635	0.000023
	K87-4	fusion	0.888403	0.000656	0.000039	0.055007	0.000066	0.001178	0.000021
M134-P11-06	B83-1			0.003951	0.000033	0.000367	0.000013	0.000200	0.000009
White mica	K83-1	382 mV	6.043E-15	0.003951	0.000033	0.000367	0.000013	0.000200	0.000009
	K83-2	403 mV	5.819E-15	0.003951	0.000033	0.000367	0.000013	0.000200	0.000009
	K83-3	423 mV	4.107E-14	0.003951	0.000033	0.000367	0.000013	0.000200	0.000009
	B83-2			0.003391	0.000036	0.000370	0.000034	0.000204	0.000014
	K83-4	430 mV	1.348E-14	0.003391	0.000036	0.000370	0.000034	0.000204	0.000014
	K83-5	460 mV	5.637E-15	0.003391	0.000036	0.000370	0.000034	0.000204	0.000014
	K83-6	574 mV	1.264E-15	0.003391	0.000036	0.000370	0.000034	0.000204	0.000014
	K83-7	900 mV	3.297E-16	0.003391	0.000036	0.000370	0.000034	0.000204	0.000014
M102-06-03	B86-1			0.003464	0.000038	0.000375	0.000023	0.000214	0.000009
White mica	K86-1	368.00W	1.479E-15	0.077405	0.000143	0.007291	0.000061	0.000248	0.000010
	K86-2	389.00W	1.605E-15	0.083689	0.000135	0.008810	0.000037	0.000306	0.000010
	K86-3	408.00W	5.174E-16	0.029331	0.000064	0.003004	0.000027	0.000232	0.000007
	K86-4	fusion	1.550E-15	0.080988	0.000083	0.008470	0.000039	0.000255	0.000012
M101-06-04	B90-1			0.004338	0.000043	0.000552	0.000039	0.000222	0.000013
White mica	K90-1	300 mV	1.407E-15	0.074682	0.000080	0.008033	0.000031	0.000268	0.000018
	K90-2	439 mV	1.055E-14	0.532069	0.000519	0.061184	0.000112	0.000917	0.000022
	K90-3	445 mV	1.448E-15	0.075817	0.000095	0.008815	0.000048	0.000306	0.000006
	B90-2			0.003413	0.000037	0.000378	0.000033	0.000243	0.000006
	K90-4	452 mV	5.572E-15	0.282011	0.000228	0.032988	0.000100	0.000564	0.000015
	K90-5	490 mV	4.284E-15	0.217596	0.000189	0.025193	0.000073	0.000463	0.000024
	K90-6	fusion	9.929E-18	0.003909	0.000034	0.000396	0.000012	0.000202	0.000013
M181-06	B92-1			0.002961	0.000022	0.000359	0.000012	0.000161	0.000011
White mica	K92-1	320 mV	1.717E-15	0.088821	0.000274	0.011794	0.000070	0.000281	0.000016
	K92-2	425 mV	7.125E-17	0.006523	0.000025	0.000760	0.000020	0.000187	0.000010
	K92-3	470 mV	4.332E-16	0.024622	0.000036	0.003301	0.000037	0.000230	0.000022
	K92-4	1111 mV	2.087E-15	0.107299	0.000156	0.014646	0.000038	0.000353	0.000018
M76-06-02	B205-1			0.003041	0.000083	0.000248	0.000014	0.000026	0.000003
White mica	K205-1	386 mV	1.545E-15	0.080280	0.000086	0.003936	0.000021	0.000071	0.000004
	K205-2	435 mV	1.057E-14	0.531748	0.000553	0.024109	0.000060	0.000320	0.000009
	K205-3	462 mV	7.940E-15	0.400034	0.000547	0.017862	0.000026	0.000237	0.000010
	B205-2			0.001879	0.000035	0.000080	0.000008	0.000046	0.000006
	K205-4	493 mV	3.585E-15	0.181123	0.000541	0.007986	0.000039	0.000133	0.000005
	K205-5	560 mV	1.910E-15	0.097373	0.000505	0.004289	0.000022	0.000088	0.000004
	K205-6	fusion	3.046E-15	0.154187	0.000446	0.006780	0.000032	0.000120	0.000005
M181-06	B92-1			0.002961	0.000022	0.000359	0.000012	0.000161	0.000011
White mica	K92-1	320 mV	1.717E-15	0.088821	0.000274	0.011794	0.000070	0.000281	0.000016
	K92-2	425 mV	7.125E-17	0.006523	0.000025	0.000760	0.000020	0.000187	0.000010
	K92-3	470 mV	4.332E-16	0.024622	0.000036	0.003301	0.000037	0.000230	0.000022
	K92-4	1111 mV	2.087E-15	0.107299	0.000156	0.014646	0.000038	0.000353	0.000018
M44-06-03	B208-1			0.001855	0.000032	0.000039	0.000008	0.000031	0.000005
White mica	K208-1	345 mV	3.348E-15	0.169243	0.000530	0.026452	0.000078	0.000387	0.000008
	K208-2	370 mV	4.064E-14	2.033947	0.005855	0.334405	0.001011	0.004320	0.000020
	K208-3	384 mV	4.991E-15	0.251428	0.000547	0.042600	0.000098	0.000566	0.000009
	B208-2			0.002133	0.000057	0.000109	0.000012	0.000044	0.000003
	K208-4	419 mV	4.287E-14	2.145633	0.004426	0.367908	0.000700	0.004671	0.000028
	K208-5	452 mV	5.143E-15	0.259307	0.000553	0.044400	0.000140	0.000588	0.000011
	K208-6	520 mV	2.025E-15	0.103366	0.000337	0.017295	0.000068	0.000241	0.000006
	K208-7	fusion	2.045E-16	0.012359	0.000050	0.001567	0.000014	0.000062	0.000004

TABLE 1
(continued)

Sample	^{37}Ar (V)	±1σ	^{36}Ar (V)	±1σ	^{40}Ar*/^{39}Ar$_k$	±1s	%^{40}Ar*	Age (Ma)	±2σ
M126-06-03	0.000561	0.000009	0.000209	0.000006					
White mica	0.000511	0.000023	0.000298	0.000009	15.842427	0.29829	89.36	557.91	±18.07
	0.000470	0.000012	0.000188	0.000010	16.339775	0.18567	100.74	572.91	±11.16
	0.000470	0.000015	0.000189	0.000008	16.464305	0.20875	101.21	576.65	±12.52
	0.000464	0.000011	0.000180	0.000012	16.405100	0.18070	100.76	574.87	±10.84
M134-P11-06	0.000515	0.000013	0.000210	0.000006					
White mica	0.000515	0.000013	0.000210	0.000006	16.589187	0.27802	94.07	580.39	±16.63
	0.000515	0.000013	0.000210	0.000006	15.550713	0.26481	100.03	549.05	±16.12
	0.000515	0.000013	0.000210	0.000006	15.181038	0.15529	100.10	537.76	±9.51
	0.000526	0.000022	0.000216	0.000009					
	0.000526	0.000022	0.000216	0.000009	15.260090	0.17890	100.88	540.18	±10.95
	0.000526	0.000022	0.000216	0.000009	16.259285	0.72339	107.52	570.49	±43.52
	0.000526	0.000022	0.000216	0.000009	15.716883	0.91520	101.08	554.10	±55.56
	0.000526	0.000022	0.000216	0.000009	14.230362	2.89660	87.29	508.40	±180.36
M102-06-03	0.000554	0.000014	0.000221	0.000006					
White mica	0.000485	0.000016	0.000235	0.000006	10.066340	0.38854	93.89	373.87	±26.07
	0.000517	0.000013	0.000220	0.000008	9.530186	0.35971	99.91	355.79	±24.38
	0.000503	0.000013	0.000224	0.000006	9.426595	0.98176	95.54	352.28	±66.66
	0.000489	0.000011	0.000210	0.000010	9.973951	0.44470	103.85	370.76	±29.89
M101-06-04	0.000537	0.000018	0.000203	0.000005					
White mica	0.000535	0.000019	0.000202	0.000006	9.431091	0.32233	100.02	352.43	±21.88
	0.000496	0.000020	0.000173	0.000008	8.844811	0.10092	101.33	332.42	±6.93
	0.000531	0.000016	0.000210	0.000009	7.977066	0.34926	92.69	302.39	±24.38
	0.000568	0.000015	0.000193	0.000004					
	0.000493	0.000018	0.000161	0.000007	8.827044	0.12140	103.03	331.81	±8.34
	0.000480	0.000026	0.000180	0.000009	8.774402	0.14950	101.37	330.00	±10.28
	0.000520	0.000012	0.000185	0.000008	158.422310	352.60046	554.22	2762.50	±6293.92
M181-06	0.000525	0.000016	0.000189	0.000005					
White mica	0.000469	0.000015	0.000181	0.000011	7.711613	0.33395	102.42	293.10	±23.43
	0.000505	0.000017	0.000187	0.000005	10.230378	5.25422	115.03	379.36	±351.43
	0.000524	0.000022	0.000185	0.000008	7.712755	0.92951	104.49	293.14	±65.21
	0.000481	0.000017	0.000188	0.000008	7.307504	0.21191	99.78	278.86	±14.99
M76-06-02	0.000343	0.000016	0.000110	0.000007					
White mica	0.000188	0.000008	0.000091	0.000007	18.572147	0.89294	91.10	638.76	±51.73
	0.000136	0.000015	0.000082	0.000014	21.704532	0.30324	98.30	727.27	±16.72
	0.000124	0.000010	0.000079	0.000007	21.885666	0.29487	97.70	732.26	±16.22
	0.000233	0.000008	0.000123	0.000005					
	0.000193	0.000009	0.000117	0.000006	22.447106	0.41057	99.10	747.64	±22.39
	0.000197	0.000010	0.000121	0.000006	22.037773	0.65519	97.47	736.44	±35.95
	0.000197	0.000006	0.000123	0.000006	22.247234	0.44299	97.99	742.18	±24.23
M181-06	0.000525	0.000016	0.000189	0.000005					
White mica	0.000469	0.000015	0.000181	0.000011	7.711613	0.33395	102.42	293.10	±23.43
	0.000505	0.000017	0.000187	0.000005	10.230378	5.25422	115.03	379.36	±351.43
	0.000524	0.000022	0.000185	0.000008	7.712755	0.92951	104.49	293.14	±65.21
	0.000481	0.000017	0.000188	0.000008	7.307504	0.21191	99.78	278.86	±14.99
M44-06-03	0.000184	0.000011	0.000122	0.000007					
White mica	0.000152	0.000009	0.000183	0.000006	5.543069	0.13090	87.31	215.37	±9.59
	0.000117	0.000008	0.000181	0.000010	5.995228	0.06607	98.40	231.86	±4.80
	0.000156	0.000014	0.000119	0.000007	5.814193	0.09994	98.93	225.28	±7.28
	0.000180	0.000010	0.000110	0.000006					
	0.000149	0.000025	0.000116	0.000027	5.801986	0.06444	99.29	224.83	±4.70
	0.000150	0.000015	0.000101	0.000019	5.788246	0.14858	99.47	224.33	±10.83
	0.000166	0.000012	0.000100	0.000006	5.968135	0.17588	101.10	230.87	±12.77
	0.000152	0.000009	0.000124	0.000007	2.450817	1.92596	35.32	98.41	±150.53

Samples were irradiated for 30 hours with Cd shielding in 5C position at McMaster Nuclear Reactor along with Hb3gr hornblende monitor (1072 Ma; Turner and others, 1971). J-values range from 0.0035309 ± 0.0000177 (=0.5% at 1σ) to 0.0035312 ± 0.0000177 (=0.5% at 1s). Data are presented following Renne and others (2009) recommendations and calculations are determined by using the ArArCALC-software of Koppers (2002).

The internal part of the GTIC reveals a magmatic fabric that is best developed in the main granodiorite. This fabric is usually strong and defined by the preferred orientation of hornblende and a strong shape-preferred orientation of diorite xenoliths showing variable degrees of flattening (figs. 14C and 14D). The steeply ESE-dipping magmatic fabric (fig. 12, stereogram 8 and fig. 13A) is locally cut by steep NE-SW striking sub-magmatic shear zones. The relationship between granodiorite, granite and its metasedimentary envelope implies a complex stoping-passive and active emplacement mechanism. For instance, there is a full coherency between foliation of migmatites, migmatitic orthogneisses and magmatic fabric in gabbros and granodiorites. Farther east, the main body of granodiorite is intruded by a late granophyric granite that has no visible magmatic fabric. Here, the relationship between the Devonian spotted slates and the granites suggests a more passive style of magma emplacement, characterized by stoping of Devonian slate blocks. The southernmost border zone of the GTIC consists of a Devonian volcano-sedimentary sequence which shows a decrease in metamorphic grade from north to south from fine-grained chlorite-sericite greenschist-facies shales and metabasites to almost unmetamorphosed rocks. The NE-SW striking metamorphic schistosity S_{2SG} (fig. 12, stereogram 9) was heterogeneously reworked by a new SW-dipping cleavage S_{3SG} (fig. 12, data included in stereogram 10). The superposed character of deformation is well developed in more competent gabbros, which show discrete D_{3SG} reworking of a heterogeneous array of D_{2SG} shear zones.

$^{40}Ar/^{39}Ar$ geochronology

$^{40}Ar/^{39}Ar$ dating via step heating of single grains of white micas was performed in order to unravel key deformational and/or cooling events and to complement the U-Pb zircon ages of Kröner and others (2010). The analytical procedure is detailed in Appendix I, and the $^{40}Ar/^{39}Ar$ results are shown in table 1.

Metamorphic and Cooling Ages from the Lake Zone

Numerous orthogneisses are exposed between the northern margin of the EC and the Khantaishir ophiolite and constitute the northernmost outcrop of the Zamtyn basement (fig. 7). These rocks may provide an age of metamorphism predating emplacement of the Eclogitic Complex. Sample M126-06-3 (45.41120N, 98.19978E; figs. 2, 15A and table 1) is a mylonitic orthogneiss composed of K-feldspar, plagioclase, quartz, white mica, epidote and chlorite. K-feldspar, plagioclase, quartz and white mica form porphyroclasts (up to 5 mm in size) that are recrystallized by brittle-ductile deformational mechanisms into a fine-grained matrix. White mica in the recrystallized domains was partially converted into very fine-grained aggregates containing chlorite. A few epidote grains occur in plagioclase aggregates. The large porphyroclasts are interpreted as relicts of the peak metamorphic assemblage, but some may be also relicts of magmatic origin. Fine-grained recrystallization is attributed to a lower greenschist-facies metamorphic overprint. One white mica grain yielded a plateau age of 573 ± 15 Ma.

Located 3.5 km east of the above sample and still on the northern margin of the Eclogite Complex, micaschists enclosing a large eclogitic lens are exposed where sample M134-P11-6 was collected (45.41141N, 98.24463E; figs. 2, 15B, and table 1). This sample is a quartzitic micaschist that contains garnet, white mica, chloritoid, chlorite, quartz, rutile and ilmenite. The metamorphic foliation is defined by white mica- (up to 3 mm) dominated bands containing minor chlorite that alternate with recrystallized quartz bands of infinite length. Elongated chloritoid porphyroblasts (up to 5 mm) preferentially occur aligned within the mica layers. Garnet (up to 5 mm) contains inclusions of quartz, rutile, ilmenite and rare white mica. This sample yielded a plateau age of 540 ± 15 Ma. Štípská and others (2010) obtained $^{40}Ar/^{39}Ar$ cooling

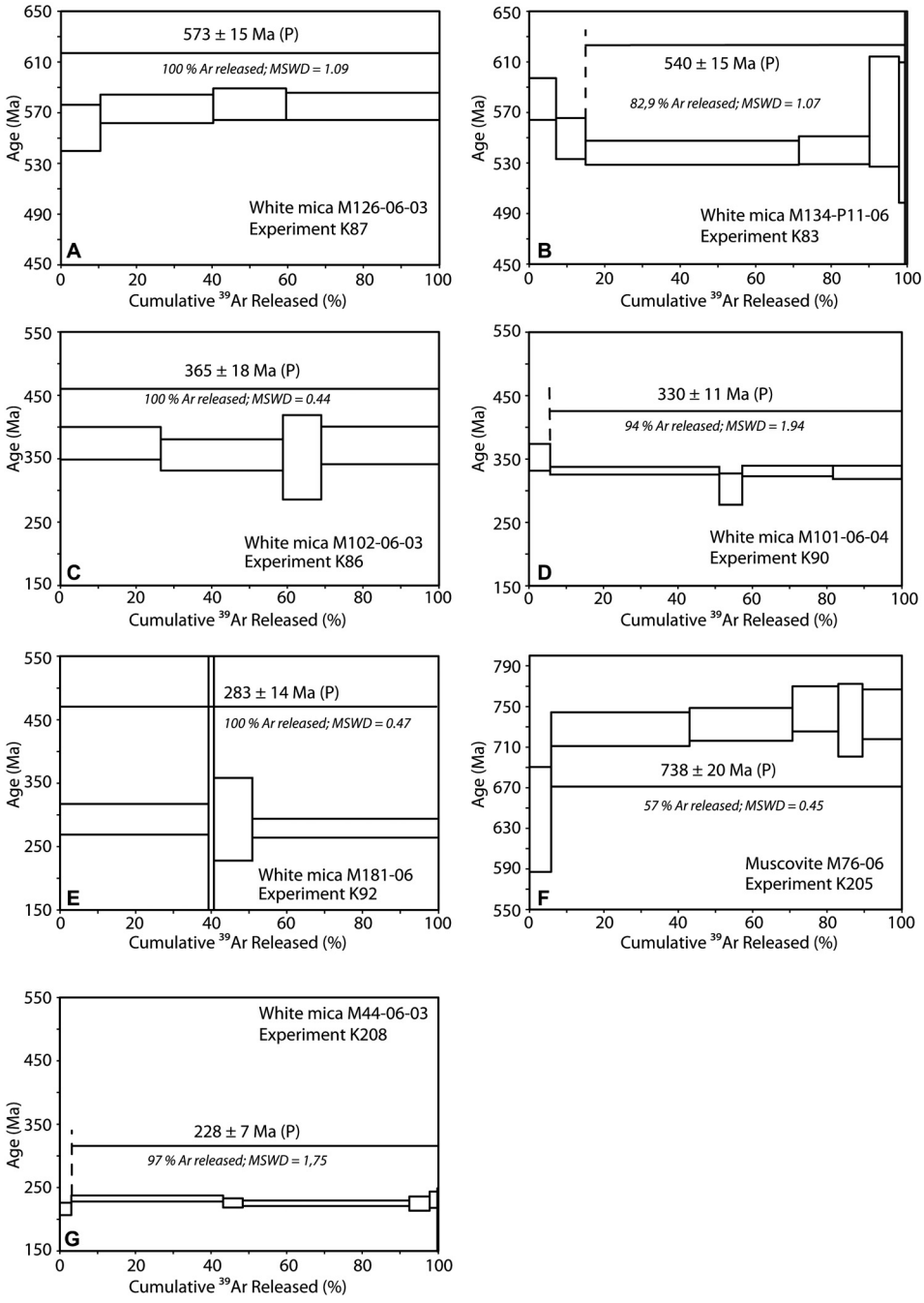

Fig. 15. $^{40}Ar/^{39}Ar$ age spectra as a function of ^{39}Ar released. Single grains were heated by a laser. The error boxes of each step are at the 2σ level. Error of the plateau ages (P) is given at the 2σ level. Ages were calculated using the ArArCalc program (Koppers, 2002). MSWD for plateau and percentage of ^{39}Ar degassed used in the plateau calculation are indicated in the table 1.

ages from two white micas oriented parallel to large clinopyroxene porhyroblasts and to the $S_{1\text{-}2E}$ planar fabric of eclogites from the same outcrop which overlap, within error, with our age (fig. 6A). Therefore, the ~540 Ma is interpreted as the minimum age for exhumation of the Eclogite Complex.

Metamorphic and Cooling Ages from the Gobi-Altai Zone

An andalusite-bearing micaschist (M102-06-3) and a white mica-bearing migmatite (M101-06-4) were collected close to Chandman village from the southern metamorphic rim of the Chandman crystalline complex in the Tugrig Formation, respectively at some 500 meters south and at few meters southwest of the intrusive contact (fig. 2 and table 1). Sample M102-06-3 (45.26035N, 97.94460E; figs. 6C and 15C) is composed of quartz, biotite, white mica, plagioclase and andalusite. It displays a S_{2G} compositional layering of quartz- and biotite-dominated layers with relatively small grain size (0.1-0.5 mm). The poikiloblasts of andalusite (up to 1 cm) include biotite, white mica and opaque minerals. Sample M101-06-4 (45.29473N, 97.81898E; fig. 15D) contains quartz, plagioclase, biotite, white mica, opaque minerals and pseudomorphs composed of white mica (after andalusite?) and white mica-chlorite (after cordierite?). The S_{2G} foliation is defined by an alternation of recrystallized quartz (up to 2 mm) layers with biotite-plagioclase rich layers. Few large white mica flakes occur aligned within the biotite-rich layers or fine-grained white mica forms part of the pseudomorphs. Large white micas from these two samples yielded plateau ages of 365 ± 18 and 330 ± 11 Ma, respectively. The age of ~365 Ma is identical to the late Devonian–early Carboniferous emplacement ages for rocks of the CCC (Kröner and others, 2010). We therefore interpret this ~365 Ma $^{40}Ar/^{39}Ar$ age as reflecting fast cooling during syn-emplacement exhumation of the southern part of the CCC. The ~330 Ma $^{40}Ar/^{39}Ar$ age may reveal a slower cooling during post-emplacement exhumation of the southwestern part of the CCC. Alternatively, this later age may reflect mixing of the ~365 Ma gas reservoir with a younger one (perhaps formed during the D_{3G} event).

A sample of strongly deformed shaly sandstone (M181-06) of Ordovician-Silurian depositional age (Rauzer and others, 1987) was collected in the eastern Gobi-Altai Zone (45.06242N, 99.50111E; figs. 2, 15E and table 1). It contains quartz, plagioclase, calcite, white mica, biotite, chlorite and opaque minerals. Within the fine-grained matrix occur sub-rounded to angular fragments of quartz and plagioclase (up to 0.5 mm), recrystallized calcite veins, a few biotite grains that are generally chloritized, and a few white mica grains. The slaty S_{3G} cleavage is of variable intensity; in strongly deformed domains chlorite, white mica and opaque minerals are commonly aligned within the foliation. This sample yielded a white mica plateau age of 283 ± 14 Ma, which we interpret to reflect the timing of low-grade metamorphism accompanying an early Permian deformation event.

In the southern Gobi-Altai Zone, an andalusite-bearing micaschist (M76-06) was collected from the northern metamorphic metapelites rimming the gneissic dome located south of Erdene village (44.87916N, 97.79470E; figs. 2, 15F and table 1). This area was mapped as Proterozoic but yielded new late Devonian zircon ages for the protoliths of some gneissic rocks (Kröner and others, 2007; Demoux and others, 2009a and Kröner and others, 2010) and an early Devonian age for a metarhyolite (Demoux and others, 2009a) located several kilometers south and 1 km SE, respectively, of our sampling locality. The above micaschist sample contains quartz, white mica, biotite, andalusite and opaque minerals. The S_{3G} metamorphic foliation is defined by quartz and biotite-white mica rich alternations with mica grains up to 1 mm and contains relict isoclinal folds. Poikiloblasts of andalusite (up to 5 mm) include biotite, white mica and opaque minerals. The $^{40}Ar/^{39}Ar$ spectrum shows a shape typical for argon loss which yielded a mean age of 738 ± 20 Ma interpreted as a cooling age of schists.

These results therefore confirm the occurrence of Proterozoic metamorphic rocks in this area as proposed by Rauzer and others (1987).

Cooling Age for the Gobi-Tienshan Intrusive Complex

In the South Gobi Zone, we collected sample M44-06-3 (43.31867N, 97.06856E; figs. 2, 15G and table 1), which is a leucocratic gneiss from the northwestern termination of the GTIC. It is composed of quartz, plagioclase, K-feldspar and white mica. Plagioclase, K-feldspar and quartz form porphyroclasts (1-2 mm in size) that are recrystallized at grain boundaries to fine-grained (0.02-0.2 mm) monomineral anastomozing ribbons defining the S_{3SG} metamorphic foliation. Large white micas, randomly oriented in low-strain domains or aligned within the anastomozing metamorphic foliation were commonly recrystallized into fine-grained aggregates (0.2 mm). Porphyroclasts of K-feldspar, quartz and plagioclase together with large white mica are interpreted as magmatic relicts whereas the recrystallized grains are attributed to the greenschist-facies D_{3SG} event. The analyzed white mica grain (fig. 15G and table 1) yielded a plateau age of 228 ± 7 Ma. This young cooling age either suggests that the argon isotopic system of the previously cooled plutonic complex was reset during middle-late Triassic deformation or that its northwestern part remained below the closure temperature for the argon system in white mica for about 70 Ma. However, this leucocratic gneiss is in intrusive contact with low-grade metasediments, attesting that the intrusive rocks cooled rapidly after their emplacement. We therefore interpret this middle-late Triassic age as reflecting deformation of the low-grade D_{3SG} in this area.

DISCUSSION

Our main aim is to understand the differences in structural styles between the Lake, Gobi-Altai and South Gobi continental Zones and the Trans-Altai oceanic Zone. An attempt is therefore made to establish relationships between the changing orientations of deformation fabrics through time in terms of changes in plate configurations so that the main patterns of the orogenic structure can be interpreted in the context of current tectonic models.

Principal Tectonic Events Affecting the CAOB in Southern Mongolia

In order to define the principal tectonic events it is necessary to correlate the spatial and temporal character of major angular unconformities with geochronological ages characterizing magmatic, volcanic and metamorphic events (fig. 3). The oldest unconformity is known from the Gobi-Altai Zone and is defined by deposition of early Ordovician sediments of the Bayantsagaan formation on metamorphosed schists of the Tugrig formation. This unconformity potentially also exists in the Mandalovoo Subzone as marked by detrital late Cambrian zircons in the Ordovician sediments and in the South Gobi Zone. Based on recent zircon ages, the age of the Ordovician unconformity correlates well with intrusive ages for dikes, granites and volcanic rocks from the Lake Zone, suggesting the existence of a major Cambro-Ordovician tectonic and thermal event affecting the Precambrian crust (D_{2Z} and D_{1G} events in fig. 16).

An early Devonian unconformity is present in the Trans-Altai and in the Gobi-Altai Zones (fig. 16) and is related to the formation of an early-middle Devonian arc in the southerly Edrengin and Dzolen Subzones and back-arc volcanism in the northern Khuvinkharin Subzone that are developed on top of distal passive margin sequences of the Trans-Altai Silurian-Devonian oceanic basin. The associated proximal margin was located in the Gobi-Altai Zone and was subsequently replaced by a back-arc system (Lamb and Badarch, 1997, 2001; Demoux and others, 2009a; Kröner and others, 2010). The early Devonian unconformity corroborates early Devonian ages for volcanic rocks dated by Helo and others (2006) (fig. 3C). This event succeeds deformation

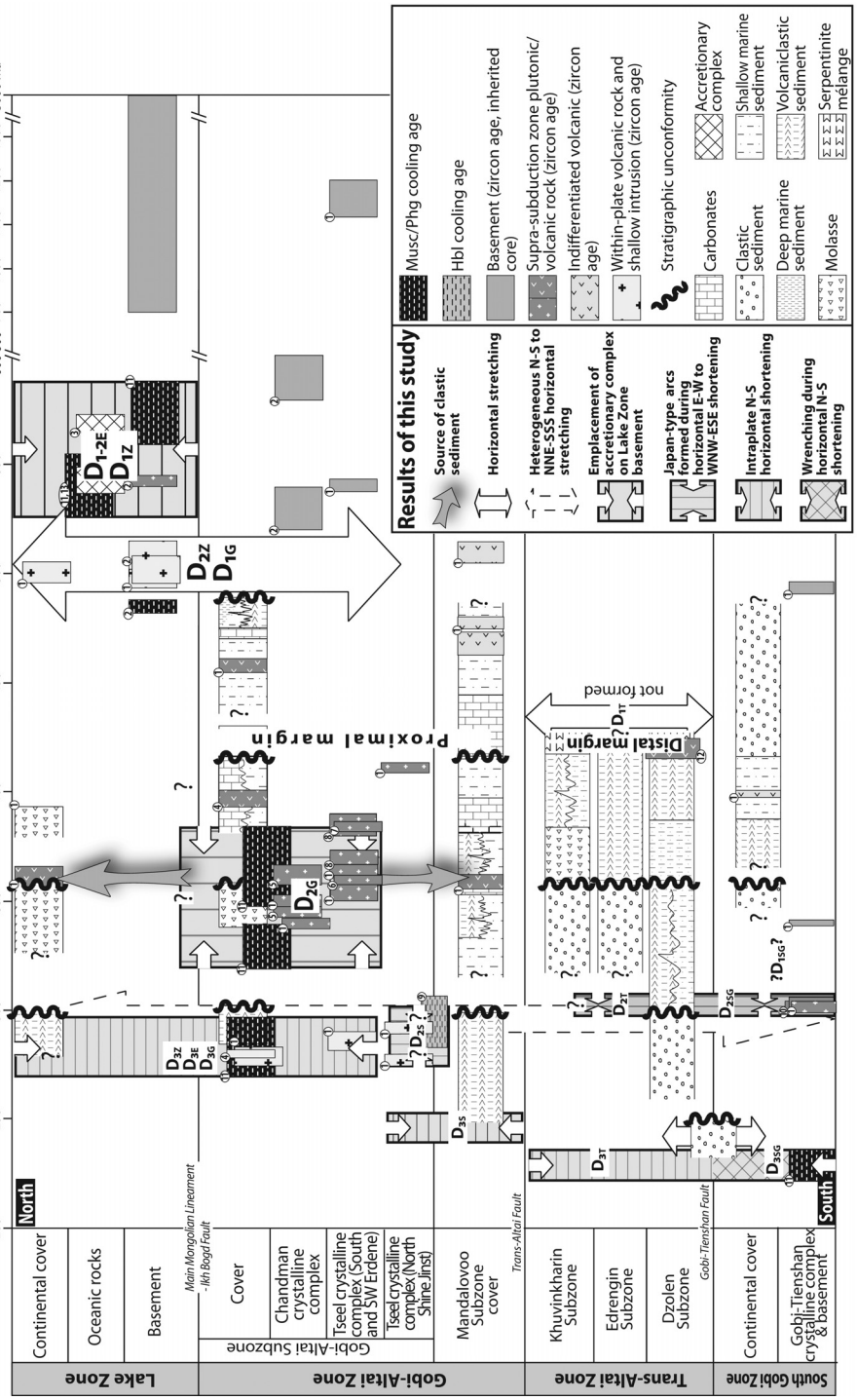

Fig. 16. Summary of tectonic chronology of SW Mongolia including published zircon ages $^{40}Ar/^{39}Ar$ mineral ages. Circled numbers in the corner of each frame refer to geochronological constraints as follows: 1)—Kršner and others (2010), 2)—Hanžl and Aichler (2007), 3)—Gibsher and others (2001), 4)—Demoux and others (2009a), 5)—Hrdličková and others (2008), 6)—Kröner and others (2007), 7)—Kozakov and others (2002), 8)—Bibikova and others (1992), 9)—Lamb and others (2008), 10)—Yarmolyuk and others (2008), 11)—this study, 12)—Helo and others (2006), 13)—Štípská and others (2010).

during greenschist-facies affecting serpentinites, ophicalcites and gabbros reported, for example, from ophiolite fragments in the Dzolen Subzone (D_{1T} event in fig. 16).

The main unconformity in the Trans-Altai Zone is located at the base of the early Carboniferous (Markova, 1975; fig. 16), which coincides with clastic sedimentation that was interpreted by some authors to have occurred in a foreland basin (Tomurtogoo and Badarch, 1997). This event was also associated with emplacement of the Dzolen ophiolites and first folding of Devonian and Carboniferous sequences during D_{2T}. It correlates with Devonian-Carboniferous intrusions of magmatic arc rocks (fig. 3B) in the Gobi-Altai Zone and clastic sedimentation in basins developed on Gobi-Altai and Lake Zone continental crust. The syntectonic intrusions and associated LP-HT metamorphism are coeval with major E-W shortening and mark the main tectonic event affecting the Silurian to early Devonian passive margin sequences of the Gobi-Altai Zone (D_{2G} event in fig. 16).

The late Carboniferous–early Permian unconformities were mainly described in the Gobi-Altai and Mandalovoo Subzones. Here, sediments filled intramontane basins and covered previously deformed late Devonian to early Carboniferous rocks (fig. 16). This unconformity reflects a surface response to crustal melting and the emplacement of alkaline granites in the Gobi-Altai Zone. The Permian tectonic evolution is also characterized by the onset of N-S compression dated at ~280 Ma by the $^{40}Ar/^{39}Ar$ method on white mica in the Gobi-Altai Zone. Late Carboniferous volcanic activity in the southern Trans-Altai and South Gobi Zones was already recognized by Markova (1975) and may be correlated with intense arc magmatism in the Gobi-Tienshan area in the South Gobi Zone in late Carboniferous time. This arc evolved in a compressive tectonic setting and marks the second major tectonic event in the CAOB of SW Mongolia (D_{2SG} event in fig. 16).

Finally, Triassic and late Jurassic unconformities were reported from the South Gobi Zone and reflect major tectonic events caused by collision of the CAOB with the Tarim and North China Cratons (Xiao and others, 2003, 2008, 2009). These events can be correlated with Triassic $^{40}Ar/^{39}Ar$ cooling ages on K-feldspar reported by Lamb and others (2008) and with our new data which indicate an important and recurrent Mesozoic shortening event.

Kinematic and Structural Model for the CAOB of Southern Mongolia

We now discuss the kinematic and temporal evolution of individual tectonic zones, and we correlate these events across the studied section of the Mongolian CAOB. The Paleozoic structural evolution of southern Mongolia is subsequently interpreted in terms of different rheological responses of crustal/lithospheric units to far-field stresses.

Early Cambrian thrusting and Early Ordovician orogenic collapse.—The oldest deformation event recognized in the southern Mongolian CAOB was related to early Cambrian thrusting of an eclogitic mélange of the Tsakhir Uul formation and Khantaishir ophiolite over the Zamtyn basement of the Lake Zone (Štípská and others, 2010) as shown by ~573 to 540 Ma $^{40}Ar/^{39}Ar$ mica ages for samples M126-06-3 and M134-P11-6 (figs. 15A and 15B). Consequently, a nappe stack developed, composed of the Khantaishir ophiolite on the top, an eclogitic mélange representing a subducted passive margin in the middle, and a deformed continental basement at the bottom. This event was responsible for the origin of $S_{1\text{-}2E}$ burial/exhumation fabrics in the eclogites as well as earliest and relict S_{1Z} fabrics in the Zamtyn basement. The direction of thrusting cannot be reconstructed from our study area, but the broadly linear E-W arrangement of the Dariv and Khantaishir ophiolite fragments parallel to the Lake Zone trend suggest that the ophiolites were emplaced approximately in the N-S direction in present coordinates (fig. 17A).

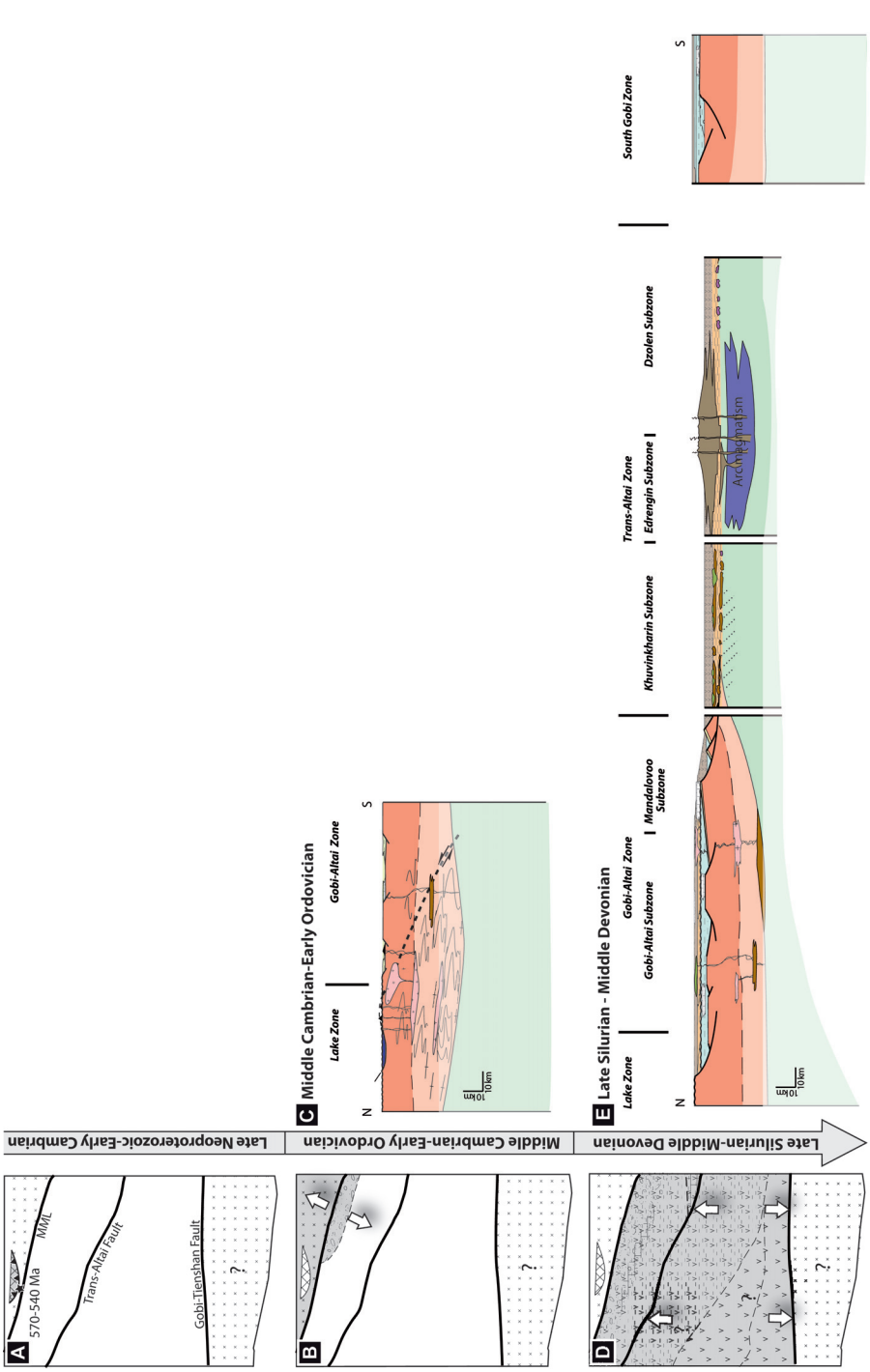

Fig. 17. Left column: Successive schematic maps showing the orientation of each deformation phase. Right column: Internal geodynamic evolution of each tectonic zone shown as idealized cross-sections through the orogen. (A) Late Neoproterozoic–early Cambrian emplacement of an accretionary complex in the Lake Zone. (B) and (C) Middle Cambrian–early Ordovician thermomechanic relaxation of the thickened Lake Zone, inducing magmatism in the Lake Zone and possibly in the Gobi-Altai Zone. (D) and (E) Late Silurian-middle Devonian oceanic back-arc and arc systems in Trans-Altai Zone. .

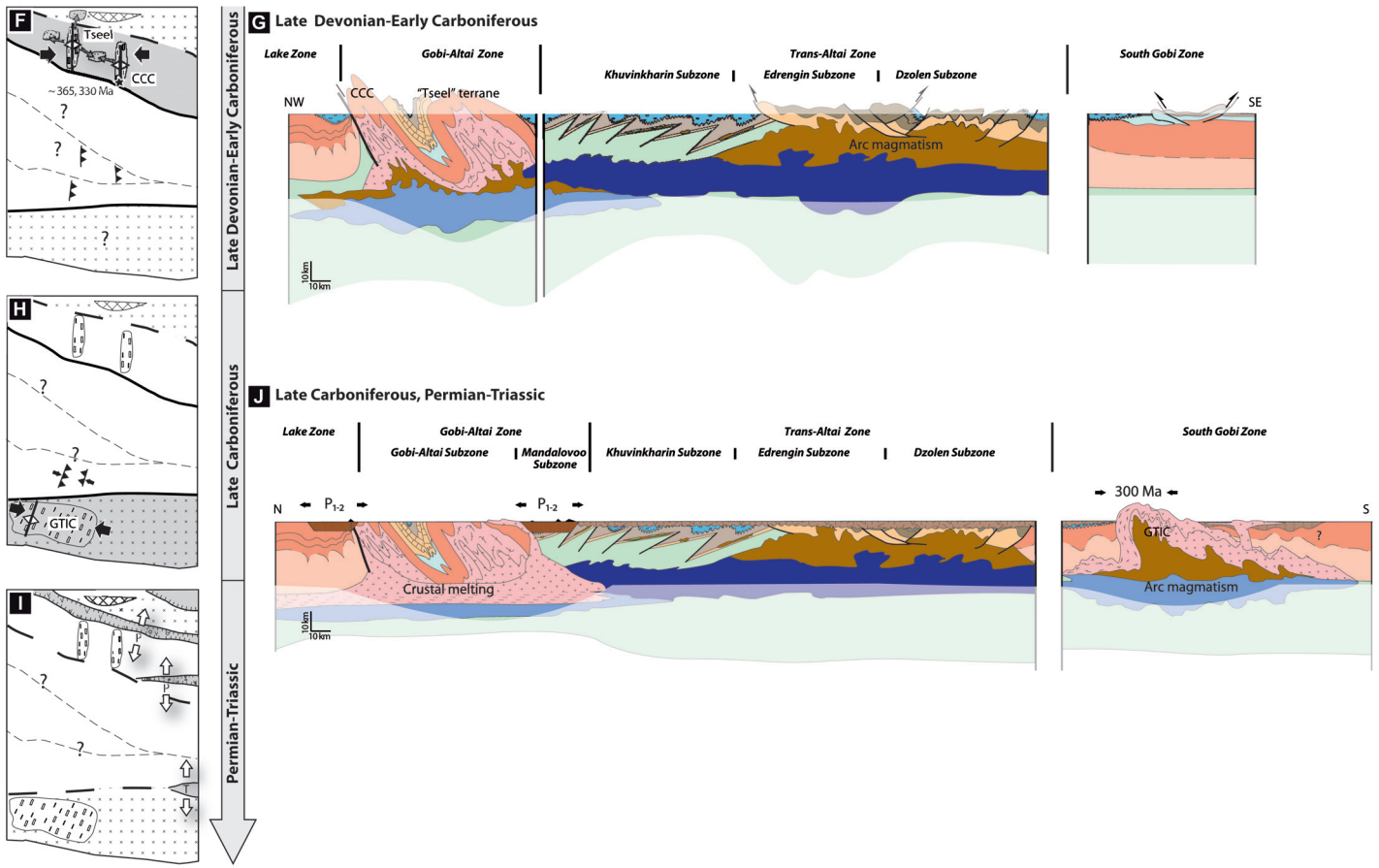

Fig. 17 (continued). (F) and (G) Late Devonian–early Carboniferous compressive arcs in the Gobi-Altai Zone with subsequent accretion to the Lake Zone. Suprastructure imbrication in the Trans-Altai Zone (this may already have occurred in middle Devonian time). (H) and (J) Late Carboniferous compressive arc in the South Gobi Zone associated with homogeneous volcaniclastic sedimentation in the Trans-Altai and South Gobi Zones. (I) and (J) Permian-Triassic marine and continental terrigenous intramontane basins. (J) Early Permian intraplate alkaline magmatism in the Gobi-Altai Zone.

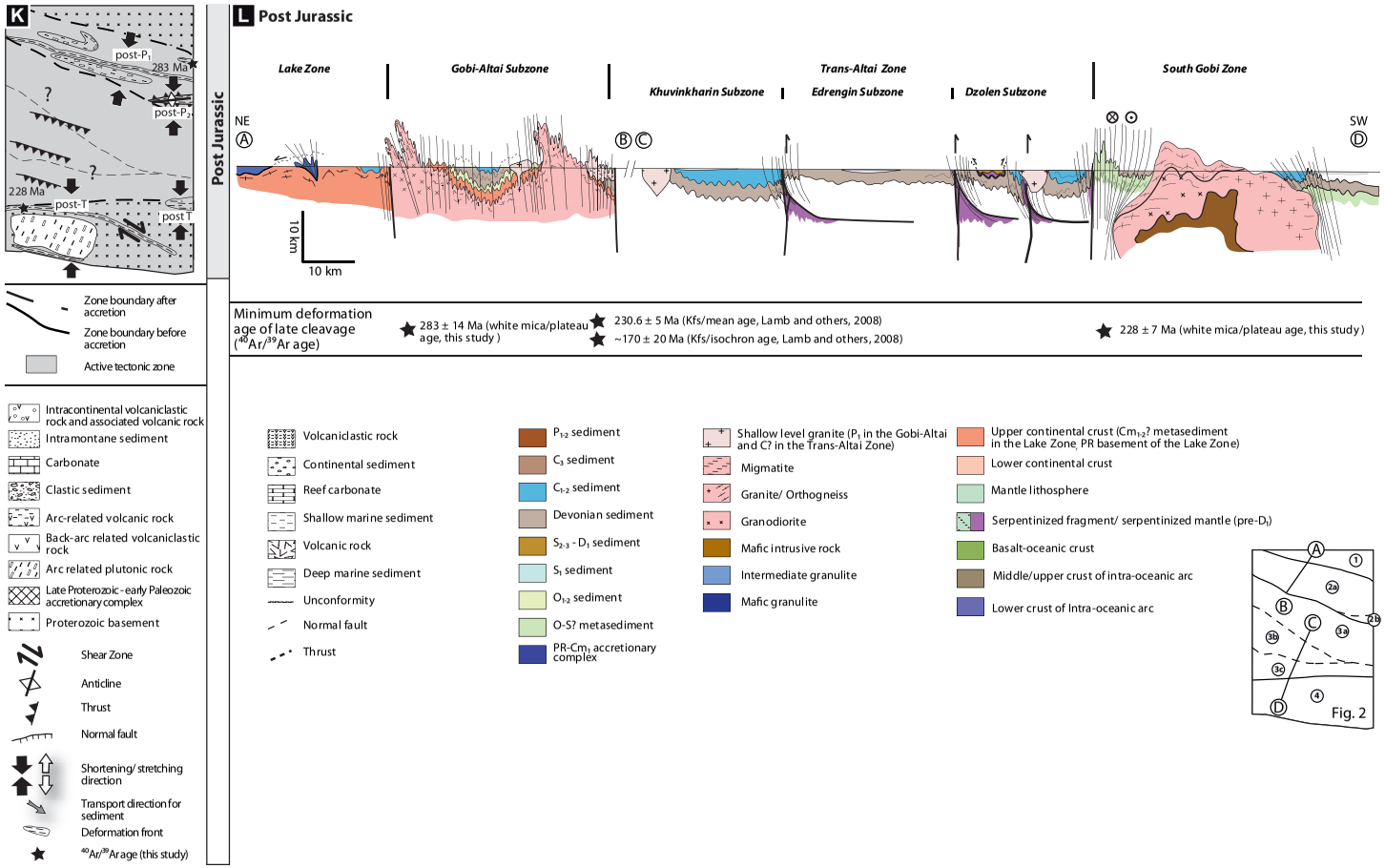

Fig. 17 (continued). (K) and (L) Post-Jurassic architecture with influence of intense late NNE-SSW to N-S shortening event, leading to present-day E-W striking zonation of the different geodynamic elements. Mineral abbreviations are after Kretz (1983)

The main sub-horizontal deformation D_{2Z} developed during amphibolite- to greenschist-facies metamorphism in the Zamtyn basement and is interpreted in terms of extensional shearing associated with major late Cambrian thermal reworking of the Lake Zone Precambrian rocks. The Eclogitic Complex as well as the Khantaishir ophiolite are therefore separated from the Zamtyn basement by a major detachment zone, partially reactivating an ancient thrust surface. The direction of detachment was probably top-to-the WSW-SW in present coordinates (figs. 17B and 17C). The formation of a flat and penetrative greenschist-facies foliation affecting the (Cambrian) Tugrig formation in the Gobi-Altai Zone must have occurred prior to the early Ordovician as documented by the unconformably overlying siliciclastic sediments of the Bayantsagaan formation. We propose that this D_{1G} vertical shortening was coeval with D_{2Z} extension affecting the Zamtyn basement of the Lake Zone (fig. 16). This follows from the fact that similar zircon ages for late Cambrian magmatic and volcanic rocks from the Lake Zone corroborate ages of clastic zircons of the early Ordovician clastic sequence of the Mandalovoo Subzone (fig. 3B). Lamb and Badarch (2001) proposed that this event does not reflect formation of an Ordovician passive margin, based on the clastic character of Ordovician sediments. We agree and suggest that the Ordovician thermal and tectono-sedimentary event may reflect equilibration of thickened crust following Cambrian nappe stacking.

Late Silurian ocean basin formation and Early Devonian development of an arc and back-arc system.—A passive margin sequence developed along the entire length of the Gobi-Altai Zone during the late Silurian and early Devonian (figs. 17D and 17E) and has been interpreted in terms of initiation of N-S stretching in present coordinates (Zonenshain, 1973; Zorin and others, 1993). Silurian sequences from the South Gobi Zone were also considered by some authors to reflect passive margin development (for example, Zaitsev and others, 1970; Zonenshain, 1973). However, the structural record of this event seems to be missing.

Late Silurian to early Devonian fabrics were reported from the Trans-Altai Zone and are represented by greenschist-facies deformation of mantle rocks associated with the development of a serpentinite mélange that contains lenses of metagabbro and strongly sheared ophicalcite (Ruzhentsev and Pospelov, 1992; Ruzhentsev, 2001). This deformation is typical for exhumation of lithospheric mantle in areas of distal passive margins (figs. 17D and 17E) as reported from several areas in the world (for example, Manatschal and others, 2006). We therefore attribute the D_{1T} deformation to lithospheric stretching preceding the formation of oceanic crust during the early Devonian as indicated by massive basalt and andesite volcanism in the Dzolen and Gurvansaykhan ranges (Lamb and Badarch, 1997, 2001). This volcanism was partly related to magmatic arc activity whereas in other sectors it reflects a back-arc environment (Lamb and Badarch, 2001; Helo and others, 2006; Demoux and others, 2009a). The direction of stretching related to distal passive margin deformation is unknown, but several authors suggested N-S stretching related to opening of a Paleozoic oceanic domain (figs. 17D and 17E) in southern Mongolia (Zonenshain, 1973; Lamb and Badarch, 2001; Badarch and others, 2002).

Late Devonian to Early Carboniferous E-W convergence.—Syn-convergent emplacement of the Chandman arc magmas in the Gobi-Altai Zone is confirmed by: 1) growth of syntectonic HT-LP mineral assemblages before and during the D_{2G} event, 2) Carboniferous zircon crystallization ages for granites and gneiss protoliths of the CCC and, 3) $^{40}Ar/^{39}Ar$ white mica cooling ages of ~365 and 330 Ma for high-grade schists of the Tugrig formation. Telescoping ages obtained from high and low closure temperature isotopic systems indicate that emplacement of granodiorites, melting of crust, cooling, and exhumation of the core of the CCC (~350-340 Ma, Kröner and others, 2010) occurred very fast. D_{2G} also affected the upper crustal Paleozoic sequences as docu-

mented by vestiges of earliest large-scale folds that were responsible for the steepening of Ordovician to early Carboniferous sedimentary strata. During E-W compression, the deep parts of the magmatic arc, together with the thermally softened Tugrig formation, were vertically extruded through moderately folded Paleozoic sequences (figs. 17F and 17G). Early Carboniferous basins are probably related to uplift of the gneiss domes and represent intramontane basins infilled during erosion of exhumed deep crustal rocks (Markova, 1975). Importantly, these siliciclastic early Carboniferous sediments containing Devonian to Carboniferous zircons extend into the Lake Zone, which suggests that both tectonic units were juxtaposed during the early Carboniferous and received sedimentary input from growing infrastructural domes located in the Gobi-Altai Zone. The late Devonian gneiss dome (~364 Ma) in the southern part of the Gobi-Altai Zone exhibits a similar tectonic evolution as the CCC but was emplaced tens of millions of years earlier, indicating that E-W emplacement of magmatic arc rocks already began during the late Devonian (figs. 17F and 17G).

The tectonic emplacement of ophiolites in the Trans-Altai Zone over Devonian sediments possibly also occurred during late Devonian to early Carboniferous shortening. According to Zonenshain and others (1975) ophiolite-derived clasts occur in Middle Devonian sediments as well as in olistolithic blocks. These authors also documented unconformable deposition of undeformed late Devonian strata over older and deformed sequences, which suggests ophiolite emplacement to have occurred in the middle Devonian. These observations corroborate those of Tomurtogoo and Badarch (1997) who interpreted early Carboniferous sediments of the Gurvansaykhan Range as a molasse related to ophiolite nappe emplacement. On the other hand, Ruzhentsev and others (1985) proposed a middle to late Carboniferous age for ophiolite nappe stacking. These authors also reported thrusting of the ophiolitic mélange over Triassic sediments, implying that ophiolite emplacement and deformation continued until the Mesozoic–potentially middle-late Jurassic (Hendrix and others, 1996) or even into the Cenozoic (Rippington and others, 2008). Our study shows that the ophiolites with an inherited mylonitic fabric were emplaced above Devonian rocks prior to the major D_{3T} event. Although structural data attesting to the kinematics of D_{2T} ophiolite nappe thrusting are missing, we can deduce the thrusting direction from early E-W folding of the Trans-Altai Devonian and Carboniferous sequences which is related to E-W directed convergence (figs. 17F and 17G). This event was most likely related to the imbrication of oceanic crust and shallow-angle thrusting of the volcanic arc over the Devonian and Caboniferous sequences as shown in figures 17F and 17G.

The South Gobi Zone reveals a greenschist-facies, thin-skinned D_{1SG} tectonic pattern typical of Ordovician and Devonian rocks that were thrust onto almost unmetamorphosed Carboniferous sediments. Low-angle shearing and thrusting along the Tömörtyn shear zone suggests a low geothermal gradient (figs. 17F and 17G). The kinematics of this deformation is difficult to determine because of strong later reworking, but the presence of an E-W subhorizontal stretching lineation associated with numerous sense of shear criteria indicate that the originally flat E-W shear fabric was steepened during N-S D_{3SG} compression. This deformation event may be of middle Carboniferous age or older because of stoping of greenschist-facies blocks in late Carboniferous granites.

Late Carboniferous E-W convergence.—Late Carboniferous convergence is documented by syntectonic emplacement of the Gobi-Tienshan Intrusive Complex in the South Gobi Zone. The syntectonic character of emplacement is revealed by steep magmatic fabrics resulting from major ESE-WNW directed shortening during HT-LP metamorphic conditions. This deformation is characterized by pure shear shortening of the deep magmatic-metamorphic edifice associated with asymmetric extrusion of

the deepest (metamorphic) part of the Gobi-Tienshan arc along its northwestern margin (figs. 17H and 17J).

Late Carboniferous to early Permian migmatites and granites from the eastern extremity of the "Tseel terrane" are spatially related to an E-W trending belt of alkaline magmatism and narrow intracontinental sedimentary basins (Kovalenko and others, 1995; Lamb and Badarch, 1997). Kovalenko and others (1995) considered this belt as an extensional zone linked to northward ridge subduction. At this stage, our structural data are not sufficient to provide a kinematic interpretation of metamorphic and magmatic fabrics as well as the geodynamic setting of sedimentary basins. However, the narrow belt of magmatic and sedimentary rocks located close to the Gobi-Altai Zone boundaries may indicate a transtensional origin associated with an important strike-slip component or closure of remnant oceanic basins (figs. 17I and 17J).

Permian to Late Triassic N-S shortening.—D_{3Z} post-Permian N-S shortening was responsible for steep and tight folding of all Lake Zone units; including Carboniferous and Permian cover sequences and lower greenschist-facies imbrication of the Khantaishir ophiolite (figs. 17K and 17L).

In the Gobi-Altai Zone, this deformation is of middle Permian age (~283 Ma, sample M181-06) and was responsible for pervasive refolding of early D_{2G} folds affecting the crystalline core of the CCC and producing a typical Type 2 "mushroom" interference pattern (Ramsay, 1967). The Paleozoic sediments attained an ubiquitous NNW-SSE striking steeply dipping cleavage S_{3G} and were folded by disharmonic folds in which the main km-scale folding was probably controlled by thick Ordovician and Devonian volcaniclastic sequences. The D_{3G} event followed shortly after deposition of early Permian clastic sediments and an important early Permian magmatic event. This short time lag between early Permian crustal melting and basin formation and N-S compression may explain the high degree of deformability in the Gobi-Altai Zone and the mechanical coupling between deep and shallow rocks during D_{3G} (figs. 17K and 17L). The thermally softened crust of the Gobi-Altai Zone may have been at least partially rheologically unstable because of major Permian magmatic reworking of this region (Kovalenko and others, 1995).

D_{3T} deformation in the Trans-Altai Zone was spatially connected with boundaries of individual subzones that represent zones of weakness and important non-coaxial deformation whereas the central parts of individual subzones recorded dominantly pure shear deformation and low strain intensities (figs. 17K and 17L). The deformation was thus partitioned in a typical manner as observed in oblique transpressive zones (Teyssier and Tikoff, 1998; Schulmann and others, 2003) which calls for a rheological and mechanical explanation. The individual subzones probably correspond to different parts of a back-arc, arc, and accretionary prism which led Badarch and others (2002) to propose their suspect terrane model for this region. In contrast, we present a model in which the boundaries between individual subzones correspond to transform faults that developed during early Devonian arc and back-arc formation. When this system was subjected to compressive stress at high angles to the back-arc ridge axis, the transform boundaries may have been reactivated as dextral strike-slip faults, and the oceanic structure of the Devonian back-arc and arc system was displaced, thus disrupting the original polarity (figs. 17K and 17L). From a mechanical point of view, the oceanic basin with a well developed transform fault system should have behaved in a different way compared to the rheologically weak Gobi-Altai continental passive margin that was dominated by felsic lithologies and was additionally weakened by the Permian thermal event.

D_{3SG} deformation in the South Gobi Zone is documented by an important dextral shear zone that affected weak Paleozoic rocks due to the indentation effect of the strong and undeformable Gobi-Tienshan pluton. In particular, D_{3SG} deformation was

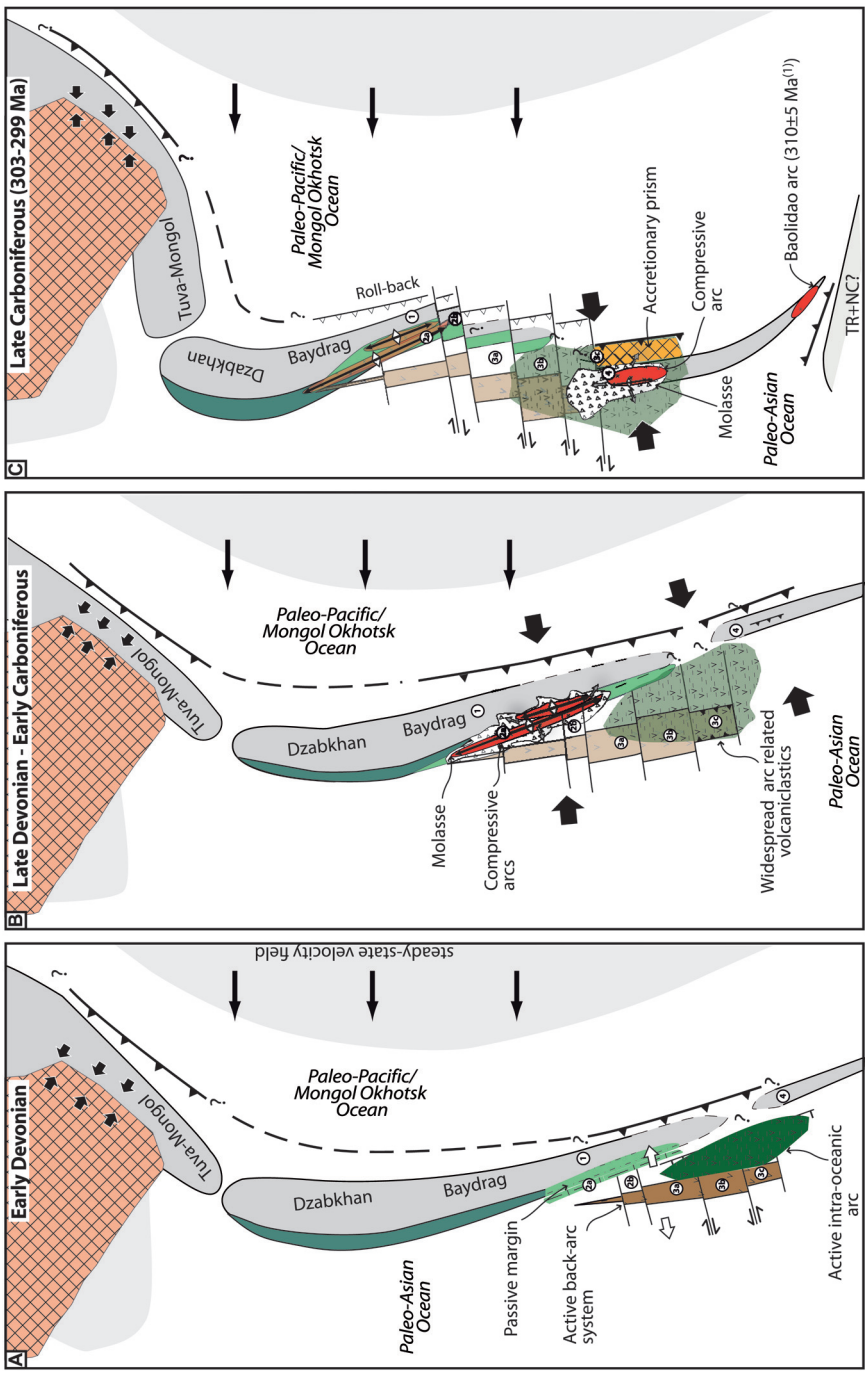

Fig. 18. Conceptual model for the Paleozoic evolution of the CAOB in SW Mongolia. (A) Early Devonian formation of island arc/back-arc systems in the rear of the N-S oriented Tuva-Mongol and Dzabkhan-Baydrag amalgamated continental ribbons. (B) Eastward migration of arcs to the continent in the Gobi-Altai Zone. (C) Locus of arc activity in the South Gobi Zone.

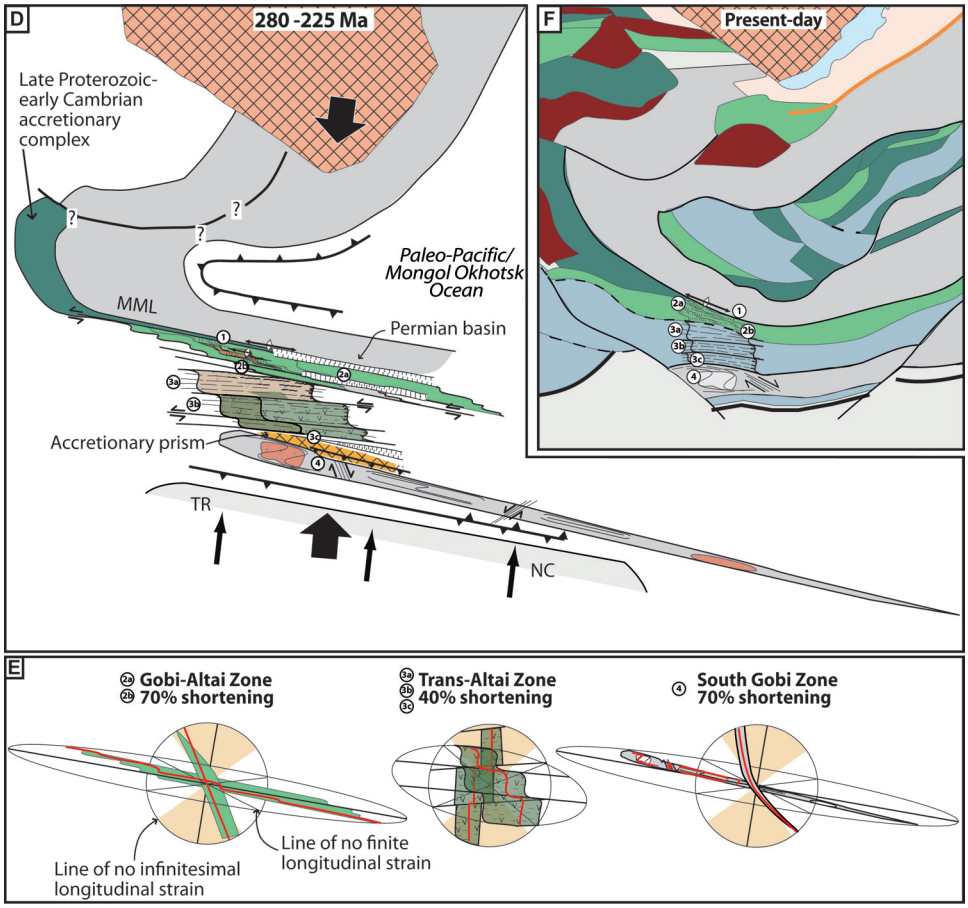

Fig. 18 (continued). (D) Orthogonal tectonic switch and onset of Permian-Triassic NNE-SSW directed shortening. Strongly contrasting deformation mechanisms between continental and oceanic domains were active as a function of the nature of the crust, the locus of Permian magmatism and the orientation of paleo-transform faults. (E) Change in shape for the bulk of each of the Gobi-Altai, Trans-Altai and South Gobi Zones as a result of a progressive pure shear represented in a strain ellipse. (F) Present-day structural trends in the study area. (1) From Chen and others (2009).

responsible for steep folding of the greenschist-facies Tömörtyn D_{1SG} mylonites together with unmetamorphosed Carboniferous rocks, whereas the D_{2SG} magmatic and migmatitic fabric remained shielded by the Gobi-Tienshan pluton carapace. This late deformation is also revealed by steep folding of early Triassic continental sequences and by the middle-late Triassic $^{40}Ar/^{39}Ar$ white mica age for the GTIC orthogneiss. Importantly, the Mesozoic D_{3SG} deformation indicates major but strongly heterogeneous shortening of the South Gobi Zone crust.

A new accretionary model for the CAOB in SW Mongolia (Fig. 18)

Previously published models for the evolution of the CAOB of Şengör and Natal'in (1996), Yakubchuk and others (2005), Zorin and others (1993), and Badarch and others (2002) are summarized in Appendix II. These models contain important elements of a large-scale geodynamic evolution, which is partly incompatible with the orthogonality, the duration, and the kinematics of deformation events as recorded in the CAOB of SW Mongolia. We therefore propose a new model that takes into account

the time and length scales of deformation events as well as their kinematic significance, compared with published paleontological and paleomagnetic constraints presented in Appendix II. This analysis shows that the orthogonal tectonics through most of the Paleozoic may have resulted from: 1) the pene-contemporaneous activity of two inward-dipping subduction zones operating at high angles to each other; 2) the westward-subduction producing an arc-back-arc domain at the rear of the Tuva-Mongol and Dzabkhan-Baydrag continental ribbons in the late Silurian and Devonian, followed by E-W shortening in the late Devonian–Carboniferous and N-S oroclinal bending during Permian-Triassic times.

A Penecontemporaneous Orthogonal Subduction System Terminated by Permo-Triassic Accretion

The model of Badarch and others (2002) assumes continuous southward migration of subduction zones and sequential northward accretion during the Devonian-Carboniferous and Permo-Triassic. However, the two parallel subduction zones spatially coinciding with the Trans-Altai and Gobi-Tienshan fault zones are not compatible with the tectonic orthogonality and time scales of tectonic events as presented in this study. Lamb and Badarch (1997, 2001) proposed a tectonic model similar to the progressive opening of the Philippine Sea, based on detailed sedimentology and volcanic geochemistry. The progressive opening of the Phillipine Sea satisfies the orthogonal evolution of an arc and back-arc assemblage (Hall, 2002; Queano and others, 2007) and can be tested as a viable model to generate the SW Mongolian CAOB.

A pre-requisite of our model is the preservation of a N-S tectonic zonation (in present coordinates), marked by the early Cambrian nappe stack of the Lake Zone in the north, the Ordovician thinned crust developed in the Gobi-Altai Zone and the Silurian to Devonian proximal and distal passive margins represented by the Gobi-Altai and Trans-Altai Zones, respectively. We also accept the polarity of the Devonian back-arc and island arc as proposed by Lamb and Badarch (1997, 2001). The development of back-arc and arc systems in the SW Mongolian part of the CAOB can be related to two well documented Paleozoic subduction zones: the E-W trending Mongol-Okhotsk suture zone in the north-east and the E-W trending Solonker suture in the south (in present-day coordinates). In order to develop the present structure of the SW Mongolian CAOB, a strongly contrasting mechanical behavior of individual tectonic zones is required during the entire tectonic evolution but specifically during Permo-Triassic times.

Our model considers the Proterozoic Tuva-Mongol and Dzabkhan-Baydrag blocks as N-S elongated microcontinents during the late Cambrian (Salnikova and others, 2001; Levashova and others, 2010). As they are both overlain by Cambrian accretionary complexes on their western margins (for example, fig. 2 of Badarch and others, 2002), we also believe that they were already stitched together in late Cambrian times. This N-S geometry is based on the existence of the Mongol-Okhotsk Ocean, which was interpreted as a N-S trending oceanic domain during the early Paleozoic (Zonenshain and others, 1978; Zorin and others, 1993; Zorin, 1999). Here, deep marine Silurian sediments are reported by Kurihara and others (2009) and clastic zircons in Devonian and Carboniferous sediments of central Mongolia show a provenance from both the Tuva-Mongol and Dzabkhan-Baydrag blocks (Kelty and others, 2008). These data corroborate the paleomagnetic reconstructions, suggesting that in Permian time, the northern margins of Mongolia and Siberia formed an angle of 80 to 120° (Zorin and others, 1993). All these observations imply that the Tuva-Mongol and Dzabkhan-Baydrag microcontinents were oriented N-S during early Paleozoic in present coordinates (fig. 18A). The paleogeographic position of the South Gobi Zone remains uncertain because neither Siberian nor North China Craton nor Tarim affinities can clearly be attributed to this region from Silurian to Permian times (Rong and others,

1995; see Appendix II for details). Therefore, the basement of the South Gobi Zone may correspond to a southern and distant part of the N-S trending trail of microcontinents. Our concept of N-S orientation of the continental blocks corroborates the model of N-S orientation of the Tarim block from the Ordovician to the Permian which may indicate a generalized trend of these microcontinents during this period (Xiao and others, 2009). Assuming a N-S orientation of these microcontinents, the opening of a Silurian to Devonian oceanic domain west of the Gobi-Altai passive margin suggests a west-dipping subduction zone located east of the Tuva-Mongol and Dzabkhan-Baydrag ribbons. The other implication of an E-W opening of the Trans-Altai back-arc basin is the E-W orientation of transform faults which will play a major role during the subsequent deformation events.

Late Devonian to Carboniferous E-W Convergence and Emplacement of Arcs

Figure 18A shows the N-S orientation of the main tectonic zones including the Mongol-Okhotsk subduction zone polarity in the early Devonian. The position of the Tuva-Mongol ribbon is in agreement with Delvaux and others (1995) who found Devonian compressive structures at the southern margin of the Siberian platform (Patom belt, fig. 1) and interpreted them in terms of NW-SE oriented collision between the northern part of the Tuva-Mongol microcontinent and Siberia. This supports a N-S pre-Devonian orientation of the Tuva-Mongol microcontinent and its westward drift during the early Devonian (fig. 18A).

A major result of our work is the interpretation of syn-convergent emplacement of magmatic arcs during E-W shortening in the Gobi-Altai Zone (figs. 4, 7 and 8), E-W shearing and shallow crustal thrusting in the area of the South Gobi Zone (figs. 13B and 17G), and emplacement of Silurian ophiolites associated with E-W folding of Devonian and early Carboniferous sequences in the Trans-Altai Zone (figs. 12 and 13). Magmatic arc activity essentially developed in the Gobi-Altai Zone and probably corresponds to eastward migration of an arc from the Trans-Altai Zone towards the trench. Sedimentological and clastic zircon studies (Lamb and Badarch, 2001; Kröner and others, 2010) report deposition of late Devonian volcanic rocks in the northern part of the Trans-Altai Zone (Khuvinkharin Subzone), in the Gobi-Altai Zone including Mandalovoo Subzone, and in the Lake Zone. This implies that all these units were already stitched together in late Devonian times and that the original polarity of the subduction zone system was preserved during the late Devonian to early Carboniferous compressive event (fig. 18B). This major shortening corroborates the NW-SE oriented collisional event in the area of the Patom belt in southern Siberia as shown in structural studies of Delvaux and others (1995) and de Boisgrollier and others (2009). NW-SE collision between Siberia and the northern part of the Tuva-Mongol continental block was coeval with E-W compressive deformation in the south, implying westward drift of the Tuva-Mongol ribbon (fig. 18B).

The E-W syn-convergent emplacement of a magmatic arc during E-W shortening was proposed in the South Gobi Zone in late Carboniferous times (figs. 12 and 13). Such compression has not been reported from the other CAOB tectonic zones, suggesting that subduction activity was concentrated in the southern part of the system. Because compression only occurred in the south, this part was displaced to the west compared to the stationary northern units (fig. 18C). We suggest that these differential movements were accommodated by dextral strike-slip movements employing previous transform zones, thereby producing an en-echelon displacement of the originally continuous and N-S trending arc and back-arc zones. The offset related to dextral strike-slip movement is most apparent in the position of the South Gobi Zone basement with respect to the southern Trans-Altai area (fig. 18C). The migration of E-W compression to the south also implies drag of the Tuva-Mongol basement around the Siberian promontory and drift of the Dzabkhan microcontinent to the west that

generated an oroclinal geometry around the southern Siberian promontory. This is consistent with the concept of Yakubchuk and others (2005) which implies Devonian oroclinal bending of the Tuva-Mongol ribbon due to draping around an obstacle (see Johnston, 2004 for explanations). In contrast to large amplitude folding as proposed by Yakubchuk (2008), other authors (for example Johnston, 2004) suggested that wrapping around an impinging salient may cause orocline formation, but the observed rotations should be small and associated with numerous strike-slip faults. The latter suggestion is more consistent with our model. This forced folding mechanism implies potentially frontal deformation, resulting in the formation of an early N-S striking compressive fabric. This is not fully compatible with the Yakubchuk (2008) concept where the accretionary prisms forming the Gobi-Altai and Trans-Altai zones only passively follow the shape of the more competent Tuva-Mongol and Dzabkhan-Baydrag microcontinents that constitute a large-scale accommodation structure (figs. 19B3, 19B4 and Appendix II).

Permian to Jurassic N-S convergence.—Our structural study shows that the major switch in orientation of the compressional axis occurred in the early Permian and that N-S shortening continued until the middle Jurassic. The deformation related to this event varies from north to south as a function of different rheological properties of the individual tectonic zones and their orientation prior to the orthogonal switch in the compressive axes. The Lake Zone reveals folding of the previously flat-lying late Cambrian fabrics, resulting in E-W striking upright folds and a steep cleavage. The fact that the Dariv, Khantaishir and Tsakhir Uul accretionary complexes are broadly aligned in an E-W direction parallel to the Main Mongolian lineament may imply passive rotation of the southern limb of the Tuva-Mongol Dzabkhan-Baydrag orocline. The important N-S shortening in the Lake Zone indicates that this fold limb already rotated to a high angle with respect to the N-S compression axis during mid-late Permian times.

The Gobi-Altai Zone preserves N-S striking planar relicts of the late Devonian to early Carboniferous E-W shortening that are locally strongly reworked by heterogeneous and recurrent E-W trending structures resulting from Permian NNE-SSW shortening. These relict fabrics can be explained by asymmetrical folding of the Gobi-Altai Zone that was originally oriented in a NNW-SSE direction. Such rheological behavior is possible due to the inherited and ubiquitous steep N-S attitude of the Devonian-Carboniferous fabric that is developed at all crustal levels of the Gobi-Altai Zone (figs. 18D and 18E). An estimate of the deformation intensity based on the passive rotation of litholigical boundaries yields about 70 percent of NNE-SSW shortening.

The Trans-Altai Zone shows a completely different structural record compared to the northerly continental domains. Here, cores of the individual subzones reveal weak structures related to Permo-Triassic shortening, whereas their margins show intense deformation associated with the exhumation of mantle rocks. This behavior may be explained by the reactivation of E-W trending transform faults which acted as sinistral strike-slip zones during NNE-SSW oriented compression. Sinistral displacement of the original early Devonian arc and back-arc structures of the Trans-Altai Zone produced an apparent N-S zonation as reported by Lamb and Badarch (2001). The weak internal deformation of rocks between the strike-slip faults can be explained by the rheological properties of stiff oceanic lithosphere which caused these rocks to be protected from strong deformation as relatively rigid blocks between rotating strike-slip faults. Bulk shortening of the Trans-Altai Zone was estimated at about 40 percent, using the same method as for the Gobi-Altai Zone (figs. 18D and 18E).

The South Gobi Zone contains relicts of NNW-SSE trending late Carboniferous fabrics registered in the syntectonic Gobi-Tienshan magmatic arc. Permo-Jurassic

shortening is heterogeneously developed here, so that the Gobi-Tienshan pluton behaved as a rigid body deflecting the ductile shear zones. This behavior may be interpreted as a result of folding of a NW-SE trending ribbon that has subsequently been stretched and unfolded in an extensional sector of finite strain. The originally steep late Carboniferous structure was protected by the carapace of the magmatic arc, whereas the remaining continental ribbon was stretched and sheared. The dextral Tömörtyn shear zone is interpreted as one of these extensional shears that developed during layer-perpendicular compression in the sense of Kidan and Cosgrove (1996). The estimated shortening of the South Gobi Zone yields a value of about 70 percent.

The regional shortening of the entire system is more than 60 percent which is in agreement with paleontological studies showing that the late Permian floral assemblage in the South Gobi Zone is a mixture of North Cathaysian (North China affinity) and Angaran (Siberian affinity) species (Johnson and others, 2008 and references therein). Dewey and others (1988) and Xiao and others (2008) interpreted this mixed floral zone as representing a major suture (Solonker suture of Xiao and others, 2003) in the late Paleozoic along which the Tarim and North China cratons collided with the southern peri-Siberian zones. Paleomagnetic studies confirm that the Tarim block did not dock with peri-Siberian zones until the early Permian (Cocks and Torsvik, 2007), accretion of North China to Mongolia occured around the early/late Permian boundary (Zorin 1999, and references therein) and to Siberia after closure of the Mongol-Okhotsk Ocean in the middle Jurassic (Cocks and Torsvik, 2007). This mid-Jurassic closure of the Mongol-Okhotsk Ocean is consistent with ages reported by Tomurtogoo and others (2005). All these data are compatible with progressive shortening of an originally N-S striking continental ribbon bordered by two oceanic domains.

CONCLUDING REMARKS

We suggest that the contrasting behavior of individual tectonic zones as described above was only possible because of the presence of paleo-transform faults which accommodated lateral displacement by discrete strike-slip partitioning mechanisms (Tikoff and Teyssier, 1994). An additional important factor was the contrasting rheological properties of individual tectonic zones. Whereas the Gobi-Altai Zone was thermally softened due to widespread Permian magmatism, the Trans-Altai Zone remained cool and competent and was therefore internally almost undeformable. In contrast, the South Gobi Zone was rheologically weaker than the Trans-Altai oceanic domain because of the late Carboniferous magmatism and a dominantly felsic composition. In addition, the distance to promontories on the northward-moving North China and Tarim cratons was probably small which makes it likely that high strain concentration was induced by indentation effects (England and Houseman, 1986; Ježek and others, 2002).

The model presented above shows a number of elements typical for SE Asia (Hall, 2009) with aligned continents and two competing subduction zones. The most important is the orthogonal tectonic switch related to N-S Permo-Triassic convergence that was responsible for major N-S shortening of the entire SW Mongolian paleo-oceanic system. It was during this event that all previously formed oceanic arc and back-arc systems, Japan-type arcs and the Dzabkhan-Baydrag microcontinent were deformed together and experienced anticlockwise rotation associated with the development of an oroclinal structure. A similar switch is only in its intial stage in the present Phillipine Sea as shown by modern palinspastic reconstructions based on GPS data from the Timor area (Pubellier and others, 2003). Nevertheless, the dominant N-S convergence is expected to propagate into the western Pacific due to continous northward drift of the Australian plate (Hall, 2002; Pubellier and others, 2003) and will eventually produce an E-W trending accretionary orogen (Hall, 2009) similar to the Mongolian CAOB.

ACKNOWLEDGMENTS

Funding through the French CNRS and Strasbourg University for fieldwork in Mongolia and a salary for Ondrej Lexa during his visit to Strasbourg are gratefully acknowledged. The grant MSM0021620855 of the Ministry of Education of the Czech Republic is acknowledged for salary and financial support of Ondrej Lexa. We thank Annie Bouzeghaia for help in drawing figures 17, 18 and 19 and Michel Manetti for help in the separation of micas. We acknowledge constructive reviews by J. F. Dewey and B. F. Windley.

Appendix I: analytical methods for $^{40}Ar/^{39}Ar$ age determinations

Mineral separates of white mica were obtained after crushing and handpicking of single grains ranging from 0.5 to 1 mm under a binocular microscope. The minerals were repeatedly cleaned ultrasonically in distilled water. The crystals were then co-irradiated for 30 h in the nuclear reactor at McMaster University in Hamilton (Canada) in position 5c, along with Hb3gr hornblende monitor (1072 Ma; Turner and others, 1971). $^{40}Ar/^{39}Ar$ analyses were performed at the Geoazur laboratory in Nice. Two minerals were heated with a CO_2 Synrad laser. The gas was purified in a stainless and glass extraction line using two Al-Zr getters (working at 400°C and ambient temperature, respectively) and a liquid nitrogen cold trap. Isotopic measurements were performed in a VG3600 mass spectrometer equipped with a Daly-photomultiplier system. Blank measurements were obtained before and after every three sample runs (table 1). The correction factors for interfering isotopes correspond to $(^{39}Ar/^{37}Ar)_{Ca} = (7.30 \pm 0.28) \times 10^{-4}$; $(^{36}Ar/^{37}Ar)_{Ca} = (2.82 \pm 0.03) \times 10^{-4}$ and $(^{40}Ar/^{39}Ar)_{K} = (2.97 \pm 0.06) \times 10^{-2}$. Ages were calculated using the decay constants of Steiger and Jäger (1977) and an air $^{40}Ar/^{36}Ar$ ratio of 298.56 ± 0.1% (at 1σ) (Lee and others, 2006). *J*-values ranged from 0.0035309 ± 0.0000177 (=0.5% at hh1s) to 0.0035312 ± 0.0000177 (=0.5% at 1s). Mass discrimination values ranged from 1.00474 to 1.00738 ± 1% (1σ) per dalton (atomic mass unit). The spectrometer sensitivity was an average 2.0 E-14 moles/V. The criteria for defining plateau ages were as follows: 1) a plateau age should contain at least 70% of the released ^{39}Ar; 2) there should be at least three successive steps in the plateau; and 3) the integrated age of the plateau should agree with each apparent age of the plateau within a 1σ error confidence interval.

Appendix II: paleogeographic and geodynamic constraints on the formation of the CAOB in SW Mongolia

We present here a review of several previous studies and geotectonic models of the CAOB so that interested readers can compare our data and interpretations with published databases.

Paleontology and Paleomagnetic Constraints

Well-studied Cambrian sequences of the Lake and Gobi-Altai Zones enclose a typical Siberian trilobite fauna and Archaeocythan reefs (Cocks and Torsvik, 2007). According to Rong and Zhang (1982), the Silurian-Devonian strata of the South Gobi Zone do not contain brachiopods (*Tuvaella*) of Siberian affinity, which according to Badarch and others (2002), may suggest that this unit is a fragment of Tarim or of the North China craton. However, maps published by Rong and others (1995) show that the location of the southernmost occurrences of this fauna is bordering the northern boundary of the South Gobi Zone (fig. 1B), which places the Trans-Altai Zone into a peri-Siberian oceanic domain in Silurian times. Furthermore, the most northern locations of the *Retziella* fauna, which is the ecological equivalent of *Tuvaella* but endemic to the Cathaysian paleogeographic province, are located south of the Solonker suture (Rong and others, 1995). Importantly, the location of the paleogeographic boundary between North Cathaysian (North China affinity) and Angaran (Siberian affinity) flora broadly follows the present 42°N parallel south of the South Gobi Zone (Dewey and others, 1988) in late Permian times (fig. 1B). The late Permian floral assemblage in the central part of the South Gobi Zone (Noyon Uul) contains a mixture of these two paleogeographic affinities (Johnson and others, 2008 and references therein). Dewey and others (1988) and Xiao and others (2008) interpreted this mixed flora zone as representing a major suture in late Paleozoic along which the Tarim and North China collided with the southern peri-Siberian zones.

The paleogeographic position of Siberia through the Paleozoic was synthetized by Cocks and Torsvik (2007). The northern drift of Siberia and Peri-cratonic terranes began in the Cambrian and peaked at either 13 cm/a between 450 and 440 Ma (Cocks and Torsvik, 2007) or at 20 to 25 cm/a in the late Devonian (Buslov and others, 2001). Apparent polar wander path in Cocks and Torsvik (2007, their figs. 3 and 4) shows counter-clockwise rotation of Siberia between 439 and 360 Ma. From the late Devonian to the Late Permian Siberia rotated again but in a clockwise sense (total rotation about 75°) while continuously drifting

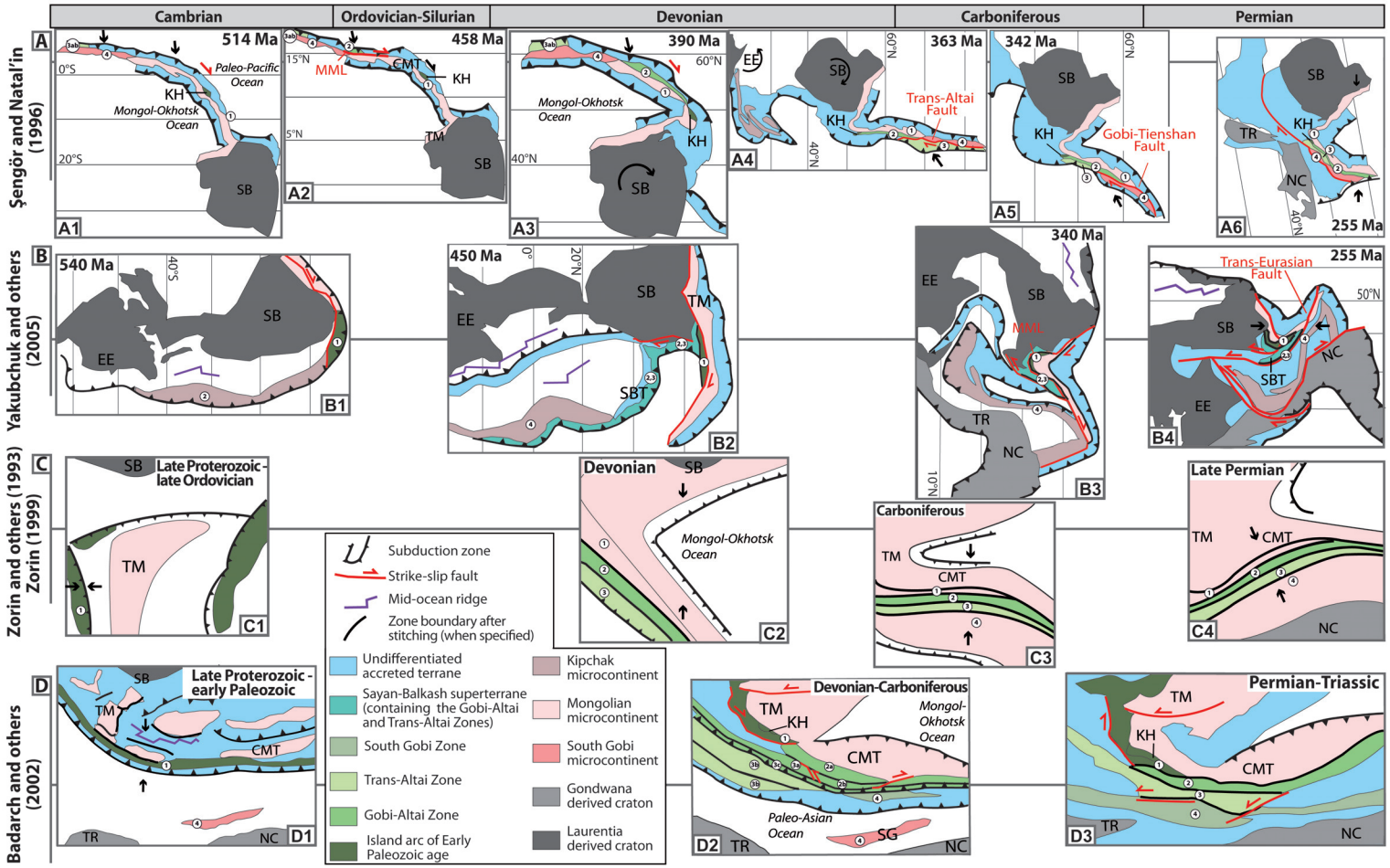

Fig. 19. Synthesis of the main published conceptual models related to the Paleozoic evolution of the CAOB in Mongolia and southern Siberia. The models (A) of Şengör and Natal'in (1996) and (B) of Yakubchuk and others (2005) take into account paleomagnetic and paleontological constraints that existed at the time of publication in contrast to models (C) of Zorin and others (1993) and (D) by Badarch and others (2002). We therefore applied the appropriate rotations around a vertical axis to the two last above-mentioned models C and D to keep consistency with models A and B. Circled numbers refer to tectonic zones as in fig. 1B. CMT: Central Mongolian Terrane; EE: East European Craton; KA: Kazakhstan terrane collage; KH: Khantaishir ophiolite complex; NC: North China Craton; SB: Siberian Craton; SBT: Sayan-Balkhash turbiditic Superterrane; SG: South Gobi Microcontinent; TM: Tuva-Mongol block; TR: Tarim Craton; (see also fig. 1A).

northward. The southern margin of Siberia still formed an angle of about 80° with respect to the northern margin of Mongolia during the late Permian (Zorin and others, 1993). As a result, the present-day tectonic zonation (fig. 1B) was almost inverted in the early Cambrian. The position between Siberia and Mongolia was mainly accomodated by the dynamics of the Mongol-Okhotsk Ocean. Kravchinsky and others (2001) suggested that the western part of the Tuva-Mongol block, which constituted the northern seabord of this ocean, was already close to Siberia in late Neoproterozoic and early Cambrian times. Accordingly, no vast oceanic domain is likely to have existed between the Mongolian Precambrian units and Siberia at this time. There is no difference between early Cretaceous paleopoles for the Siberian and Mongolian sides of the Mongol-Okhotsk suture, confirming a pre-early Cretaceous (Cogné and others, 2005), most likely Jurassic (Kravchinsky and others, 2002) closure of the Mongol-Okhotsk Ocean. The Tarim block was docked to peri-Siberian zones during the Permian (Li and others, 1988a, 1988b) and experienced little or no apparent polar wander since the Carboniferous (Gilder and others, 2008). The North China block accreted with Mongolia in the late Permian to earliest Triassic (Xiao and others, 2008) and with Siberia after closure of the Mongol Okhotsk Ocean but not until the Jurassic (Cocks and Torsvik, 2007).

Review of Published Tectonic Models for the CAOB (Fig. 19)

The four conceptual models presented in figure 19 focus on the growth of the CAOB through the Paleozoic by accretion onto the Siberian craton. The first group of models (Şengör and others, 1993; Şengör and Natal'in, 1996, fig. 19A; Yakubchuk and others, 2005; Yakubchuk, 2008, fig. 19B; Zorin and others, 1993; Zorin, 1999, fig. 19C) suggests that the CAOB formed by imbrication of at least one oroclinally folded Precambrian continental ribbon, beginning in the late Neoproterozoic to early Cambrian. The second group of models (Badarch and others, 2002; Windley and others, 2007, fig. 19D) refutes the existence of a single pre-accretionary continental ribbon and prefers an Indonesian-type of geodynamic scenario with subduction zones operating since the beginning of the Neoproterozoic. An analysis of the above geotectonic models is carried out in order to find the most plausible evolutionary scenario which satisfies the results of our structural study.

Single Arc Oroclinal bending models.—The main mechanism involved in the model of Şengör and others (1993) and Sengör and Natal'in (1996) is the shaving off and slicing of accretionary wedges formed along a long island arc (the Kipchak arc). This mechanism can only operate for: 1) oblique and steady-state subduction allowing strike-slip movement to occur parallel to the arc, and 2) a straight and elongated magmatic zone enhancing arc parallel strike-slip movement.

At the end of the Proterozoic, a narrow and elongate sliver of Precambrian continental crust was detached from the Siberian nucleus and rotated counterclockwise with the rotation axis located at the hinge of the Tuva-Mongol Massif. Thus, the oroclinal nature of the orogen was already acquired in Cambrian times. The continental ribbon composed of both the Tuva-Mongol Massif and the South Gobi microntinent was bounded by two subduction zones with opposite polarities which produced peripherally growing accretionary wedges (fig. 19A1 at 514 Ma). These accretionary complexes were duplicated by right-lateral strike-slip faulting along the margin of the straight continental ribbon. The Gobi-Altai Zone (a Cambrian to Silurian accretionary complex) was transported parallel to the Lake Zone through pre-Devonian movement along the Main Mongolian Lineament (fig. 19A2 at 458 Ma). This episode was followed by translation of the Trans-Altai Zone and its attached Gobi-Altai Zone along the Trans-Altai fault during the late Devonian (figs. 19A3 and 19A4 at 390 and 363 Ma, respectively). Finally, the South Gobi Zone was detached, translated and attached to the Trans-Altai Zone during early Carboniferous movement along the Gobi-Tienshan fault zone (figs. 19A5 and 19A6 at 342 and 255 Ma, respectively).

The models of Yakubchuk and others (2005) and Yakubchuk (2008) represent a modification of the concept of Şengör and others (1993). The controlling features for the accretion of the CAOB in these models are: (1) clockwise rotation of Siberia during the middle Devonian to Carboniferous and, (2) northward drift of the joined North China and Tarim cratons from the Devonian to the late Paleozoic. The rotation of Siberia was responsible for oroclinal bending of the Tuva-Mongol and Kipchak ribbon continents (figs. 19B1 and 19B2 at 540 and 450 Ma, respectively) that were isoclinally folded and amalgamated during ongoing collision with the southern continental masses (figs. 19B3 and 19B4 at 340 and 255 Ma, respectively).

The figure 19B1 shows that the composite Tuva-Mongol and Kipchak ribbon was detached from Siberia and the East European Craton (Baltica) during the Cambrian, due to opening of a large back-arc basin located above a west-dipping subduction zone. From the end of the Cambrian to the Silurian (fig. 19B2), the Tuva-Mongol ribbon continent was separated from the remaining Kipchak ribbon and translated dextrally along the northern margin of the Siberian craton. At the same time, the northern part of the remaining Kipchak ribbon collided with the eastern margin of Siberia. The Gobi-Altai and Trans-Altai Zones were generated in Ordovician time as accretionary wedges of the Kipchak subduction system [Sayan-Balkhash turbiditic Superterrane of Yakubchuk and others (2005)], whereas the South Gobi Zone was located far to the south of the Kipchak ribbon (fig. 19B2 at 450 Ma). During the Silurian to middle

Devonian, the Tuva-Mongol arc and the Kipchak and Sayan-Balkash superterranes were amalgamated (fig. 19B3 at 340 Ma), generating large-scale folding and producing a large orocline. The South Gobi Zone was located at the highly attenuated limb of the folded Kipchak ribbon which was progressively accreted to the eastern long limb of the Tuva-Mongol orocline. Finally, the entire system was affected by late Permian, predominantly left-lateral, strike-slip movement coinciding with the Main Mongolian Lineament and the Gobi-Tienshan fault zones as a result of indentation effects of the combined North China and Tarim cratons. The principal offset occurred along the late Paleozoic to early Triassic Trans-Eurasian sinistral strike-slip fault with an offset of as much as 1000 km (fig. 19B4 at 255 Ma).

Zorin and others (1993) and Zorin (1999) presented a model for closure of the Mongol-Okhotsk Ocean which is geometrically similar to the oroclinal bending. However, according to these authors, the Tuva-Mongol microcontinent was not attached to the Siberian craton in early Cambrian times and, therefore, a folding event is not specified. The Tuva-Mongol Masssif represented an E-W elongated continental ribbon that was flanked by two opposite oceanward-directed subduction zones on its northern and southern margins. The southern island arc generated the Lake Zone whereas the northern one produced the Bayankhongor ophiolite (figs. 1B and 19C1 in late Neoproterozoic to late Ordovician times). E-W collision between the Tuva-Mongol Massif, the Lake Zone island arc and the Siberian craton occurred at the end of the Cambrian. Orthogonal middle Ordovician accretion of the Lake Zone with the Tuva-Mongol continent was followed by late Ordovician to late Silurian accretion of the Bayankhongor island arc. During the Devonian, the Tuva-Mongol Peninsula rotated counterclockwise progressively closing the Mongol-Okhotsk Ocean until the late Permian. The ocean was consumed through two continentward-inclined subduction zones, both beneath Siberia and the Tuva-Mongol ribbon. The Ordovician to Devonian Gobi-Altai and Trans-Altai passive margins were located south of the Lake Zone and were tectonically inverted during the Devonian. This event was associated with the formation of a north-directed subduction zone riming the southern part of the Trans-Altai Zone (the Dzolen Subzone) (fig. 19C2 in Devonian time). In early Carboniferous times, the South Gobi microcontient collided with the entire system, thus closing the marine domain south of the Trans-Altai and Gobi-Altai Zones (fig. 19C3 in Carboniferous time). The subduction zone jumped south of the South Gobi microcontinent until the amalgamation of the North China craton with the Peri-Siberian domain which was completed in late Permian times (fig. 19C4 in the late Permian).

Exotic terranes accretion models.—Badarch and others (2002), Windley and others (2007), Kröner and others (2007) and Xiao and others (2009) proposed evolutionary models for the CAOB by opening and closure of small ocean basins and accretion of back-arcs, island arcs and small basement nuclei. Badarch and others (2002) divided the Tuva-Mongol Massif into six different blocks and the eastern Central Mongolian Assemblage into three separate cratonic terranes (fig. 19D1). The Lake Zone was interpreted as an island arc and the Bayankhongor ophiolite as back-arc oceanic crust of early Cambrian age and related to a subduction zone inclined towards the continent (for example Khain and others, 2003). Frontal N-S accretion of the Lake Zone to the southern part of the Central Mongolian Assemblage was expected to have occurred in the early Cambrian to middle Ordovician (fig. 19D1, in the late Neoproterozoic–early Paleozoic). In Devonian-Carboniferous times (fig. 19D2), the Gobi-Altai and Trans-Altai Zones were generated during the development of a new southward-directed subduction zone whereas the earlier subduction zone in the north still operated and produced an accretionary wedge—the Dzolen Subzone. Stacking of the northern part of the Trans-Altai and the southern Mandalovoo Subzone occurred through strike-slip at this time. The South Gobi Zone was interpreted as a composite domain, containing fragments of a back-arc that formed along strike of the Trans-Altai Zone and the South Gobi microcontinent. Formation of the South Gobi Zone and the actual geometry of the Gobi-Altai and the Trans-Altai Zones were acquired during Permian-Triassic strike-slip displacement along the Gobi-Tienshan and Tost faults (Lamb and others, 1999) (fig. 19D3 at Permian-Triassic time).

REFERENCES

Alekseyeva, R. E., 1993, Biostratigraphy of Devonian of Mongolia: Moscow, Nauka Press, Transactions of Joint Soviet-Mongolian Paleontological Expedition, 135 p. (in Russian).

Amantov, V. A., Blagonravov, V. A., Borzakovskiy, Y. A., Durante, M. V., Zonenshain, L. P., Luvsandanzan, B., Matrosov, P. S., Suyetenko, O. D., Filippova, I. B., and Hasin, R. A., 1970, Main features of Paleozoic stratigraphy of Mongolian People's Republic, *in* Zaitsev, N. S., Luvsandanzan, B., and Marinov, N. A., editors, Stratigraphy and tectonics of the Mongolian People's Republic: Moscow, Nauka Press, p. 8–63 (in Russian).

Badarch, 1990, ms, Tectonics of the south Mongolian fold belt: Ulaanbaatar, Töv, Mongolia, Mongolian Academy of Sciences and Mongolian Technical University, Ph. D. thesis (in Russian).

Badarch, G., Cunningham, W. D., and Windley, B. F., 2002, A new terrane subdivision for Mongolia: implications for the Phanerozoic crustal growth of Central Asia: Journal of Asian Earth Sciences, v. 21, p. 87–110, doi: 10.1016/S1367-9120(02)00017-2.

Baljinnyam, I., Bayasgalan, A., Borisov, B. A., Cisternas, A., Dem'yanovich, M. G., Ganbaatar, L., Kochetkov, V. M., Kurushin, R. A., Molnar, P., Philip, H., and Vashchilov, Y. Y., 1993, Ruptures of major earthquakes and active deformation in Mongolia and its surroundings: Geological Society of America, Memoir 181, 62 p.

Bayasgalan, A., Jackson, J., and McKenzie, D., 2005, Lithosphere rheology and active tectonics in Mongolia: relations between earthquake source parameters, gravity and GPS measurements: Geophysical Journal International, v. 163, p. 1151–1179, doi: 10.1111/j.1365-246X.2005.02764.x.

Bibikova, E. V., Kirnozova, T. I., Kozakov, I. K., Kotov, A. B., Neymark, L. A., Gorokhovskiy, B. M., and Shuleshko, I. K., 1992, U-Pb ages for polymetamorphic complexes on the southern flank of Mongolian and Gobi-Altai: Geotectonics, v. 26, p. 166–172.

Buslov, M. M., Saphonova, I. Yu., Watanabe, T., Obut, O. T., Fujiwara, Y., Iwata, K., Semakov, N. N., Sugai, Y., Smirnova, L. V., and Kazansky, A. Yu., 2001, Evolution of the Paleo-Asian Ocean (Altai-Sayan Region, Central Asia) and collision of possible Gondwana-derived terranes with the southern marginal part of the Siberian continent: Geosciences Journal, v. 5, p. 203–224, doi: 10.1007/BF02910304.

Calais, E., Vergnolle, M., San'kov, V., Lukhnev, A., Miroshnitchenko, A., Amarjargal, S., and Déverchère, J., 2003, GPS measurements of crustal deformation in the Baikal-Mongolia area (1994-2002): Implications for current kinematics of Asia: Journal of Geophysical Research, v. 108, 2501, 13 p., doi: 10.1029/2002JB002373.

Chen, B., Jahn, B. M., and Tian, W., 2009, Evolution of the Solonker suture zone: Constraints from zircon U-Pb ages, Hf isotopic ratios and whole-rock Nd-Sr isotope compositions of subduction- and collision-related magmas and forearc sediments: Journal of Asian Earth Sciences, v. 34, p. 245–257, doi: 10.1016/j.jseaes.2008.05.007.

Cocks, L. R. M., and Torsvik, T. H., 2007, Siberia, the wandering northern terrane, and its changing geography through the Palaeozoic: Earth-Science Reviews, v. 82, p. 29–74, doi: 10.1016/j.earscirev.2007.02.001.

Cogné, J. P., Kravchinsky, V. A., Halim, N., and Hankard, F., 2005, Late Jurassic–Early Cretaceous closure of the Mongol-Okhotsk Ocean demonstrated by new Mesozoic palaeomagnetic results from the Trans-Baikal area (SE Siberia): Geophysical Journal International, v. 163, p. 813–832, doi: 10.1111/j.1365-246X.2005.02782.x.

Collins, W. J., 2002a, Nature of extensional accretionary orogens: Tectonics, v. 21, 24 p., doi: 10.1029/2000TC001272.

——— 2002b, Hot orogens, tectonic switching, and creation of continental crust: Geology, v. 30, p. 535–538, doi: 10.1130/0091-7613(2002)030<0535:HOTSAC>2.0.CO;2.

Cunningham, W. D., Windley, B. F., Dorjnamjaa, D., Badamgarov, J., and Saandar, M., 1996, Late Cenozoic transpression in southwestern Mongolia and the Gobi-Altai-Tien Shan connection: Earth and Planetary Science Letters, v. 140, p. 67–81, doi: 10.1016/0012-821X(96)00048-9.

de Boisgrollier, T., Petit, C., Fournier, M., Leturmy, P., Ringenbach, J. C., San'kov, V. A., Anisimova, S. A., and Kovalenko, S. N., 2009, Palaeozoic orogeneses around the Siberian craton: Structure and evolution of the Patom belt and foredeep: Tectonics, v. 28, 18 p., TC1005, doi: 10.1029/2007TC002210, 2009.

Delvaux, D., Moeys, R., Stapel, G., Melnikov, A., and Ermikov, V., 1995, Palaeostress reconstructions and geodynamics of the Baikal region, Central Asia, Part I. Palaeozoic and Mesozoic pre-rift evolution: Tectonophysics, v. 252, p. 61–101, doi: 10.1016/0040-1951(95)00090-9.

Demoux, A., Kröner, A., Hegner, E., and Badarch, G., 2009a, Devonian arc-related magmatism in the Tseel terrane of SW Mongolia: chronological and geochemical evidence: Journal of the Geological Society, London, v. 166, p. 459–471, doi: 10.1144/0016-76492008-090.

Demoux, A., Kröner, A., Liu, D., and Badarch, G., 2009b, Precambrian crystalline basement in southern Mongolia as revealed by SHRIMP zircon dating: International Journal of Earth Sciences, v. 98, p. 1365–1380, doi: 10.1007/s00531-008-0321-4.

Dewey, J. F., Shackleton, R. M., Chang, C. F., and Sun, Y. Y., 1988, The tectonic evolution of the Tibetan Plateau: Philosophical Transactions of the Royal Society of London, v. A327, p. 379–413.

England, P., and Houseman, G., 1986, Finite strain calculations of continental deformation; 2. Comparison with the India-Asia collision zone: Journal of Geophysical Research, B, v. 91, p. 3664–3676, doi: 10.1029/JB091iB03p03664.

Gibsher, A. S., Khain, E. V., Kotov, A. B., Sal'nikova, E. V., Kozakov, I. K., Kovach, V. P., Yakovleva, S. Z., and Fedoseenko, A. M., 2001, Late Vendian age of the Han-Taishiri ophiolite complex in western Mongolia: Russian Geology and Geophysics, v. 42, p. 1110–1117.

Gilder, S. A., Gomez, J., Chen, Y., and Cogné, J. P., 2008, A new paleogeographic configuration of the Eurasian landmass resolves a paleomagnetic paradox of the Tarim Basin (China): Tectonics, v. 27, TC1012, 19 p., doi: 10.1029/2007TC002155.

Hall, R., 2002, Cenozoic geological and plate tectonic evolution of SE Asia and the SW Pacific: Computer-based reconstructions, model and animations: Journal of Asian Earth Sciences, v. 20, p. 353–431, doi: 10.1016/S1367-9120(01)00069-4.

——— 2009, The Eurasian SE Asian margin as a modern example of an accretionary orogen: Geological Society, London, Special Publication, v. 318, p. 351–372, doi: 10.1144/SP318.13.

Hanžl, P., and Aichler, J., 2007, Geological survey of the Mongolian Altay at a scale 1:50,000 (Zamtyn nurru—50): Prague, Czech Republic, Czech Geological Survey, Final Report, 389 p.

Helo, C., Hegner, E., Kröner, A., Badarch, G., Tomurtogoo, O., Windley, B. F., and Dulski, P., 2006, Geochemical signature of Paleozoic accretionary complexes of the Central Asian Orogenic Belt in South Mongolia: Constraints on arc environments and crustal growth: Chemical Geology, v. 227, p. 236–257, doi: 10.1016/j.chemgeo.2005.10.003.

Hendrix, M. S., Graham, S. A., Amory, J. Y., and Badarch, G., 1996, Noyon Uul syncline, southern Mongolia: Lower Mesozoic sedimentary record of the tectonic amalgamation of central Asia: Geological Society of America Bulletin, v. 108, p. 1256–1274, doi: 10.1130/0016-7606(1996)108<1256:NUSSML>2.3.CO;2.

Hrdličková, K., Bolormaa, K., Buriánek, D., Hanžl, P., Gerdes, A., and Janoušek, V., 2008, Petrology and age of metamorphosed rocks in tectonic slices inside the Paleozoic sediments of the eastern Mongolian Altay, SW Mongolia: Journal of Geosciences, v. 53, p. 139–165.

Hutton, D. H. W., and Dewey, J. F., 1986, Palaeozoic terrane accretion in the western Irish Caledonides: Tectonics, v. 5, p. 1115–1124, doi: 10.1029/TC005i007p01115.
Hutton, D. H. W., and Reavy, R. J., 1992, Strike-slip tectonics and granite petrogenesis: Tectonics, v. 11, p. 960–967, doi: 10.1029/92TC00336.
Ingram, G. M., and Hutton, D. H. W., 1994, The Great Tonalite Sill: emplacement into a contractional shear zone and implications for late Cretaceous to early Eocene tectonics in southeastern Alaska and British Columbia: Geological Society of America Bulletin, v. 106, p. 715–728, doi: 10.1130/0016-7606(1994)106<0715:TGTSEI>2.3.CO;2.
Jahn, B. M., 2004. The Central Asian Orogenic Belt and growth of the continental crust in the Phanerozoic, *in* Malpas, J., Flechter, C. J. N., Ali, J. R., and Aitchison, J. C., editors, Aspects of the tectonic evolution of China: Geological Society, London, Special Publications, v. 226, p. 73–100, doi: 10.1144/GSL.SP.2004.226.01.05.
Ježek, J., Schulmann, K., and Thompson, A. B., 2002, Strain partitioning in front of an obliquely convergent indenter, *in* Bertotti, G., Schulmann, K., and Cloethingh, S., editors, Continental collision and the tectonosedimentary evolution of forelands: European Geophysical Society, Stephan Mueller Special Publication Series, v. 1, p. 93–104.
Johnson, C. L., Amory, J. A., Zinniker, D., Lamb, M. A., Graham, S. A., Affolter, M., and Badarch, G., 2008, Sedimentary response to arc-continent collision, Permian, southern Mongolia: Geological Society of America Special Papers, v. 436, p. 363–390, doi: 10.1130/2008.2436(16).
Johnston, S. T., 2001, The Great Alaskan Terrane Wreck: Reconciliation of paleomagnetic and geological data in the Northern Cordillera: Earth and Planetary Science Letters, v. 193, p. 259–272, doi: 10.1016/S0012-821X(01)00516-7.
——— 2004, The New Caledonia-D'Entrecasteaux orocline and its role in clockwise rotation of the Vanuatu–New Hebrides Arc and formation of the North Fiji Basin: Geological Society of America Special Papers, v. 383, p. 225–236, doi: 10.1130/0-8137-2383-3(2004)383[225:TNCOAI]2.0.CO;2.
Kelty, T. K., Yin, A., Dash, B., Gehrels, G. E., and Ribeiro, A. E., 2008, Detrital-zircon geochronology of Paleozoic sedimentary rocks in the Hangay-Hentey basin, north-central Mongolia: Implications for the tectonic evolution of the Mongol-Okhotsk Ocean in central Asia: Tectonophysics, v. 451, p. 290–311, doi: 10.1016/j.tecto.2007.11.052.
Khain, E. V., Bibikova, E. V., Sal'nikova, E. B, Kröner, A., Gibsher, A. S., Didenko, A. N., Degtyarev, K. E., and Fedotova, A. A., 2003, The Palaeo-Asian ocean in the Neoproterozoic and early Palaeozoic: new geochronologic data and palaeotectonic reconstructions: Precambrian Research, v. 122, p. 329–358, doi: 10.1016/S0301-9268(02)00218-8.
Kidan, T. W., and Cosgrove, J. W., 1996, The deformation of multilayers by layer-normal compression; an experimental investigation: Journal of Structural Geology, v. 18, p. 461–474, doi: 10.1016/0191-8141(95)00099-Y.
Koppers, A. A. P., 2002, ArArCALC-software for $^{40}Ar/^{39}Ar$ age calculations: Computer & Geosciences, v. 28, p. 605–619, doi: 10.1016/S0098-3004(01)00095-4.
Kovalenko, V. I., Yarmolyuk, V. V., and Bogatikov, O. A., 1995, Magmatism, geodynamics and metallogeny of Central Asia: Moscow, MIKO, Commercial Herald Publishers, 272 p.
Kozakov, I. K., Glebovitsky, V. A., Bibikova, E. V., Azimov, P. Y., and Kirnozova, T. I., 2002, Hercynian granulites of Mongolian and Gobian Altai: geodynamic setting and formation conditions: Doklady Earth Sciences, v. 386, p. 781–785.
Kravchinsky, V. A., Konstantinov, K. M., and Cogné, J. P., 2001, Palaeomagnetic study of Vendian and Early Cambrian rocks of South Siberia and Central Mongolia: Was the Siberian platform assembled at this time?: Precambrian Research, v. 110, p. 61–92, doi: 10.1016/S0301-9268(01)00181-4.
Kravchinsky, V. A., Sorokin, A. A., and Courtillot, V., 2002, Paleomagnetism of Paleozoic and Mesozoic sediments from the southern margin of Mongol-Okhotsk ocean, far eastern Russia: Journal of Geophysical Research B: Solid Earth, v. 107, 2253, 22 p., doi: 10.1029/2001JB000672.
Kretz, R., 1983, Symbols for rock-forming minerals: American Mineralogist, v. 68, p. 277–279.
Kröner, A., Windley, B. F., Badarch, G., Tomurtogoo, O., Hegner, E., Jahn, B. M., Gruschka, S., Khain, E. V., Demoux, A., and Wingate, M. T. D., 2007, Accretionary growth and crust formation in the Central Asian Orogenic Belt and comparison with the Arabian-Nubian shield: Geological Society of America, Memoir, v. 200, p. 181–209, doi: 10.1130/2007.1200(11).
Kröner, A., Lehmann, J., Schulmann, K., Demoux, A., Lexa, O., Tomurhuu, D., Štípská, P., Otgonbator, D., Liu, D. Y., and Wingate, M. T. D., 2010, Lithostratigraphic and geochronological constraints on the evolution of the Central Asian Orogenic Belt in SW Mongolia: Early Paleozoic rifting followed by late Paleozoic accretion: American Journal of Science, v. 310, p.
Kurihara, T., Tsukada, K., Otoh, S., Kashiwagi, K., Chuluun, M., Byambadash, D., Boijir, B., Gonchigdorj, S., Nuramkhan, M., Niwa, M., Tokiwa, T., Hikichi, G., and Kozuka, T., 2009, Upper Silurian and Devonian pelagic deep-water radiolarian chert from the Khangai-Khentei belt of Central Mongolia: Evidence for Middle Paleozoic subduction-accretion activity in the Central Asian Orogenic Belt: Journal of Asian Earth Sciences, v. 34, p. 209–225, doi: 10.1016/j.jseaes.2008.04.010.
Lamb, M. A., and Badarch, G., 1997, Paleozoic sedimentary basins and volcanic arc systems of southern Mongolia: new stratigraphic and sedimentologic constraints: International Geology Review, v. 39, p. 542–576, doi: 10.1080/00206819709465288.
——— 2001, Paleozoic sedimentary basins and volcanic arc systems of southern Mongolia: New geochemical and petrographic constraints, *in* Hendrix, M. S., and David, G. A., editors, Paleozoic and Mesozoic tectonic evolution of Central and Eastern Asia: From continental assembly to intracontinental deformation, Boulder, Colorado: Geological Society of America, Memoir, v. 194, p. 117–149, doi: 10.1130/0-8137-1194-0.117.

Lamb, M. A., Hanson, A. D., Graham, S. A., Badarch, G., and Webb, L. E., 1999, Left-lateral sense offset of Upper Proterozoic to Paleozoic features across the Gobi Onon, Tost, and Zuunbayan faults in southern Mongolia and implications for other central Asian faults: Earth and Planetary Science Letters, v. 173, p. 183–194, doi: 10.1016/S0012-821X(99)00227-7.

Lamb, M. A., Badarch, G., Navratil, T., and Poier, R., 2008, Structural and geochronologic data from the Shine Jinst area, eastern Gobi-Altai, Mongolia: Implications for Phanerozoic intracontinental deformation in Asia: Tectonophysics, v. 451, p. 312–330, doi: 10.1016/j.tecto.2007.11.061.

Lee, J.-Y., Marti, K., Severinghaus, J. P., Kawamura, K., Yoo, H.-S., Lee, J. B. and Kim, J. S., 2006, A redetermination of the isotopic abundances of atmospheric Ar: Geochimica et Cosmochimica Acta, v. 70, p. 4507–4512, doi: 10.1016/j.gca.2006.06.1563.

Levashova, N. M., Kalgyn, V. M., Gibsher, A. S., Yff, J., Ryabinin, A. B., Meert, J. G., and Malone, S. J., 2010, The origin of the Baydaric microcontinent, Mongolia: Constraints from paleomagnetism and geochronology: Tectonophysics, v. 485, p. 306–320, doi: 10.1016/j.tecto.2010.01.012.

Li, Y. P., Zhang, Z. K., McWilliams, M., Sharps, R., Zhai, Y. J., Li, Y. A., Li, Q., and Cox, A., 1988a, Mesozoic paleomagnetic results of the Tarim craton: Tertiary relative motion between China and Siberia: Geophysical Research Letters, v. 15, p. 217–220, doi: 10.1029/GL015i003p00217.

Li, Y. P., McWilliams, M., Cox, A., Sharps, R., Li, Y. A., Gao, Z. J., Zhang, Z. K., and Zhai, Y. J., 1988b, Late Permian paleomagnetic pole from dikes of the Tarim craton, China: Geology, v. 16, p. 275–278, doi: 10.1130/0091-7613(1988)016<0275:LPPPFD>2.3.CO;2.

Lister, G. S., Forster, M. A., and Rawling, T. J., 2001, Episodicity during orogenesis, *in* Miller, J. A., Holdsworth, R. E. Buick, I. S., and Hand, M., editors, Continental Reactivation and Reworking: Geological Society, London, Special Publications, v. 184, p. 89–113, doi 10.1144/GSL.SP.2001.184.01.06.

Manatschal, G., Engström, A., Desmurs, L., Schaltegger, U., Cosca, M., Müntener, O., and Bernoulli, D., 2006, What is the tectono-metamorphic evolution of continental break-up: The example of the Tasna Ocean-Continent Transition: Journal of Structural Geology, v. 28, p. 1849–1869, doi: 10.1016/j.jsg.2006.07.014.

Marinov, N. A., Zonenshain, L. P., and Blagonravov, V. A., 1973, Geology of the Mongolian People's Republic: Moscow, Nedra, 782 p. (in Russian).

Markova, N. G., 1975, Stratigraphy of the early and Middle Paleozoic of Western Mongolia: Moscow, Nauka Press, Transactions of Joint Soviet-Mongolian Scientific Research Geological Expedition, 12, 119 p. (in Russian).

Minzhin, C., Badarch, G., and Tungalag, F., 1993, Stratigraphy of the Shine Jinst Paleozoic deposits: Mongolian Technical University Scientific Transactions, v. 3, p. 3–19 (in Mongolian).

Pubellier, M., Ego, F., Chamot-Rooke, N., and Rangin, C., 2003, The building of pericratonic mountain ranges: Structural and kinematic constraints applied to GIS-based reconstructions of SE Asia: Bulletin de la Societe Geologique de France, v. 174, p. 561–584, doi: 10.2113/174.6.561.

Queano, K. L., Ali, J. R., Milsom, J., Aitchison, J. C., and Pubellier, M., 2007, North Luzon and the Philippine Sea Plate motion model: Insights following paleomagnetic, structural, and age-dating investigations: Journal of Geophysical Research B: Solid Earth, v. 112, 44 p., B05101, doi: 10.1029/2006JB004506.

Ramsay, J. G., 1967, Folding and fracturing of rocks: New York, McGraw-Hill Book Company, 568 p.

Rauzer, A. A., Zhanchiv, D. I., Golyakov, V. I., Ykhina, I. F., Ivanov, I. G., Tsukernik, A. B., Afonin, V. V., Smirnov, I. G., Bykhover, V. I., Kravtsev, A. V., Baatarkhuyag, A., Skoryukin, M. I., Khodikov, I. V., Mantsev, N. V., Okaemov, S. V., Mischin, V. A., and Enkhsajkhan, T., 1987, Report on results of geological survey at a scale of 1: 200,000, performed in southeast part of the Mongolian Altay, Mongolian National Republic in 1983–1986: Moscow, Tekhnoexport, 769 p. (in Russian).

Renne, P. R., Deino, A. L., Hames, W. E., Heizler, M. T., Hemming, S. R., Hodges, K. V., Koppers, A. A. P., Mark, D. F., Morgan, L. E., Phillips, D., Singer, B. S., Turrin, B. D., Villa, I. M., Villeneuve, M., and Wijbrans, J. R., 2009, Data reporting norms for $^{40}Ar/^{39}Ar$ geochronology: Quaternary Geochronology, v. 4, p. 346–352, doi: 10.1016/j.quageo.2009.06.005.

Rippington, S., Cunningham, D., and England, R., 2008, Structure and petrology of the Altan Uul ophiolite: New evidence for a Late carboniferous suture in the Gobi-Altai, southern Mongolia: Journal of the Geological Society, London, v. 165, p. 711–723, doi: 10.1144/0016-76492007-091.

Rong, J. Y., and Zhang, Z.-X., 1982, A southward extension of *Tuvaella* brachiopod, fauna: Lethaia, v. 15, p. 133–147, doi: 10.1111/j.1502-3931.1982.tb01985.x.

Rong, J. Y., Boucot, A. J., Zheng, Y., and Strusz, D. L., 1995, Biogeographical analysis of the Silurian brachiopod faunas, chiefly from Asia and Australia: Lethaia, v. 28, p. 39–60, doi: 10.1111/j.1502-3931.1995.tb01592.x.

Ruzhentsev, S. V., 2001, The Variscan belt of south Mongolia and Dzungaria, *in* Dergunov, A. B., editor, Tectonics, Magmatism, and Metallogeny of Mongolia: London, Routledge, p. 61–94.

Ruzhentsev, S. V., and Pospelov, I. I., 1992, The South Mongolian variscan fold system: Geotectonics, v. 26, p. 383–395.

Ruzhentsev, S. V., Badarch, G., and Voznesenskaya, T. A., 1985, Tectonics of the Trans-Altai zone of Mongolia (Gurvansaykhan and Dzolen ranges): Geotectonics, v. 19, p. 276–284.

Ruzhentsev, S. V., Rotman, K. S., and Minzhin, C., 1991, The formation time of the south Mongolian ocean: Doklady Akademii Nauk SSSR, v. 319, p. 451–455 (in Russian).

Salnikova, E. B., Kozakov, I. K., Kotov, A. B., Kröner, A., Todt, W., Bibikova, E. V., Nutman, A., Yakovleva, S. Z., and Kovach, V. P., 2001, Age of Palaeozoic granites and metamorphism in the Tuvino-Mongolian Massif of the Central Asian Mobile Belt: loss of a Precambrian microcontinent: Precambrian Research, v. 110, p. 143–164, doi: 10.1016/S0301-9268(01)00185-1.

Schulmann, K., Thompson, A. B., Lexa, O., and Jezek, J., 2003, Strain distribution and fabric development modeled in active and ancient transpressive zones: Journal of Geophysical Research—Solid Earth, v. 108, 2023, 15 p., doi: 10.1029/2001JB000632.

Schulmann, K., Kröner, A., Hegner, E., Wendt, I., Konopásek, J., Lexa, O., and Štípská, P., 2005, Chronological constraints on the pre-orogenic history, burial and exhumation of deep-seated rocks along the eastern margin of the Variscan orogen, Bohemian Massif, Czech Republic: American Journal of Science, v. 305, p. 407–448, doi: 10.2475/ajs.305.5.407.

Schulmann, K., Lexa, O., Štípská, P., Racek, M., Tajčmanová, L., Konopásek, J., Edel, J. B., Peschler, A., and Lehmann, J., 2008, Vertical extrusion and horizontal channel flow of orogenic lower crust: key exhumation mechanisms in large hot orogens?: Journal of Metamorphic Geology, v. 26, p. 273–297, doi: 10.1111/j.1525-1314.2007.00755.x.

Şengör, A. M. C., and Natal'in, B. A., 1996, Paleotectonics of Asia: fragments of a synthesis, *in* Yin, A., and Harrison, M., editors, The Tectonic Evolution of Asia: Cambridge, Cambridge University Press, p. 486–640.

Şengör, A. M. C., Natal'in, B. A., and Burtman, V. S., 1993, Evolution of the Altaid tectonic collage and Paleozoic crustal growth in Eurasia: Nature, v. 364, p. 299–307, doi: 10.1038/364299a0.

Sinitsyn, V. M., 1956, Principal elements of geological structure of Gobi: Bulletin, MOIL, Geology, v. 61, 6 p. (in Russian).

Steiger, R. H., and Jäger, E., 1977, Subcommission on geochronology: Convention on the use of decay constants in geo- and cosmochronology: Earth and Planetary Science Letters, v. 36, p. 359–362, doi: 10.1016/0012-821X(77)90060-7.

Štípská, S., Schulmann, K., Lehmann, J., Corsini, M., Lexa, O., and Tomurhuu, D., 2010, Early Cambrian eclogites in SW Mongolia: Evidence that the Paleo-Asian Ocean suture extends further east than expected: Journal of Metamorghic Geology, doi: 10.1111/j.1525-1314.2010.00899.x.

Tapponnier, P., and Molnar, P., 1979, Active faulting and Cenozoic tectonics of the Tien Shan, Mongolia, and Baykal regions: Journal of Geophysical Research, v. 84, p. 3425–3459, doi: 10.1029/JB084iB07p03425.

Teyssier, C., and Tikoff, B., 1998, Strike-slip partitioned transpression of the San Andreas fault system; a lithospheric-scale approach, *in* Holdsworth, R. E., Strachan, R. A., and Dewey, J. F., editors, Continental transpressional and transtensional tectonics: Geological Society, London, Special Publications, v. 135, p. 143–158, doi: 10.1144/GSL.SP.1998.135.01.10.

Tikoff, B., and Teyssier, C., 1994, Strain modeling of displacement-field partitioning in transpression orogens: Journal of Structural Geology, v. 16, p. 1575–1588, doi: 10.1016/0191-.8141(94)90034-5.

Tomurtogoo, O., 1997a, A new tectonic scheme of the Paleozoides in Mongolia: Mongolian Geoscientist, v. 3, p. 12–19.

——— 1997b, A new tectonic scheme of the Paleozoides in Mongolia, *in* Zhiqin, X., Yufeng, R., and Xiaping, Q., editors, Orogenic Belts Geological Mapping, Proceedings of the 30th International Geological Congress: Utrecht, The Netherlands, VSP, v. 7, p. 75–82.

——— 1998, Geological map of Mongolia: Ulaanbaatar, Mineral Resources Authority of Mongolia, Mongolian Academy of Sciences, scale 1:1 000 000 (with English summary).

Tomurtogoo, O., and Badarch, G., 1997, Serpentinite mélange of the Ongon Ylaan range in the Variscides of South Mongolia: Mongol Orny Geodynamic for Metallogeny, v. 14, p. 35–48 (in Russian).

Tomurtogoo, O., Windley, B. F., Kröner, A., Badarch G., Liu, D. Y., 2005, Zircon age and occurrence of the Adaatsag ophiolite and Muron shear zone, central Mongolia: constraints on the evolution of the Mongol-Okhotsk ocean, suture and orogen: Journal of the Geological Society, London, v. 162, p. 125–134, doi: 10.1144/0016-764903-146.

Turner, G., Huneke, J. C., Podosek, F. A., and Wasserburg, G. J., 1971, ^{40}Ar-^{39}Ar ages and cosmic ray exposure ages of Apollo 14 samples: Earth and Planetary Science Letters, v. 12, p. 19–35, doi: 10.1016/0012-821X(71)90051-3.

Walker, R. T., Nissen, E., Molor, E., and Bayasgalan, A., 2007, Reinterpretation of the active faulting in central Mongolia: Geology, v. 35, p. 759–762, doi: 10.1130/G23716A.1.

Windley, B. F., Alexeiev, D., Xiao, W., Kröner, A., and Badarch, G., 2007, Tectonic models for accretion of the Central Asian Orogenic Belt: Journal of the Geological Society, London, v. 164, p. 31–47, doi: 10.1144/0016-76492006-022.

Xiao, W., Windley, B. F., Hao, J., and Zhai, M., 2003, Accretion leading to collision and the Permian Solonker suture, Inner Mongolia, China: Termination of the central Asian orogenic belt: Tectonics, v. 22, 1069, 20 p., doi: 10.1029/2002TC001484.

Xiao, W., Han, C., Yuan, C., Sun, M., Lin, S., Chen, H., Li, Z., Li, J., and Sun, S., 2008, Middle Cambrian to Permian subduction-related accretionary orogenesis of Northern Xinjiang, NW China: Implications for the tectonic evolution of central Asia: Journal of Asian Earth Sciences, v. 32, p. 102–117, doi: 10.1016/j.jseaes.2007.10.008.

Xiao, W., Windley, B. F., Yuan, C., Sun, M., Han, C. M., Lin, S. F., Chen, H. L., Yan, Q. R., Liu, D. Y., Qin, K. Z., Li, J. L., and Sun, S., 2009, Paleozoic multiple subduction-accretion processes of the southern Altaids: American Journal of Science, v. 309, p. 221–270, doi: 10.2475/03.2009.02.

Yakubchuk, A., 2008, Re-deciphering the tectonic jigsaw puzzle of northern Eurasia: Journal of Asian Earth Sciences, v. 32, p. 82–101, doi: 10.1016/j.jseaes.2007.10.009.

Yakubchuk, A. S., Shatov, V. V., Kirwin, D., Edwards, A., Tomurtogoo, O., Badarch, G., and Buryak, V. A., 2005, Gold and Base Metal Metallogeny of the Central Asian Orogenic Supercollage: Economic Geology, 100th Anniversary Volume, p. 1035–1068.

Yarmolyuk, V. V., and Tikhonov, V. I., 1982, Late Paleozoic magmatism and fault tectonics of the Transaltai Gobi (Mongolian People's Republic): Geotectonics, v. 16, p. 123–130.

Yarmolyuk, V. V., Kovalenko, V. I., Sal'nikova, E. B., Kovach, V. P., Kozlovsky, A. M., Kotov, A. B., and Lebedev, V. I., 2008, Geochronology of igneous rocks and formation of the Late Paleozoic south Mongolian active margin of the Siberian continent: Stratigraphy and Geological Correlation, v. 16, p. 162–181, doi: 10.1134/S0869593808020056.

Zaitsev, N. S., Luwsandansan, B., Marinov, N. A., Menner, V. V., Pavlova, T. G., Peive, A. V., Timofeev, P. P., Tomurtogoo, O., and Yanshin, A. L., 1970, Stratigraphy and Tectonics of the Mongolian Peoples Republic, v. 1: Moscow, Nauka Press, Transactions of Joint Soviet-Mongolian Scientific Research Geological Expedition, 148 p. (in Russian).

Zheng, Y., Zhang, Q., Wang, Y., Liu, R., Wang, S. G., Zuo, G., Wang, S. Z., Lkaasuren, B., Badarch, G., and Badamgarav, Z., 1996, Great Jurassic thrust sheets in Beishan (North Mountains)-Gobi areas of China and southern Mongolia: Journal of Structural Geology, v. 18, p. 1111–1126, doi: 10.1016/0191-8141(96)00038-7.

Zonenshain, L. P., 1973, The evolution of Central Asiatic geosynclines through sea-floor spreading: Tectonophysics, v. 19, p. 213–232, doi: 10.1016/0040-1951(73)90020-6.

Zonenshain, L. P., Suyetenko, O. D., Jamyandamba, L., and Eengin, G., 1975, Structure and the axial part of South Mongolian eugeosyncline in the Dzolen Range: Geotectonics, v. 9, p. 214–220.

Zonenshain, L. P., and Kuzmin, M. I., 1978, Khan-Taishir ophiolite complex in western Mongolia and problems of ophiolites: Geotectonics, v. 1, p. 19–42.

Zorin, Y. A., 1999, Geodynamics of the western part of the Mongolia-Okhotsk collisional belt, Trans-Baikal region (Russia) and Mongolia: Tectonophysics, v. 306, p. 33–56, doi: 10.1016/S0040-1951(99)00042-6.

Zorin, Yu. A., Belichenko, V. G., Turutanov, E. Kh., Kozhevnikov, V. M., Ruzhentsev, S. V., Dergunov, A. B., Filippova, I. B., Tomurtogoo, O., Arvisbaatar, N., Bayasgalan, Ts., Biambaa, Ch., and Khosbayar, P., 1993, The South Siberia-Central Mongolia transect: Tectonophysics, v. 225, p. 361–378, doi: 10.1016/0040-1951(93)90305-4.